BATTELLE-NORTHWEST
RECEIVED
MAY 28 1970
CIRCULATING
COPY
TECHNICAL INFO. SECTION

BNWL-1381-1
UC-80

2-
5-70

REACTOR PHYSICS QUARTERLY REPORT
JANUARY, FEBRUARY, MARCH 1970

May 1970

AEC RESEARCH &
DEVELOPMENT REPORT

ROUTE TO

BNWL-1381-1

BATTELLE NORTHWEST
BATTELLE MEMORIAL INSTITUTE PACIFIC NORTHWEST LABORATORIES
BATTELLE BOULEVARD, P. O. BOX 999, RICHLAND, WASHINGTON 99352

LEGAL NOTICE

This report was prepared as an account of Government sponsored work. Neither the United States, nor the Commission, nor any person acting on behalf of the Commission:

A. Makes any warranty or representation, expressed or implied, with respect to the accuracy, completeness, or usefulness of the information contained in this report, or that the use of any information, apparatus, method, or process disclosed in this report may not infringe privately owned rights; or

B. Assumes any liabilities with respect to the use of, or for damages resulting from the use of any information, apparatus, method, or process disclosed in this report.

As used in the above, "person acting on behalf of the Commission" includes any employee or contractor of the Commission, or employee of such contractor, to the extent that such employee or contractor of the Commission, or employee of such contractor prepares, disseminates, or provides access to, any information pursuant to his employment or contract with the Commission, or his employment with such contractor.

PACIFIC NORTHWEST LABORATORY
RICHLAND, WASHINGTON
operated by
BATTELLE MEMORIAL INSTITUTE
for the
UNITED STATES ATOMIC ENERGY COMMISSION UNDER CONTRACT AT(45-1)-1830

3 3679 00061 6674

BNWL-1381-1
UC-80,
Reactor Technology

REACTOR PHYSICS QUARTERLY REPORT
JANUARY, FEBRUARY, MARCH 1970

By

The Staff of
Reactor Physics Department
L. C. Schmid, Manager
Physics Research Department
E. D. Clayton, Manager
and
Reactor Physics and Operations
of the FFTF
R. E. Heineman, Manager

May 1970

FIRST UNRESTRICTED DISTRIBUTION MADE MAY 22 '70

BATTELLE MEMORIAL INSTITUTE
PACIFIC NORTHWEST LABORATORIES
RICHLAND, WASHINGTON 99352

Printed in the United States of America
Available from
Clearinghouse for Federal Scientific and Technical Information
National Bureau of Standards, U.S. Department of Commerce
Springfield, Virginia 22151
Price: Printed Copy $3.00; Microfiche $0.65

REACTOR PHYSICS QUARTERLY REPORT
JANUARY, FEBRUARY, MARCH 1970

FOREWORD

The objective of the Reactor Physics Quarterly Report is to inform the scientific community in a timely manner of the technical progress made on the many phases of reactor physics work within the laboratory. The report contains brief technical discussions of accomplishments in all areas where significant progress has been made during the quarter. The results presented herein should be considered preliminary, and do not constitute final publication of the work. A list of publications and papers issued during the last quarter is included in the report. Anyone desiring additional information concerning the work reported herein is encouraged to contact the author directly.

PREVIOUS REPORTS IN THIS SERIES

HW-42182	October, November, December	1955
HW-43441	January, February, March	1956
HW-44525	April, May, June	1956
HW-47012	July, August, September	1956
HW-48893	October, November, December	1956
HW-50598	January, February, March	1957
HW-51983	April, May, June	1957
HW-53492	July, August, September	1957
HW-54591	October, November, December	1957
HW-55879	January, February, March	1958
HW-56919	April, May, June	1958
HW-57861	July, August, September	1958
HW-59126	October, November, December	1958
HW-60220	January, February, March	1959
HW-61181	April, May, June	1959
HW-62727	July, August, September	1959
HW-63576	October, November, December	1959
HW-64866	January, February, March	1960
HW-66215	April, May, June	1960
HW-67219	July, August, September	1960
HW-68389	October, November, December	1960
HW-69475	January, February, March	1961
HW-70716	April, May, June	1961
HW-71747	July, August, September	1961
HW-72586	October, November, December	1961
HW-73116	January, February, March	1962
HW-74190	April, May, June	1962
HW-75228	July, August, September	1962
HW-76128	October, November, December	1962
HW-77311	January, February, March	1963
HW-77871	April, May, June	1963
HW-79054	July, August, September	1963
HW-80020	October, November, December	1963
HW-81659	January, February, March	1964
HW-83187	April, May, June	1964
HW-84369	July, August, September	1964
HW-84608	October, November, December	1964
BNWL-95	January, February, March	1965
BNWL-149	April, May, June	1965
BNWL-193	July, August, September	1965
BNWL-222	October, November, December	1965
BNWL-284	January, February, March	1966
BNWL-315	April, May, June	1966
BNWL-340	July, August, September	1966
BNWL-400	October, November, December	1966
BNWL-472	January, February, March	1967
BNWL-534	April, May, June	1967

BNWL-634	July, August, September	1967
BNWL-685	October, November, December	1967
BNWL-775	January, February, March	1968
BNWL-887	April, May, June	1968
BNWL-921	July, August, September	1968
BNWL-985	October, November, December	1968
BNWL-1053	January, February, March	1969
BNWL-1150	April, May, June	1969
BNWL-1240	July, August, September	1969
BNWL-1304	October, November, December	1969

CONTENTS

SUMMARY 1.1
REACTOR THEORY AND CODE DEVELOPMENT. 2.1
Code Modifications 2.1
Calculation of 2-Table Sets of S_N Parameters in HRG 2.1
RSYN Development 2.6
THERMAL REACTORS 3.1
Effect of ^{241}Pu Decay on k, ... 3.1
Measurement of k, for a ThO_2-$^{233}UO_2$ HTGR Lattice at Room Temperature 3.6
Initial HTLTR Measurements with HTGR Lattice . 3.16
Critical Experiments in UO_2-2 wt% PuO_2 Fueled-H_2O Moderated Assemblies 3.20
FAST REACTORS 4.1
Calculational Comparison of Fast Neutron Cavity and Full Size Fast Critical Assembly Experiments . . 4.1
Neutronic Calculations for Fast Reactor Fuel Transient Tests . . 4.10
A New Computational System for Fast Reactor Accident Investigation . . 4.22
On the Treatment of Spatial Feedback Effects in Fast Reactor Accident Analyses . . 4.25
Stability Analysis of the Fast Test Reactor . . 4.28
Notes on the Use of the "Engineering Mockup" as a Nuclear Design Tool . . 4.31
Inverse Multiplication Monitoring of Subcritical Reactivity Changes in FTR . 4.34
Central Fuel and Peripheral Control Ring Reactivity Worths in the FTR-2 Critical . . 4.37
FTR Core Flux Monitoring 4.41
Effect of Cobalt Content in Steel on Shield Requirements 4.47
Radiation Levels in Heat Transport Cell . . 4.48

Neutron Attenuation Characteristics of Stainless Steels 4.53
ZPPR/FTR-2 Shield Experiments 4.57
PUBLICATIONS AND PRESENTATIONS 6.1
Publications 6.1
Presentations. 6.1
DISTRIBUTION Distr-1

REACTOR PHYSICS QUARTERLY REPORT

January, February, March 1970

1.0 SUMMARY

REACTOR THEORY AND CODE DEVELOPMENT

A transverse buckling option and a "white" albedo boundary condition option have been added to the THERMOS/BATTELLE code. An error was corrected in the anisotropy correction option, and the cell smear routine has been modified to make it more useful.

An option has been added to the slowing down spectrum code HRG to permit the calculation and punching of 2-table sets of S_n parameters based on an improved, "extended," transport approximation.

Expressions have been derived which will allow the three-dimensional flux synthesis code RSYN to use trial functions generated in cylindrical and hexagonal geometry in addition to the currently available rectangular geometry.

THERMAL REACTORS

Critical experiments were completed in the PRCF in a H_2O-moderated lattice (1.06 in. square pitch) of UO_2-4 wt% PuO_2 fuel rods.

The effect of ^{241}Pu decay and ^{241}Am buildup in plutonium fueled reactor lattices with a high ^{241}Pu content has an important bearing on the way that recycled plutonium can be most effectively used in thermal power reactors. An analytical study was made to determine the change in the infinite medium neutron multiplication factor, ∇k_∞, for a 4-in. square pitch graphite lattice fueled with 1/2-in. diameter UO_2-2.6 wt% PuO_2 (29% ^{240}Pu, 5% ^{241}Pu) Zircaloy clad rods, assuming the half life of ^{241}Pu is about 13 years. The neutronic parameters for

this lattice, including k_∞, were measured in the Physical Constants Testing Reactor (PCTR) in November, 1966. During the 3-1/4 years that have passed since this measurement, 16% of the ^{241}Pu in these rods has decayed to ^{241}Am. The value for Δk_∞ (calculated to be about -0.013) can be obtained experimentally by a simple remeasurement of the amount of absorber to achieve null reactivity in the lattice.

Room temperature measurements of k_∞ for a ThO_2-$^{233}UO_2$ HTGR lattice have been completed in the PCTR. Preliminary results indicate a small disagreement with theory which is probably due to an inadequate treatment of end effects. The room temperature results will be used to normalize the measurements at elevated temperatures to be performed in the HTLTR.

The first experimental information over the design temperature range (25 to 1000 °C) has been obtained in the High Temperature Lattice Test Reactor. An experimental lattice composed of a $^{235}UC_2$-ThO_2-C fuel mixture contained in graphite blocks was the subject of the measurement to determine k_∞ as a function of temperature.

FAST REACTORS

A calculational comparison of Fast Neutron Cavity (FNC) and full-size fast critical assembly experiments has shown the feasibility of measuring fast reactor neutronic parameters in the PCTR, HTLTR or both. The equilibrium neutron energy spectrum of a large FBR can be duplicated in small fast reactor lattice zones, containing 70 to 80 kg of plutonium, in a coupled fast-thermal reactor core. A broad range of investigations that could be carried out in a fast neutron cavity has been identified. The fissile fuel inventory required for these experiments is an order of magnitude smaller than that required for full size critical assemblies.

Multiplication calculations were done to determine the specific physics calculations of the EBR-II/TREAT and GETR/TREAT experiments during transient tests.

New computational methods of treating fast reactor excursions have been developed and are illustrated by examples taken from work on the Fast Test Reactor (FTR). In one development, the multichannel neutronics heat transfer program, MELT-11, is coupled to the two dimensional disassembly program, VENUS. A second development makes use of a lumped nuclear model coupled with a space-dependent feedback model to reduce the need for a complete space-time treatment of important feedback effects.

The current work in experimental reactor physics being performed in support of the FTR is described. An analysis is shown of the degree to which the FTR hexagonal core structure can be mocked up by the rectangular ZPR structure. A calculation is given which shows the errors incurred by inferring subcritical reactivity from subcritical flux levels measured by chambers at various positions in and around the FTR core. Such information will be used in implementing a subcritical reactivity monitor for the FTR. Another experiment is described in which the reactivity of control element poison placed at the core-reflector boundary is measured alternately with that of plutonium fuel removed from the center of the core. Although the poison effect can be calculated to within about 10%, the effect of removal of up to 32 kg of plutonium is overestimated by the same 30% noted in many other critical experiments.

Analyses were made to estimate the radiation environment for both in-vessel and out-of-vessel neutron detectors to assist in the design of the instrument system for the Fast Test Reactor (FTR). The analyses include the effect of stored fuel

in the sodium annulus between the radial shield and the vessel as well as the time-dependent behavior following shut down of the reactor.

It was shown that the cobalt content in stainless steel will dictate shielding requirements for FTR components such as the core support structure.

If access is required to one of the three FTR heat transport system cells while the reactor is being operated at two-thirds power, isolation valves are needed in the primary sodium lines that leak less than one or two gallons per hour.

Calculations indicate that different neutron attenuation characteristics are anticipated for Types 304 and 316 stainless steel because of the molybdenum content of the latter. The decision to employ Type 316 steel in FTR makes those shielding calculations based on Type 304 steel slightly conservative.

A comparison of analyses with experimental measurements of the neutron and gamma distribution throughout the ZPPR mockup of the FTR radial reflector and shield indicate that use of these analytical techniques and nuclear data are expected to result in a realistic preliminary shield design.

2.0 REACTOR THEORY AND CODE DEVELOPMENT

CODE MODIFICATIONS

C. L. Bennett

The following modifications to THERMOS/BATTELLE have been completed.

1) A transverse buckling option of the simple DB^2 form has been added. The radial, axial, or planer buckling is calculated from the input dimensions which may or may not include the extrapolation distances. The extrapolation distances would normally be calculated internally in this option.

2) A "white" albedo boundary condition option has been added to the cylindrical-geometry ray-tracing method. The boundary albedo can be specified for either the whole thermal range or each speed.

3) An error in the anisotropic scattering correction option (neglecting isotopes used in the cell not on the library) has been corrected.

4) The cell smear routine has been modified to correctly produce a complete spatially-collapsed-cell macroscopic-cross-section set which can be punched out on cards in a format compatable with its use in a succeeding THERMOS case as an added material used in the cell but not provided in the library.

CALCULATION OF 2-TABLE SETS OF S_N PARAMETERS IN HRG

J. L. Carter

For some time, the epithermal spectrum code HRG has had available an option of punching a 2-table set of parameters

for use in S_N codes such as DTF-IV. In this option, the entry for group g in the a_g position of the first table is (0), the flux weighted total cross section. Bell et al.[1] show that generally it is better to use the extended transport approximation, which gives

$$\sigma_g = \sigma_{t,g}(2) - \sigma_{2g}(2) \tag{1}$$

for a 2-table set. Here the subscript 2 refers to the second Legendre moment of the scattering cross section in the laboratory system and the 2 in parentheses indicates the cross sections should be weighted over the energies of group g by the second Legendre moment of the angular flux. An option has now been added to HRG to permit punching 2-table sets of S_N parameters based on this extended transport approximation.

Because evaluation of Equation (1) requires knowledge of the second Legendre moments of both the angular flux and the scattering cross section (neither of which is directly available in HRG), some auxiliary calculations must be done. Bell et al.[1] show that, for the unknown flux moment, an adequate approximation is

$$\phi_2(E) \propto \phi_1(E)/\Sigma_{tr}(E) \tag{2}$$

where $\phi_1(E)$ is the first Legendre moment of the flux, i.e., the current, and $\Sigma_{tr}(E)$ is the macroscopic transport cross section. These latter quantities are available in HRG for each fine group, so that the fine group analog of Equation (2) can readily be found.

Finding the second Legendre moment of the scattering cross section is more difficult, but sufficient information is available so that a reasonable approximation can be made if we can assume that the only anisotropy is that of elastic scattering and that this is linearly anisotropic in the center

of mass system. In this case, the microscopic cross section in energy and solid angle for a particular isotope is, in usual notation,

$$\sigma_s(E,\mu_c) = \frac{\sigma_s(E)}{4\pi} \quad [1 + \omega_1^c(E)\mu_c]. \tag{3}$$

In the laboratory system, the cross section for this isotope is

$$\sigma_s(E,\mu_L) = \frac{\sigma_s(E)}{4\pi}\sum_{\ell=0}^{\infty} \omega_\ell^L(E) \; P_\ell(\mu_L). \tag{4}$$

The transformation matrix relating these two sets of ω's is well-known;[2] we only need values for ℓ=0,1,2. For $\gamma = 1/A << 1$, these are

$$\omega_0^L(E) = 1 \tag{5a}$$

$$\omega_1^L(E) = 2\gamma + (1 - \frac{3}{5}\gamma^2)\; \omega_1^c(E) \tag{5b}$$

$$\omega_2^L(E) = \gamma^2[1 + 0(\gamma^2)] + 2\gamma[1 + 0(\gamma^2)]\; \omega_1^c(E) \tag{5c}$$

where only terms to order γ^2 are given explicitly for $\omega_2^L(E)$. The angular moments we seek are not the ω_ℓ^L themselves, but instead the coefficients of the expansion

$$\sigma_s(E,\mu_L) = \sum_{\ell=0}^{\infty} \frac{2\ell + 1}{4\pi}\; \sigma_\ell(E)\; P_\ell(\mu_L). \tag{6}$$

From Equation (4) it follows that

$$\sigma_\ell(E) = \frac{\omega_\ell^L(E)\; \sigma_s(E)}{2\ell + 1}. \tag{7}$$

Now $\omega_1^c(E)$ can be eliminated between Equations (5b) and (5c) and (7) can be used to express $\sigma_2(E)$ in terms of $\sigma_1(E)$ and $\sigma_0(E)$.

In fine group form, the result can be written

$$\sigma_{2,n} = \frac{6}{5}\,\frac{\gamma[1 + 0(\gamma^2)]}{1 - \frac{3}{5}\gamma^2}(\sigma_{1,n} - \frac{2}{3}\gamma\sigma_{0,n})$$

$$+ \frac{1}{5}\gamma^2\,[1 + 0(\gamma^2)]\sigma_{0,n} \qquad \gamma << 1. \tag{8}$$

For an individual isotope, Equation (8) gives the second Legendre moment we seek.

Many HRG nuclides are individual isotopes and $a_{0,n}$ and $a_{1,n}$ are available for them, so that $a_{2,n}$ can be found if γ is known. We can readily find γ from the knowledge that the scattering is isotropic in the center of mass system at sufficiently low energies. Thus, we can choose a low energy fine group m for which scattering is isotropic and find γ from

$$\frac{\sigma_{1,m}}{\sigma_{0,m}} = \frac{2}{3}\gamma. \tag{9}$$

For these nuclides, a_g in Equation (1) can be found by averaging $a_{t,n} - \sigma_{2,n}$ over all fine groups n in g, where $a_{2,n}$ is found from Equations (8) and (9), and where, from (2), the weighting function is $J_n/\Sigma_{tr,n}$.

The option which has been added assumes that this same procedure can also be used for the remaining HRG nuclides and for the macroscopic cross section. This extension of the application of Equations (8) and (9) needs justification. What is obtained from (9) is an average value $\overline{\gamma}$, where

$$\overline{\gamma} = \frac{\sum_i \gamma_i N_i\,\sigma^i_{0,m}}{\sum_i N_i\,\sigma^i_{0,m}} \tag{10}$$

and the index i refers to the component isotopes.

It is not immediately clear that $\bar{\gamma}$ is appropriate for use in Equation (8). For one thing, other averages such as $\overline{\gamma^2}$ are needed in (8), and $\overline{\gamma^2} = \bar{\gamma}^2$ may be a poor approximation even for group m. In addition, if the ratios of the component σ_0's vary from group to group, $\bar{\gamma}_m = \bar{\gamma}_n$ may also be a poor approximation. If the γ_i are nearly equal, however, as in those HRG nuclides which represent elements, it is clear from Equation (10) and its analogs for higher powers of γ_i that $\overline{\gamma^P} \approx \bar{\gamma}^P$ and $\bar{\gamma}$ can be used in (8) with little error. Where the γ_i are widely different (as in the HRG use of H_2O and D_2O as nuclides and as is usually the case for the components of macroscopic cross sections for a cell), the accuracy of the approximation can best be determined by testing actual data. Because $\gamma = \bar{\gamma} << 1$ is not true for these cases, another problem arises in using (8), i.e., the leading terms in γ do not reduce to the correct limit as $\gamma \to 1$. This deficiency can be largely overcome by adding terms in γ^2 in (8), with adjustable coefficients chosen to give the correct values as $\gamma \to 1$. When this is done, (8) is replaced by

$$\sigma_{2,n} = \frac{6}{5}\gamma\left(\frac{1 - \frac{3}{8}\gamma^2}{1 - \frac{3}{5}\gamma^2}\right)\left(\sigma_{1,n} - \frac{2}{3}\gamma\sigma_{0,n}\right) + \frac{1}{5}\gamma^2\left(1 + \frac{1}{4}\gamma^2\right)\sigma_{0,n}. \tag{11}$$

A test case has been run to compare the macroscopic value, the a_g of (1), with the sum of the microscopic values of the individual components. In the test case Equations (9) and (11) were used to find each fine group $a_{2,n}$ and the weighting function of $J_n/\Sigma_{tr,n}$ was used in averaging over the fine groups in g. In addition, a 0.5 in. fuel rod containing a mixture of plutonium and uranium oxide clad with zirconium in a geometry with a fuel/water ratio of about 1 was assumed for

the calculation. Three broad groups were used, with lower energy limits of 1.17×10^4, 2.38, and 0.683 eV. The percent differences between the macroscopic and sum of microscopic values of Equation (1) were -1.8, 9.0, and 3.4 for the three groups. The H_2O was treated as a nuclide in this case. A separate estimate of the error in treating H_2O as a nuclide rather than as 2H + O is about 3% in the lower energy fine groups and 6% in the higher energy fine groups.

Although these results indicate that an uncertainty of the order of 10% is introduced by extending Equations (9) and (11) to macroscopic cross sections, the accuracy is usually better than that of the basic assumption of linearly anisotropic scattering of the center-of-mass system. Therefore a more elaborate treatment of the available data is not warranted at this time.

References

1. G. I. Bell, G. E. Hansen, and H. A. Sandmeier. "Multitable Treatments of Anisotropic Scattering in S_N Multigroup Transport Calculations," Nuc. Sci. Eng., vol. 28, pp. 376-383. 1967.

2. Reactor Physics Constants, 2nd Ed., ANL-5800, pp. 50-51. Argonne National Laboratory, Argonne, Illinois, July 1963.

RSYN DEVELOPMENT

R. D. Johnson

RSYN[1] solves the three-dimensional, multigroup reactor diffusion equations by the method of flux synthesis. The two-dimensional diffusion code 2DB[2] generates the trial functions in the horizontal planes from which the full three-dimensional solution is synthesized. The currently operational version of RSYN accepts only trial functions

with rectangular geometry. Expressions have been derived which, when programmed, will extend the flexibility of RSYN by allowing utilization of trial functions generated by 2DB in cylindrical and hexagonal geometry. Availability of the extended RSYN is expected to be June 1970.

References

1. H. S. Zwibel. "A Multigroup 3D Synthesis Code," Reactor Physics Quarterly Report, October, November, December, 1968, BNWL-985. Battelle-Northwest, Richland, Washington, February 1969.

2. W. W. Little, Jr. and R. W. Hardie. 2DB User's Manual--Revision I. BNWL-831 Rev. 1. Battelle-Northwest, Richland, Washington, June 1969.

3.0 THERMAL REACTORS

EFFECT OF ^{241}Pu DECAY ON k_∞

D. F. Newnian and C. R. Gordon

Important questions have recently arisen concerning the effect of ^{241}Pu decay and ^{241}Am buildup on reactor physics parameters of plutonium fueled lattices.[1] Since the half life of ^{241}Pu is 13 to 15 years, the amount of fissile fuel in rods with high ^{241}Pu content can change significantly over a few years resulting in a change in the infinite medium neutron multiplication factor, k_∞, for a lattice fueled with this type of material. This change, which can be measured in the Physical Constants Testing Reactor (PCTR), can be directly related to ^{241}Pu decay and ^{241}Am buildup in the fuel rods. Correlation of the change in k, of a lattice containing fuel with a high ^{241}Pu content, measured over a period of several years with calculations and/or isotopic measurements properly accounting for the change in ^{241}Pu and ^{241}Am densities, will permit evaluation of the uncertainties in theoretical predictions of the reactivity effect. Effects of this kind have an important bearing on the way that recycled plutonium can be most effectively utilized in thermal power reactors.

UO_2-2.6 wt% PuO_2 Lattice

The infinite medium neutron multiplication factor, k_∞, for a 4-in. square pitch graphite lattice fueled with 1/2-in. diameter UO_2-2.6 wt% PuO_2 (29% ^{240}Pu, 5% ^{241}Pu) Zircaloy clad rods was measured in the PCTR during November, 1966.[2] During the 3-1/4 years that have passed since this measurement, 16% of the ^{241}Pu in these rods has decayed to ^{241}Am. Isotopic densities for the UO_2-2.6 wt% PuO_2 fueled graphite lattice both in November, 1966, and February, 1970 are given in Figure 3.1, assuming the half life of ^{241}Pu is 13 years. This ^{241}Pu loss

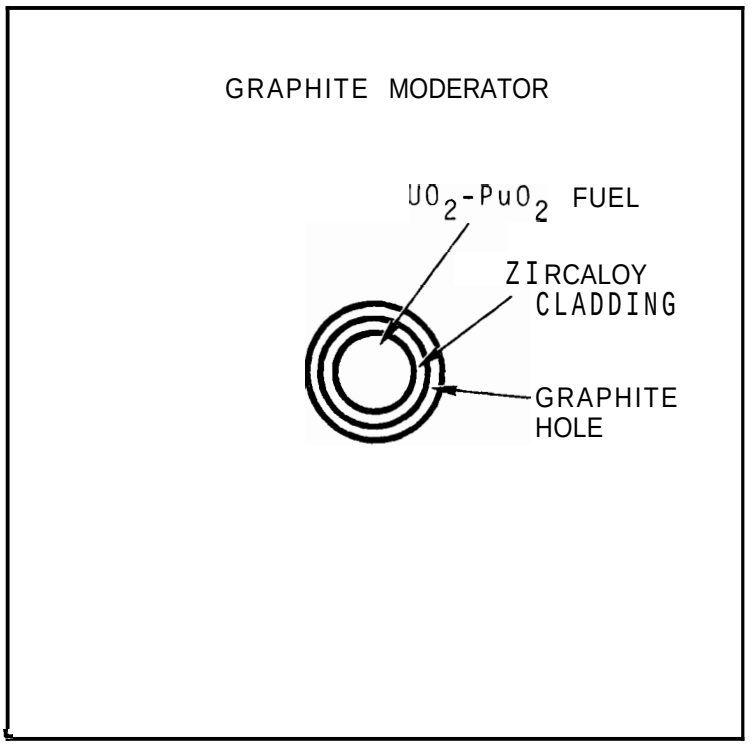

Region	Radius (cm)	Isotope	Nuclei Density (nuclei/cm^3 × 10^{-24}) November, 1966	February, 7970
Fuel	0.6375	^{235}U	3.81×10^{-5}	3.81×10^{-5}
		^{238}U	2.09×10^{-2}	2.09×10^{-2}
		O	4.38×10^{-2}	4.38×10^{-2}
		^{239}Pu	3.61×10^{-4}	3.61×10^{-4}
		^{240}Pu	1.63×10^{-4}	1.63×10^{-4}
		^{241}Pu	2.57×10^{-5}	2.16×10^{-5}
		^{242}Pu	6.72×10^{-6}	6.72×10^{-6}
		^{241}Am	5.98×10^{-6}	1.01×10^{-5}
Clad	0.7188	Zr	4.14×10^{-2}	4.14×10^{-2}
Air	0.9220	N	3.98×10^{-5}	3.98×10^{-5}
		O	$1.07 \quad 10^{-5}$	1.07
Graphite	5.7320	C	8.01×10^{-2}	8.01×10^{-2}
		N	1.14×10^{-5}	1.14×10^{-5}
		O	3.06×10^{-6}	3.06×10^{-6}

FIGURE 3.1. **UO_2-2.6 wt% PuO_2 (29% ^{240}Pu, 5% ^{241}Pu) 1/2 in. Diameter Rod, 4-in. Square Pitch Graphite Lattice**

amounts to approximately 0.75% of the total fissile inventory in the fuel. The change in the infinite medium neutron multiplication factor, k,, due to the decay of ^{241}Pu and buildup of ^{241}Am was inferred using previously measured reaction rates and making nuclei density corrections. The value for nk, = -0.012 ± 0.002 is of sufficient magnitude to permit precise measurement of the ^{241}Pu decay effect.

Theoretical Predictions

A two-energy group theoretical model was used to predict the effect of ^{241}Pu decay and ^{241}Am buildup on the infinite medium neutron multiplication factor, k_∞, for the UO_2-2.6 wt% PuO_2 fueled graphite lattice. Thermal group constants were calculated for the lattice, properly accounting for the change in ^{241}Pu and ^{241}Am densities (given in Figure 3.1), using the Battelle Revised THERMOS code.[3] Epithermal group constants were calculated using the HRG[4] code with appropriate isotopic densities. The equilibrium fluxes, ϕ_1' and ϕ_2', at the center of the lattice in the fundamental mode (just critical) environment were calculated from the two group constants using the multigroup diffusion code HFN[5] to perform criticality searches. The infinite medium neutron multiplication factor is defined[6] by the expression:

$$k_\infty = \frac{\text{Total neutron production}}{\text{Total neutron absorption}} = \frac{\nu_1 \Sigma_1^f \phi_1' + \nu_2 \Sigma_2^f \phi_2'}{\Sigma_1^a \phi_1' + \Sigma_2^a \phi_2'}$$

All quantities used to evaluate the change in k_∞ due to the decay of ^{241}Pu and buildup of ^{241}Am, Δk_∞, are given in Table 3.1. The principal contributor to Δk_∞ is the change in the thermal group η, having a fractional change $\Delta\eta/\eta$ = -0.0084 Fractional change in the thermal neutron utilization of the fuel, $\Delta f/f$, was less than -0.00019. It appears that the effect of ^{241}Pu decay and ^{241}Am buildup on the infinite medium

TABLE 3.1. **UO_2 -2.6 wt% PuO_2 Fueled** Graphite Lattice Constants

Thermal (E < 0.683 eV) Group Constants	(November 1966)	(February 1970)
$\nu\Sigma_f$	6.4980×10^{-3}	6.4265×10^{-3}
Σ_a	4.1373×10^{-3}	4.1274×10^{-3}
η	1.6589	1.6449
f	0.9467	0.9466
Epithermal (E > 0.683 eV) Group Constants		
$\nu\Sigma_f$	2.5091×10^{-4}	2.4698×10^{-4}
Σ_a	5.2976×10^{-4}	5.3281×10^{-4}
ηf	0.4736	0.4635
p	0.8472	0.8464
Central Equilibrium Flux Ratio		
$\frac{\phi_1'}{\phi_2'}$	1.6236	1.6145
k_∞	1.3818	1.3684
	1.376 ± 0.006 Experimental Value (Ref 2)	

Change in k_∞ Due to ^{241}Pu Decay and ^{241}Am Buildup

Δk_∞	= -0.0134	(Theoretical Prediction)
	= -0.012 ± 0.002	(Inferred from Measured Reaction Rates Using Nuclei Density Corrections)

multiplication factor, k_∞, can be measured by a simple remeasurement of the amount of copper necessary to achieve null reactivity in the lattice. These measured values for Δk_∞ will have much smaller errors than the error associated with the absolute value for k_∞ in a single measurement. The number of contributing sources of uncertainty are considerably reduced when only the relative change in k_∞ is desired.

References

1. V. O. Uotinen. The Effect of ^{241}Pu Decay on the Analysis of Plutonium Critical Experiments, BNWL-SA-3157. Battelle-Northwest, Richland, Washington, March 1970, Submitted for publication in Nuclear Science and Engineering.

2. N. A. Hill. "PCTR Experiments," Plutonium Utilization Program Annual Report, Fiscal Year 1967, BNWL-624. pp. 3.22 - 3.31. Battelle-Northwest, Richland, Washington, January 1968.

3. D. R. Skeen and L. J, Page. THERMOS/BATTELLE, the Battelle Version of the THERMOS Code, BNWL-516. Battelle-Northwest, Richland, Washington, September 1967.

4. J. L. Carter, Jr. "Effective Cross Sections for Resonances in HRG," and "Computer Code Abstracts," Reactor Physics Quarterly Report, July, August, September, 1966, BNWL-340. Battelle-Northwest, Richland, Washington, October 1966.

5. J. R. Lilley. Computer Code HFN - Multigroup, Multiregion Neutron Diffusion Theory in One Space Dimension, HW-71545. General Electric Company, Richland, Washington, November 1961. Available from Clearinghouse for Federal Scientific and Technical Information, Springfield, Virginia.

6. E. P. Lippincott, C. R. Richey, and D. D. Lanning. "Definition of the Infinite Neutron Multiplication Factors Measured by the PCTR Poisoned and Unpoisoned Technique," Reactor Physics Quarterly Report, July, August, September 1969, BNWL-1240. Battelle-Northwest, Richland, Washington, November 1969.

MEASUREMENT OF k_∞ FOR A ThO_2-$^{233}UO_2$ HTGR LATTICE AT ROOM TEMPERATURE

E. P. Lippincott

As part of a program to measure the nuclear parameters of High Temperature Gas-Cooled Reactor (HTGR) lattices in the High Temperature Lattice Test Reactor (HTLTR), a lattice containing ^{233}U and thorium has been constructed. This lattice is the second of a series of planned HTGR experiments and is similar to the first lattice[1] except for the substitution of ^{233}U for the ^{235}U used previously. Measurements were made with the test lattice at room temperature in the Physical Constants Test Reactor (PCTR) prior to loading the lattice into the HTLTR. The PCTR was employed to allow greater flexibility in the measurement of small reactivity effects and to facilitate the foil irradiations necessary to evaluate cell absorptions.

Description of Test Lattice

The lattice was constructed of graphite fuel blocks 3.75 in. square by 24 in. long (Figure 3.2). Each block contains 25 fuel channels, 0.470 in. in diameter, on a 0.75 in. square pitch. The channels are filled with a fuel mixture containing ThO_2-$^{233}UO_2$ pyrocoated particles, ThO_2 powder, and graphite. Both ends of the channels are sealed with graphite end plugs 1/2 in. in length. The ThO_2-$^{233}UO_2$ particles were prepared by ORNL and are composed of a microsphere core about 300 μ in diameter containing one part $^{233}UO_2$ and three parts $^{232}ThO_2$. The pyrocarbon coating has a thickness of about 100 u.

Loading the fuel mixture into the graphite blocks was performed in a glove box. After blending the fuel mixture, it was loaded via a funnel into the fuel channels and vibrated to achieve good density and uniform loading. Each finished block

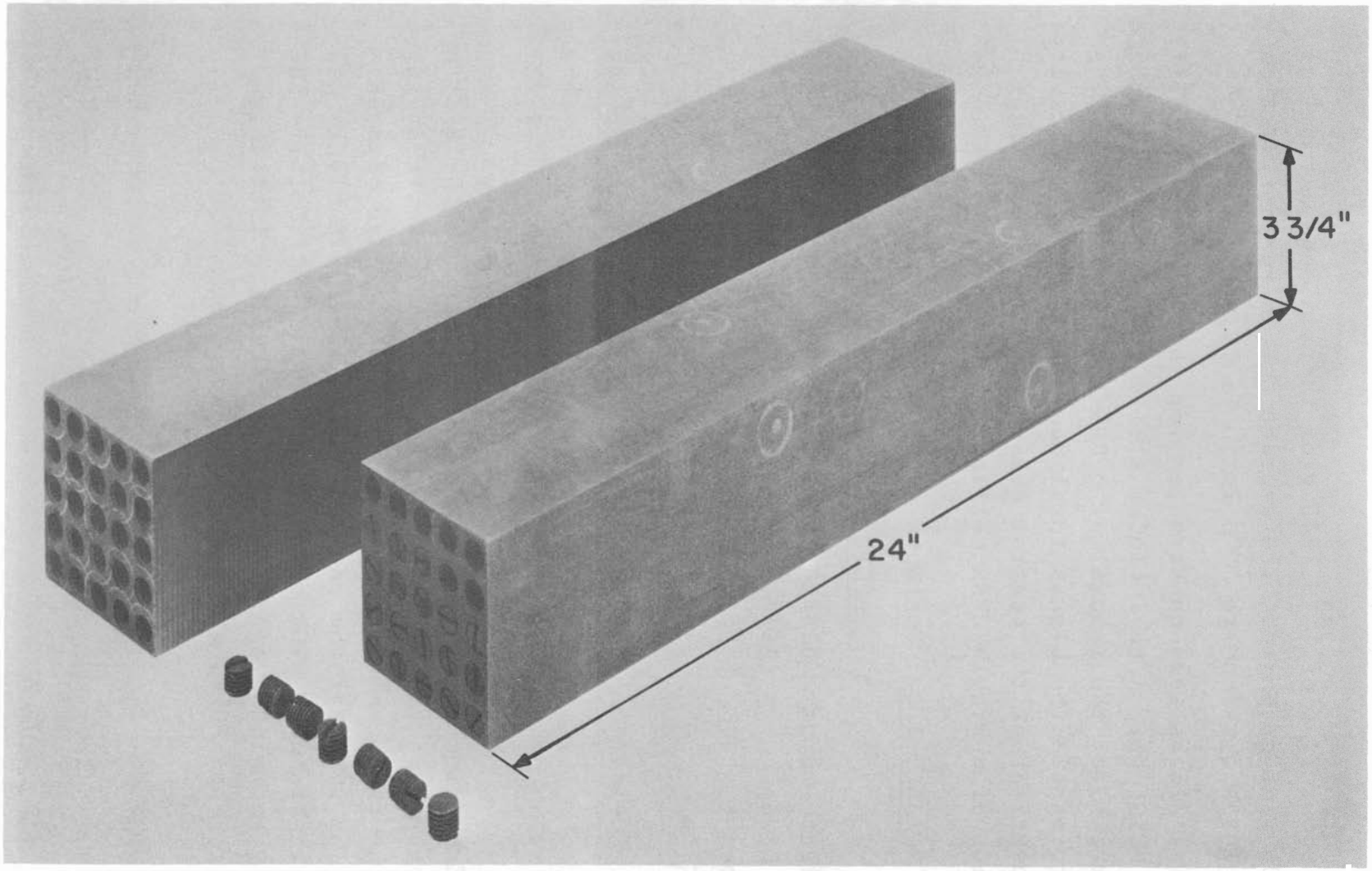

Neg 0680747-3

FIGURE 3.2. HTGR Fuel Elements

contains about 14 g of ^{233}U, 740 g of thorium, and a total of about 7800 g of graphite. The average carbon-to-thorium atom ratio is 205 and carbon-to-^{233}U ratio is 11,000.

Special blocks were constructed for the PCTR measurements. The four PCTR central cell blocks are identical to the standard blocks except for the removal of 0.005 in. of graphite on the outside to enable the blocks to slide in and out of the cavity. The compositions of the central cell blocks and the average composition of a single HTGR cell are given in Table 3.2.

TABLE 3.2. Contents of **HTGR** Fuel Blocks

	PCTR Central Blocks, g				Single Cell Mean, g
Block Weight - empty	6188.8	6299.2	6208.5	6428.2	251.25
Graphite Powder	1534.2	1527.7	1519.7	1514.	60.96
Pyro-carbon	54.1	53.8	53.6	53.4	2.15
Total carbon	7777.1	7880.7	7881.8	7995.6	314.35
^{232}Th	755.57	752.38	748.46	745.63	30.02
^{233}U	13.97	13.91	13.84	13.79	0.5551
Total U	14.32	14.26	14.19	14.14	0.5691
^{16}O	106.2	105.7	105.2	104.8	4.22

The fuel blocks were loaded in the PCTR in an 8 by 8 array. Special short blocks were constructed to fit at the front and rear of the four central cell blocks and the twelve adjacent blocks. The space at the ends of the remaining 48 blocks was filled with standard HTGR blocks laid across horizontally and vertically and with graphite bars. The complete lattice, as installed in the PCTR, is shown in Figure 3.3.

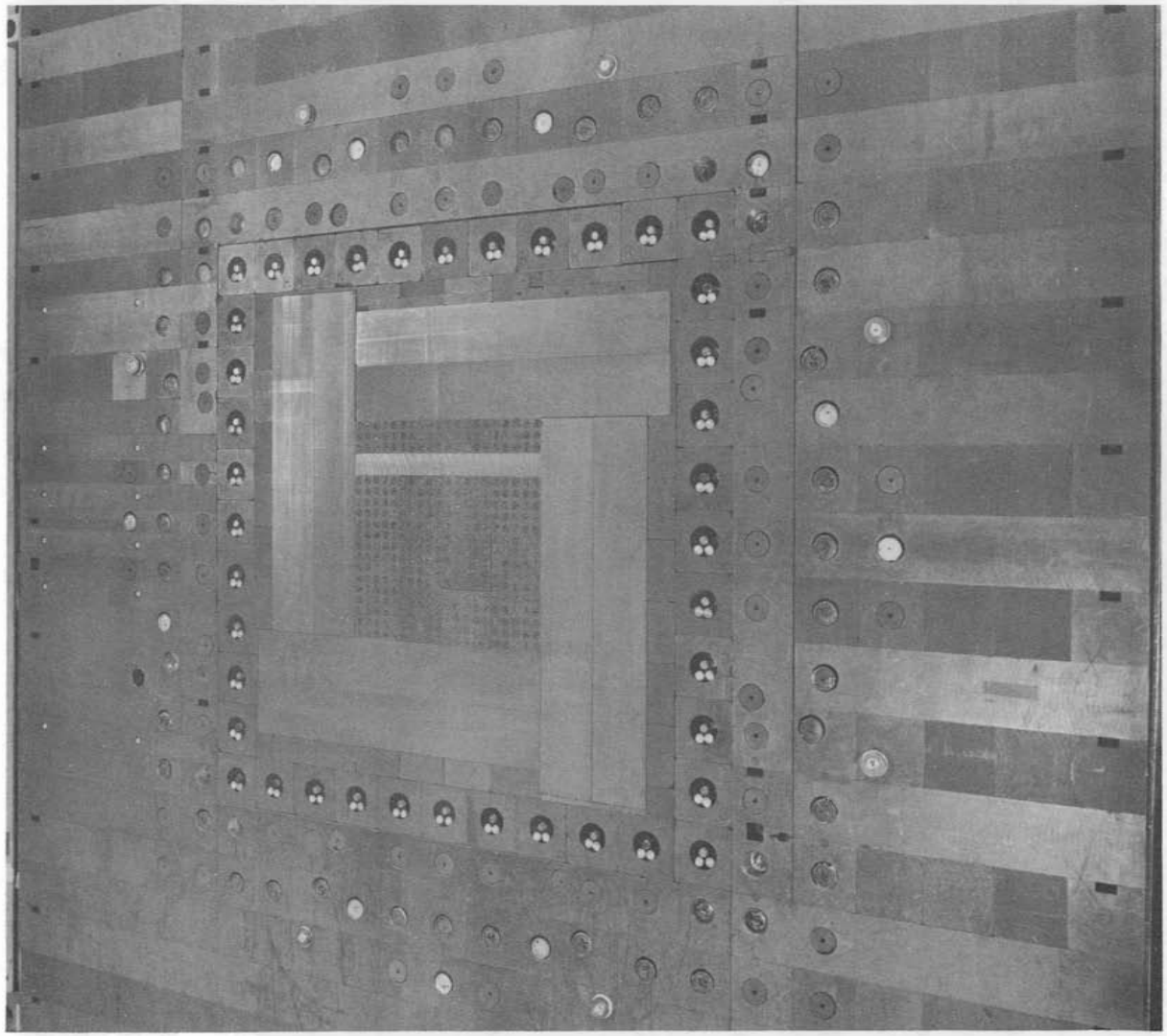

Neg 0691770-1

FIGURE 3.3. PCTR Loading-HTGR Lattice ThO_2-$^{233}UO_2$ HTGR Lattice in PCTR

Experimental Measurements

Measurements were made in the PCTR to determine k_∞ by both the unpoisoned technique[2] and the standard PCTR poisoned technique.[3] In addition to the foil irradiations and reactivity measurements required to determine k_∞, measurements of other reactivity effects were made to determine differences between blocks. These results will be used to better normalize the later experiments in the HTLTR. Relative reactivity measurements made in the final reactor configuration are summarized in Table 3.3. The quoted errors are estimated from the repeatability of the measurements on the HTGR lattice. From these measurements, the value of the mass of copper needed to reduce the central cell reactivity worth to zero was found to be 318.0 ± 2.2 g.

TABLE 3.3. Relative Reactivity Worths in the PCTR

	Unpoisoned Measurement
PCTR Central Cells	10.24 ± 0.044
Copper in void	0.0322 ± 0.0002¢/g
Graphite in void	0.795 ± 0.029¢/kg
HTLTR Central Cells	10.98 ± 0.064
PCTR end caps	1.74 ± 0.054
HTLTR end caps	2.10 ± 0.074

Gold cadmium ratio measurements were made to determine the flux match. The initial loading with a single natural uranium element in each position in the buffer region resulted in a slightly soft spectrum: the cadmium ratio increases with distance from the center of the reactor. An average over the central cell compared to two blocks further out was used as a criterion to determine the match. This criterion indicated a radial mismatch of 5.2%. The axial match was more difficult

to determine owing to theasymmetry created by the end caps. The flux peak in the end caps measured by a copper absorber was found to be about 8% greater than the flux at the center of the block. A comparison made between the cadmium ratio at the center of the block and that in the end buffers indicated that the flux was only about 0.4% harder in the end buffers, and this was considered a good match.

The addition of another natural uranium element and a copper jacketed mixed oxide element to each position in the buffer in order to harden the flux resulted in the flux being 0.3% harder radially and 0.7% harder axially, using the above criterion. A later irradiation was made with this loading to obtain improved data, and at this time the radial match was 0.7% harder and the axial 1.7% harder. The results listed in Table 3.3 are obtained from this latter measurement.

The foil irradiations to determine the cell absorptions and obtain cadmium ratio data were carried out using the special fuel block shown in Figure 3.4. This block had the fuel in two channels contained in removable aluminum cylinders between which foils could be inserted. Calculations have shown that the flux perturbations caused by these cylinders were negligible.[4] Special foils were constructed to fit in the fuel channels. Foils made of (1) copper metal, (2) thorium metal, and (3) foils containing a ^{233}U-thorium-graphite mixture identical to the fuel were used. The latter two foils were used to evaluate the absorptions in ^{233}U and thorium. The copper foils were used to integrate the flux over the cell and evaluate the absorptions in the other cell components.

Following the unpoisoned measurements, the test lattice was poisoned by placing strips of copper, 0.005 in. thick, on

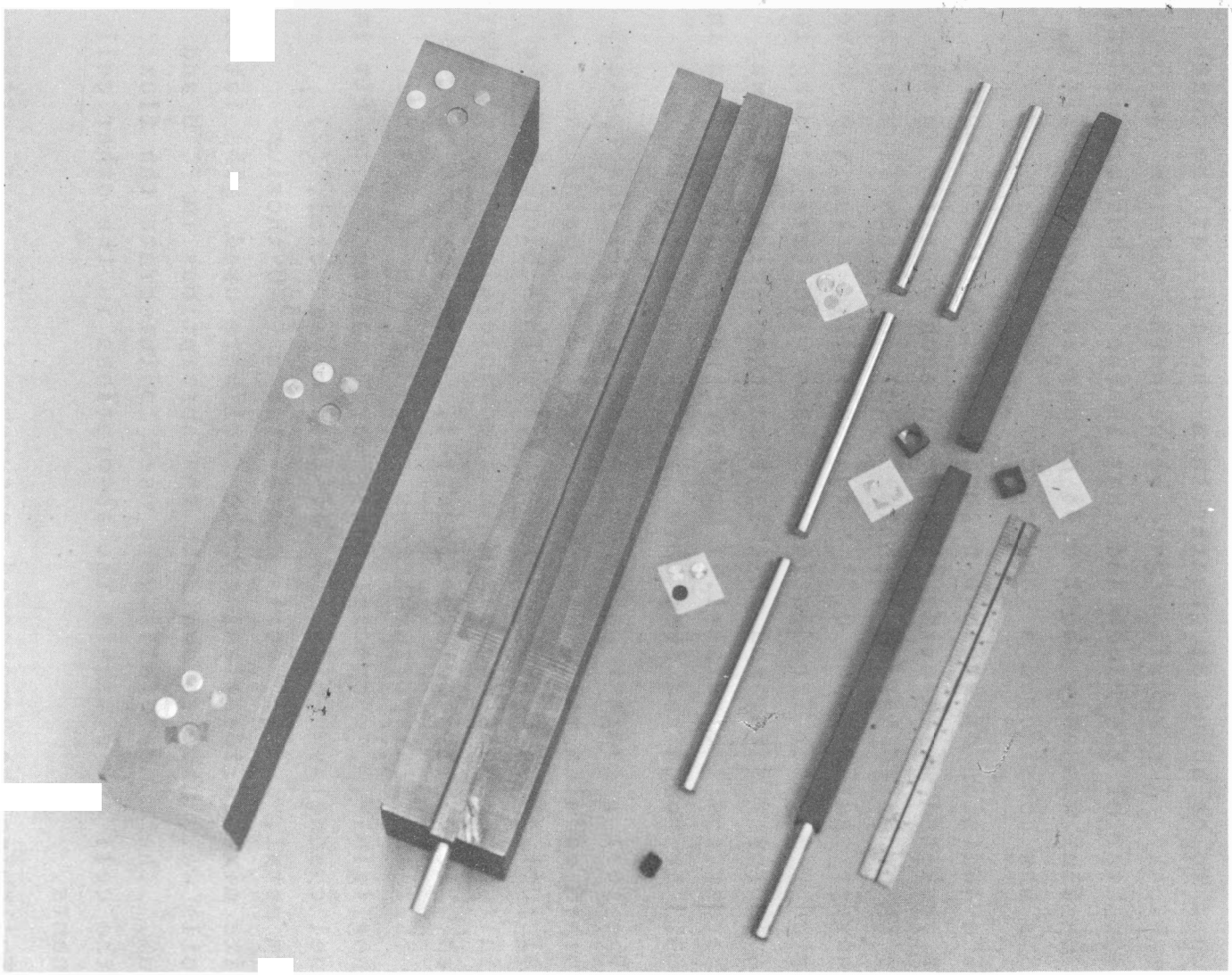

Neg0691770-3

FIGURE 3.4. Special HTGR Fuel Blocks Used in Foil Irradiation

the edge of each block (408.9 g on the central four blocks). The mass of copper required to reduce the reactivity worth of the central cell to zero was found to be -92.3 g in this case, for a net copper mass of 316.6 g. This result is in good agreement with the 318 g determined during the unpoisoned measurements.

Evaluation of k_∞

The reactivity worth of the block end caps was subtracted from the total cell reactivity, and this value of the cell worth, together with the copper worth from Table 3.3 and absorptions in the central cell and copper evaluated using foil measurements, were used to calculate k,. The value of k_∞ was found using the two-group expression:[5]

$$k_\infty = 1 - \left(\frac{\Delta\rho^{cell}}{\Delta\rho^{cu}}\right) \frac{(\Sigma\phi V)_2^{Cu}}{(\Sigma\phi V)_2^{cell}} + \frac{(\phi_1^{+}\Sigma_1\phi_1)^{Cu}}{(\phi_2'\Sigma_2\phi_2)}$$

$$-\frac{(1+\tau B^2)\ (1+L^2B^2)\ (1-p)\ L^2B^2}{1 + (1-p)\ L^2B^2} + \frac{\tau B^2\ (1+L^2B^2)\ \left[\tau B^2 - n_1 f_1\ (1-p)\right]}{1 + \tau B^2 - \eta_1 f_1\ (1-p)}$$

The k, defined in this expression is for fluxes in the fundamental mode (a bare critical system). The formula expresses k_∞ - 1 as a sum of a main term involving experimental quantities (except for the correction for epithermal absorption in copper), and two correction terms which are evaluated using calculated quantities. Evaluation of this formula results in a k, equal to 1.058 for the lattice with the worth of the graphite on the cell ends subtracted. The first correction term contributes -0.0066 to k_∞ and the second -0.0048 for an overall correction of -0.011.

The evaluation of k_∞ by the poisoned technique is similar to the above. In this case, the second correction term will be replaced by a different correction term which is primarily dependent on the change in relative thermal neutron absorptions in the moderator with the copper present. Since the foil analysis is not yet complete, this term has not been fully evaluated. However, this correction will have the same sign as the correction term determined for the unpoisoned case above. The values of k_∞ determined by the two techniques are in good agreement, if this latter correction term is neglected.

Calculations of k_∞ were made for comparison with experiment using GRANIT,[6] a modification of THERMOS[7] which includes effects of particle sizes in the fuel, and EGGNIT,[8] for the epithermal effects. These codes also supplied the calculation of the correction terms in the above evaluation of k_∞. These calculations result in a theoretical k_∞ of 1.046.

Several factors can contribute to the above difference. Some small corrections to the foil activation measurements and renormalization of the fission foils may result in a change of 1 or 2 milli-k. Adequately accounting for the effect of the end caps may result in a larger correction to the experimental cell worth than was used in these evaluations.

Other Results

By removing singly each of the four central cell blocks from the reactor, the variation among the blocks was measured. This variation was found to be 4.7%. After correcting for the difference in graphite weight among the blocks, this difference was reduced to 2.4%, which is about the limit of error of the measurement. Thus, an uncertainty of less than this magnitude would be expected in $k_\infty - 1$ from this source.

Evaluation of k_∞ and foil measurements permits the calculation of a spectrum-averaged value of η using the expression:

$$\frac{1}{\hat{\eta}^{233}} = \frac{1}{k_\infty} + \frac{1}{(\nu\Sigma_f)^{233}} \left[\left(\frac{\nu^{232}}{k_\infty} - 1 \right) \Sigma_f^{232} - \Sigma_c^{232} - \Sigma_a^{cell} \right]$$

where Σ_a^{cell} includes all cell absorptions other than in ^{232}Th or ^{233}U. A preliminary value of $\bar{\eta}^{233}$ has been found to be 2.25 ± 0.13. The rather large uncertainty results mainly from uncertainties in the foil data and will be reduced when a more thorough analysis of these data is completed. This uncertainty is much larger than the uncertainty in k_∞ because resonance captures in ^{232}Th have to be accurately evaluated. The end effect problem that affects k_∞ also affects the value of $\hat{\eta}^{233}$ determined by this method.

References

1. *E. P. Lippincott. "HTLTR Measurements on HTGR Lattice," Reactor Physics Department Technical Activities Quarterly Report, April, May, June, 1968, BNWL-887. p. 372. August 1968.*

2. *R. E. Heineman. "On the Interpretation of Reactivity Measurements of Reactor Media," Trans. Am. Nucl. Soc., vol. 8, p. 532. 1965.*

3. *D. J. Donahue, et al. "Determination of k_∞ from Critical Experiments with the PCTR," Nucl. Sci. Eng., vol. 4, p. 297. 1958.*

4. *G. E. Hansen, private communication.*

5. *E. P. Lippincott, et al. "Definition of the Infinite Neutron Multiplication Factors measured by the PCTR Poisoned and Unpoisoned Technique," Reactor Physics Quarterly Report, July, August, September 1969, BNWL-1240, pp. 2.3. Battelle-Northwest, Richland, Washington, November 1969.*

6. *C. L. Bennett, private communication.*

7. H. C. Honeck. THERMOS, A Thermalized Transport Theory Code for Reactor Lattice Calculations, BNL-5826. Brookhaven National Laboratory, September 1961.

8. C. R. Richey. EGGIVIT: A Multigroup Cross Section Code, BNWL-1203. Battelle-Northwest, Richland, Washington, November 1969.

INITIAL HTLTR MEASUREMENTS WITH HTGR LATTICE

T. J. Oakes

The first measurements over the temperature range 25 to 1000 °C have been completed in the High Temperature Lattice Test Reactor (HTLTR). In addition to obtaining the desired experimental data, a number of administrative and operational problems that were resolved should lead to more efficient use of the facility in future experimental programs. The first lattice investigated is designated as the High Temperature Gas-cooled Reactor #1 (HTGR-1) and has been described in an earlier quarterly report.[1] In brief, the test lattice consists of a $^{235}UC_2$-ThO_2-C fuel mixture contained in graphite fuel blocks. Each fuel block consists of a 3-3/4 × 3-3/4 × 24 in. block of graphite containing twenty-five 0.470 in. diameter fuel holes equally spaced in a 5 × 5 array of 3/4 in. pitch. The holes are filled with a mixture of graphite particles, ThO_2 particles, and pyrolytic carbon coated fully-enriched UC_2 spheres. The amounts of the fuel components are adjusted to give a nominal C/Th ratio of 200 and a nominal C/^{235}U ratio of 6000.

Initially, the reactor was loaded with the HTGR test lattice and a driver fuel/temperature shim configuration such that measurements were conducted up to 300 °C. The overall reactor temperature coefficient was increasingly negative at this point and, above this temperature, the available excess

reactivity was insufficient to allow further reactivity measurements. Subsequently, the reactor fuel configuration was changed and some moveable poison/fuel rods[2] were added to the reactor perimeter to permit the addition of reactivity at higher temperatures. Following this modification, measurements were performed at 550, 700, and 1000 °C.

At each temperature the measurements consisted of determining the relative worth of: a 4-block HTGR central cell, a single HTGR block, a single HTGR block with V_2O_3 replacing the ThO_2 in the fuel mix, a standard absorber (Cu), and single blocks containing absorbing materials of interest (Rh, HfO_2, Sm_2O_3). Following the completion of the reactivity versus temperature measurements, the reactor was returned to room temperature and a set of foil irradiations were conducted to determine absorption rates in the various cell components.

The foil activation data together with the room temperature reactivity data will be used to deduce k_∞^* via the unpoisoned technique.[3] The expression to be used for this purpose is as follows:

$$k_\infty^* = 1 - \left(\frac{\Delta\rho^{cell}}{\Delta\rho^{cu}}\right) \frac{(\Sigma_{a_2}\phi_2 V)^{abs}}{(\Sigma_{a_2}\phi_2 V)^{cell}} \left\{1 + \left[\frac{\phi_1^+}{\phi_2^+}\right] \frac{(\Sigma_{a_1}\phi_1)^{abs}}{(\Sigma_{a_2}\phi_2)^{abs}}\right\} \quad (1)$$

$$+ f(B^4) + g\,(\Delta\phi, \Delta\phi^+)$$

where $f(B^4)$ and $g\,(\Delta\phi, \Delta\phi^+)$ are correction terms for leakage and flux mismatch.

The variation of $\frac{\Delta\rho^{cell}}{\Delta\rho^{abs}}$ as a function of temperature is shown in Figure 3.5. Since $k_\infty^* \simeq 1 - \left(\frac{\Delta\rho^{cell}}{\Delta\rho^{abs}}\right)$, it is apparent that these HTLTR measurements provide a determination of $k_\infty^*(T)$.

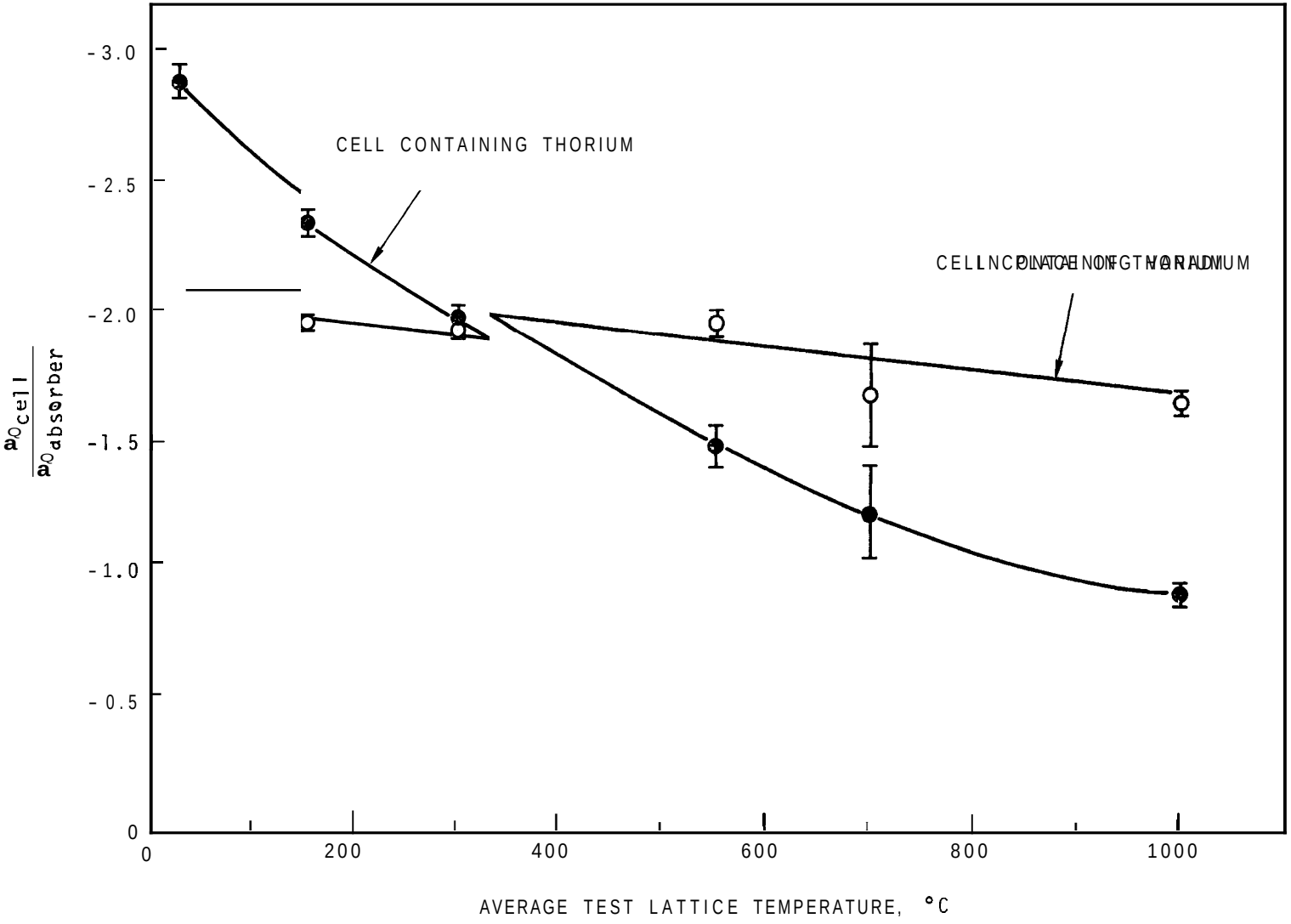

FIGURE 3.5. **Measured Ratios of Cell Reactivity Worth to Absorber Reactivity Worth for a Lattice Cell with and Without Thorium Resonance Capture**

L-1381-1

Also shown on Figure 3.5 is $\frac{\Delta\rho^{u/v}}{\Delta\rho^{abs}}$ versus T for HTGR-1. The quantity ($\Delta\rho^{u/v}$) is the reactivity worth of a single HTGR block with V_2O_3 replacing ThO_2. The ratio $\frac{\Delta\rho^{u/v}}{\Delta\rho^{abs}}$ is used in an expression similar to (1) above to infer k_∞^* (T) for this lattice with the thorium resonance capture removed and the l/v thorium captures simulated by vanadium. The doppler coefficient for the ThO_2 in the HTGR fuel assembly can be obtained from the difference between k_∞^*(T) with and without the thorium resonance capture.(4)

Analysis of the foil activation data is in progress. These data, when used in Equation (1), will provide the absolute normalizations needed to translate the reactivity ratios of Figure 3.5 into values of k_∞^*(T), with and without thorium resonance capture.

References

1. F. P. Lippincott. Reactor Physics Department Technical Activities QuarterZy Report, April, May, June 1968, BNWL-887, p. 3.72. Battelle-Northwest, RichZand, Washington, November 1968.

2. J. G. Holt. Reactor Physics QuarterZy Report, October, November, December 1969, BNWL-1304, p. 3.15. Battelle-Northwest, RichZand, Washington, February 1970.

3. E. P. Lippincott, C. R. Richey, and D. D. Lanning. Reactor Physics QuarterZy Report, July, August, September 1969, BNWL-1240, p. 2.3. Battelle-Northwest, RichZand, Washington, November 1969.

4. C. R. Richey. Reactor Physics Department Technical Activities QuarterZy Report, April, May, June 1967, BNWL-534, p. 3.19. Battelle-Northwest, RichZand, Washington, January 1968.

CRITICAL EXPERIMENTS IN UO_2-2 wt% PuO_2 FUELED-H_2O MODERATED ASSEMBLIES

W. P. Stinson

Critical experiments were conducted in the Plutonium Recycle Critical Facility (PRCF) to obtain data for verifying the accuracy of neutronic design methods. The fuel rods contained UO_2-2 wt% PuO_2 with 8% ^{240}Pu[1] and the moderator was H_2O. The core consisted of the fuel (1/2 in. diameter rods) in a 1.06 in. square lattice pitch loaded to form a cylinder 36 in. in height and a radius equivalent to 150 fuel rods when critical. The measurements conducted on this core were:

- Critical size
- Kinetic parameters (β/ℓ)
- Flux distributions
- Void coefficient
- Approach-to-critical.

Approach-to-critical data were taken as a check on the techniques used in similar type measurements made in the Critical Approach Facility (CAF). The critical loading inferred from the subcritical approach was 150.1 ± 0.03 rods which agrees well with the actual critical loading of 150.1 ± 0.05 rods.

The kinetics measurements were made by recording and analyzing the reactor noise. The preliminary value of β/ℓ obtained is 76 ± 3 sec^{-1}. The flux distribution was measured by scanning the fuel rods for fission product decay gamma rays. Empty thin wall aluminum tubes were placed in interstitial positions in the central part of the core to obtain data from which the void coefficient can be determined. Analysis of the data is continuing to obtain final values.

Reference

1. L. C. Schmid et al. "Fuel Description," Reactor Physics Data for the Utilization of Plutonium in Thermal Reactors, BNWL-801, p. A2. Battelle-Northwest, Richland, Washington, May 1968.

4.0 FAST REACTORS

CALCULATIONAL COMPARISON OF FAST NEUTRON CAVITY AND FULL SIZE FAST CRITICAL ASSEMBLY EXPERIMENTS

D. F. Newman

Continuing studies of the possible application of the Physical Constants Testing Reactor (PCTR) and the High Temperature Lattice Test Reactor (HTLTR) to fast reactor neutronics experiments have shown the feasibility of Liquid Metal Fast Breeder Reactor (LMFBR) and Gas Cooled Fast Breeder Reactor (GCFBR) lattice measurements in these facilities. A large Fast Neutron Cavity (FNC) assembly in the central region of the test reactor, surrounding a small fast reactor lattice zone, provides the neutronic coupling between the fast and thermal reactor zones.[1] Current studies have been directed toward understanding the neutron spectrum buffering requirements for a small fast reactor lattice zone in the FNC. The results of one-dimensional spherical transport theory calculations have shown that the neutron spectrum and the reaction rates in the central 3.6 liters of a 150 liter fast reactor lattice zone in the FNC duplicates the environment in a fast reactor critical assembly to within a few percent.

GCFBR Lattice Application

The dilute Gas Cooled Fast Breeder Reactor (GCFBR) lattice studied (U/Pu = 7.10) is typical of the central 900 liter zone of the 330 MW, GCFBR demonstration plant proposed by Gulf General Atomic.[2,3] A bare sphere of this GCFBR lattice has a critical volume of 3600 liters, while the GCFBR zone in the FNC requires less than 4.3% of this volume.

Calculations were performed for a GCFBR lattice zone in the PCTR-FNC at room temperature and for a full-size, fast critical assembly of the GCFBR lattice (U/Pu = 7.10). A one-dimensional diffusion theory code, 1DX,[4] was used for

generating effective nuclear cross sections, using data in the 26-group Russian format. These cross sections were employed in the multigroup transport theory code, DTF-IV,[5] using isotropic scattering and S-4 approximations for the reactor calculations. The comparison of the neutron spectrum at the center of the GCFBR lattice in the PCTR-FNC relative to the center of the GCFBR full sized critical assembly is shown in Figure 4.1. The results illustrate the neutron spectrum adjustment, at neutron energies less than 10 keV, that can be obtained by varying the thickness of a natural boron liner in the FNC.

This liner has little effect on the neutron spectrum at higher energies. The comparison of the ^{239}Pu fission rate at the center of the GCFBR lattice zone installed in the PCTR-FNC with that present in the full-size GCFBR critical lattice, illustrated in Figure 4.2, shows excellent agreement. A similar comparison for the ^{238}U absorption rate at the center of the GCFBR lattice, shown in Figure 4.3, is also in excellent agreement. If one calculates the infinite lattice multiplication factor, k_∞^*, for the GCFBR array in the FNC and for a bare critical sphere of a GCFBR, the agreement is very good.

$$k_\infty^* = \frac{\text{Total production}}{\text{Total absorption}} = \frac{\sum_{i=1}^{26} (\nu\Sigma_f\phi)i}{\sum_{i=1}^{26} (\Sigma_a\phi)i} = \begin{cases} 1.3636 \text{ critical} \\ \\ 1.3648 \text{ FNC} \end{cases}$$

These results indicate that precise integral neutronics experiments can be performed on this GCFBR lattice in the PCTR and HTLTR facilities at large cost savings for fuel, when compared with full-size critical assemblies.

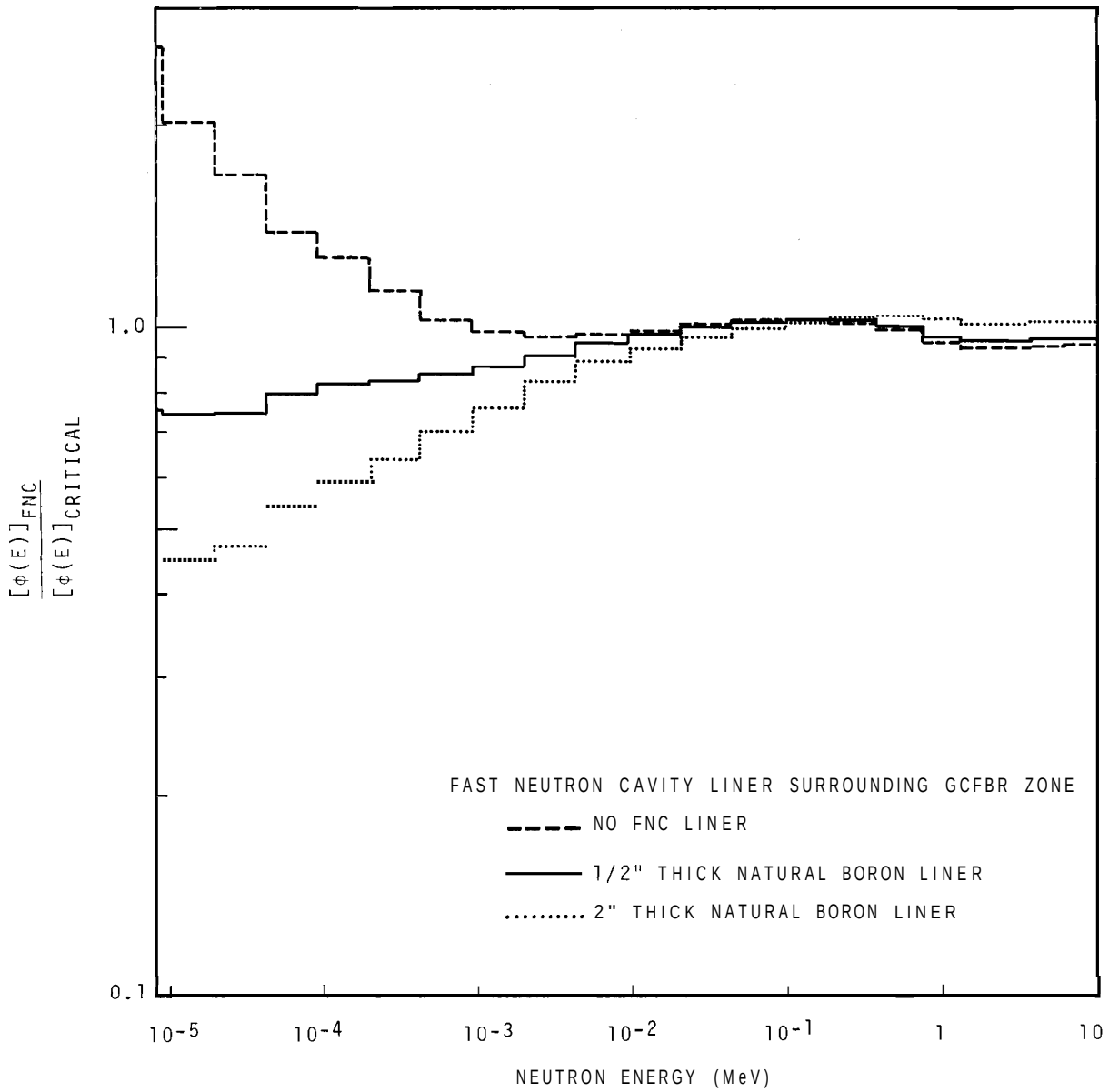

FIGURE 4.1. Comparison of Neutron Spectra at the Center of the GCFBR Lattice in the PCTR/FNC, Relative to a Bare Critical Assembly

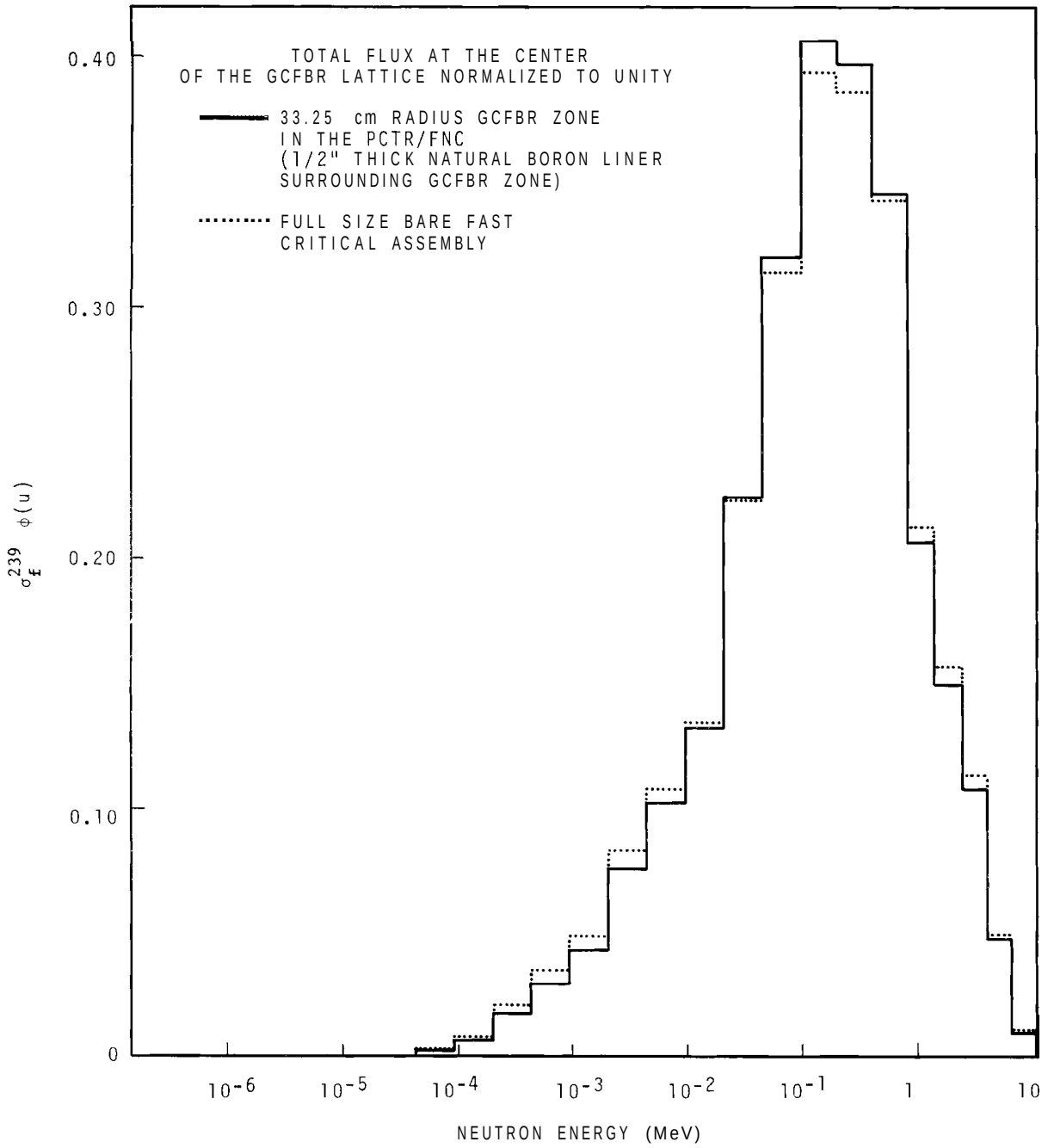

FIGURE 4.2. Comparison of ^{239}Pu Fission Rates at the Center of the GCFBR Lattice in the PCTR/FNC, and in a Bare Critical Assembly

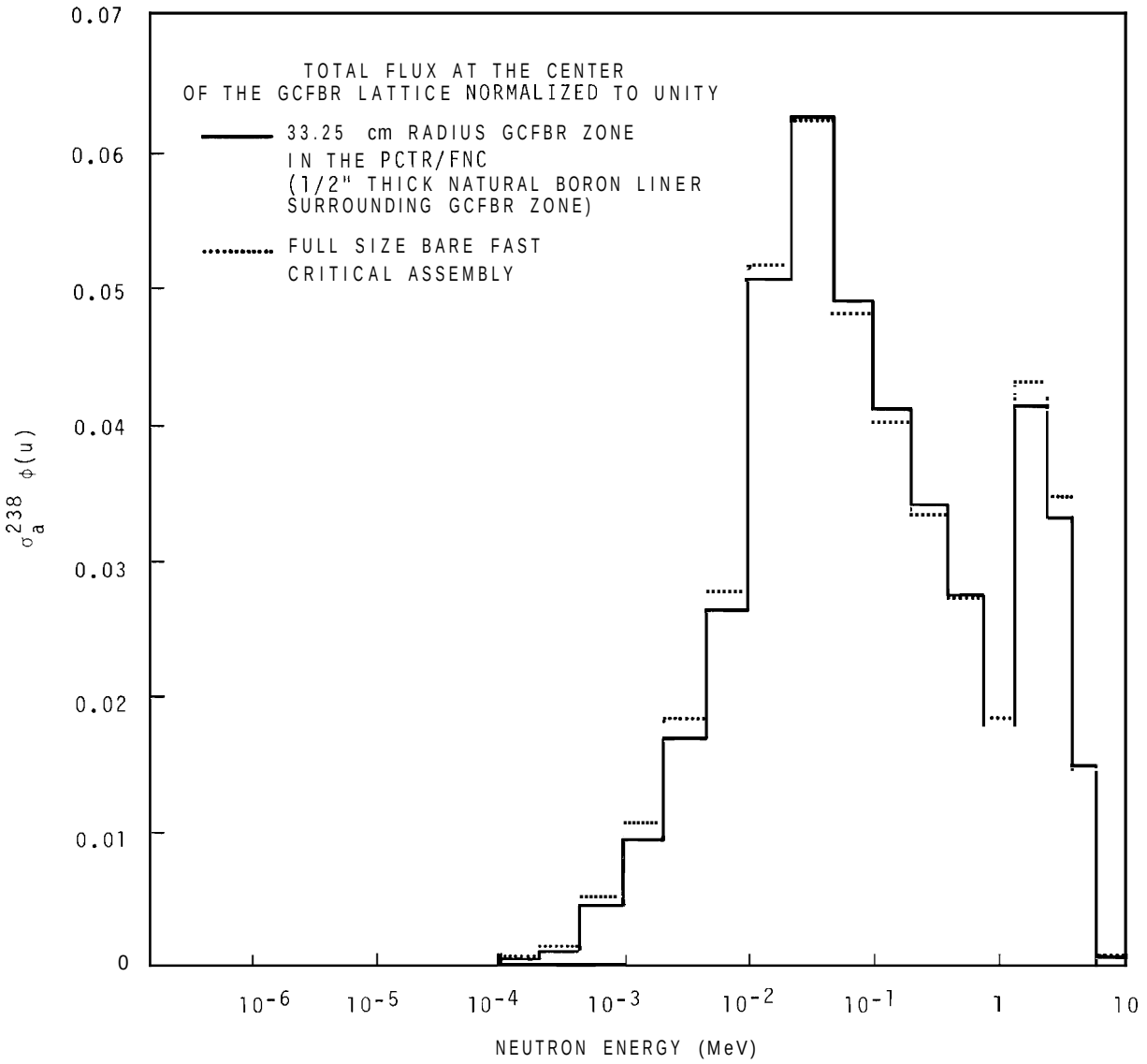

FIGURE 4.3. Comparison of ^{238}U Absorption Rates at the Center of the GCFBR Lattice in the PCTR/FNC, and in a Bare Critical Assembly

LMFBR Lattice Application

Calculational comparisons between PCTR-FNC zone loading and full-size critical assembly experiments, similar to those discussed for the GCFBR lattice, were made for a LMFBR lattice. The LMFBR lattice chosen for this study is the FTR driver fuel lattice, consisting of $U(Nat)O_2$-25 wt% PuO_2 fuel pins[6] with 316 stainless steel clad and structural support, in sodium coolant at room temperature. Neutron spectra at the center of (1) a full-size critical assembly of FTR driver fuel, and (2) a 107 liter zone of FTR driver fuel in the center of the PCTR-FNC, are compared in Figure 4.4. The neutron spectra are matched within a few percent at all neutron energies of interest ($4 \times 10^{-6} \leq E \leq 10$ MeV). At the center of the FTR driver lattice, reaction rate contributions are negligible for neutrons with energies less than 4 eV. Since the multigroup cross sections for the FTR driver fuel lattice are identical in both calculations, the energy dependent neutron spectral mismatch, shown in Figure 4, is directly proportional to the mismatch in the energy dependent reaction rates for all cell constituents. The infinite lattice multiplication factor, k_∞^*, at the center of the FTR driver fuel zone in the PCTR-FNC was matched within 2% of the value calculated at the center of a full-size critical assembly of the same fuel. Adjustment of the neutron spectrum in the PCTR-FNC by varying the thickness of a natural boron liner in the FNC, as illustrated for the GCFBR lattice zone in Figure 4.1, can reduce the difference in k_∞^* comparisons to a few milli-k.

Experiments Considered Feasible in a Fast Neutron Cavity

The ability to adjust the neutron energy spectrum in a small test zone of a fast reactor lattice constructed in a fast neutron cavity so that the equilibrium spectrum in the test zone duplicates that of a full-size critical assembly

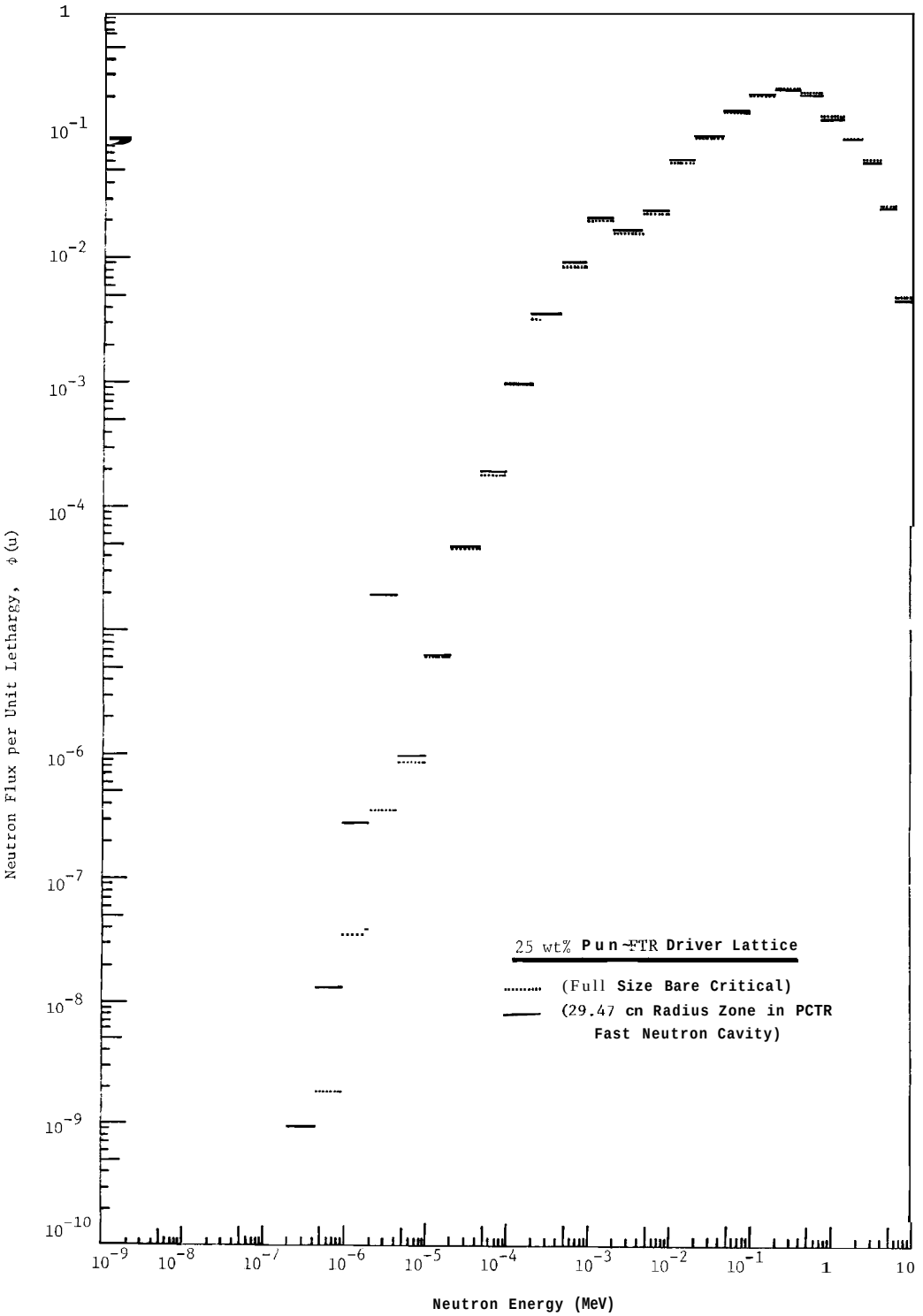

FIGURE 4.4. Calculated Comparison of Neutron Spectra at the Center of the FTR Driver Lattice in a Bare Critical Assembly and in the PCTR/FNC.

forms the basis for zoned fast reactor experiments. Calculational comparisons have shown that the equilibrium neutron spectrum in the critical assembly can be duplicated in small fast reactor lattice zones containing 70 to 80 kg of plutonium, which represents a savings of an order of magnitude in cost for fuel when compared with full-size critical assemblies. A list of experiments considered feasible in a fast neutron cavity is presented in Table 4.1. This list is not necessarily complete, but is only intended to be indicative of the rather broad range of investigations that could be carried out in such a facility.

References

1. D. F. Newman. "Fast Reactor Experiments in the PCTR," Reactor Physics Quarterly Report, October, November, December 1969, BNWL-1304, pp. 4.1 - 4.10. Battelle-Northwest, Richland, Washington, February 1970.

2. C. Maeder, J. Peak, J. Tschirky. "Reactivity Insertions in GCFR Cores Simulating Hypothetical Severe Accidents," Trans. Am. Nuc. Soc., vol. 12, p. 826. 1969.

3. A. Baxter, C. Maeder. "Effects of Data Uncertainties on as-cooled Fast Reactor Stability," Trans. Am. Nuc. Soc., vol. 12, p. 914. 1969.

4. R. W. Hardie and W. W. Little, Jr. 1DX, A One-dimensional Diffusion Code for Generating Effective Nuclear Cross Sections, BNWL-954. Battelle-Northwest, Richland, Washington, March 1969.

5. K. D. Lathrop. DTF-IV, A FORTRAN-IV Program for Solving the Multigroup Transport Equation with Anisotropic Scattering, LA-3373. Los Alamos Scientific Laboratory, Los Alamos, New Mexico, 1965.

6. C. L. Brown and C. A. Rogers, "Criticality Experiments with 25 wt% PuO_2 - $U(Nat)O_2$ Fuel Pins in Water," Reactor Physics Quarterly Report, October, November, December 1969, BNWL-1304, pp. 4.11 - 4.14. Battelle-Northwest, Richland Washington, February 1970.

TABLE 4.1. Experiments Considered Feasible in a Fast Neutron Cavity

I. Neutron reaction rates in the equilibrium spectrum of a fast breeder reactor core.

- A. Foil activation ratios
- B. "Fission detector ratios
- C. Neutron spectrum averaged cross sections
- D. $\bar{\eta}$ and $\bar{\alpha}$ for ^{239}Pu from neutron balance
- E. Detailed neutron spectrum measurements (between 300 eV and 2 MeV) using proton-recoil detectors.
- F. Neutron spectrum (spanning neutron energies from thermal to 18 MeV) using multiple foil activation method.

II. Normalized reactivity coefficients in the equilibrium spectrum

- A. Sample worths relative to boron, lithium, and other materials.
- B. Central void effects and moderator coefficients
- C. Reactivity coefficient of expansion
- D. Leakage independent temperature coefficient
- E. Doppler coefficient (25 to 1000 °C)

} Entire test core at uniform temperature in HTLTR-FNC

III. Heterogeneity Effects

- A. Detailed spatial variation in unit cell reaction rates using foil activation.
- B. Reactivity effects of heterogeneity for central cells of same composition
  1. Homogenous central cell
  2. Platelet geometry
  3. Rodded fuel geometry
- C. Control rod effectiveness (change in k_∞^* of the core material at equilibrium)
- D. Local control rod flux perturbation measurements

IV. Fuel or test assembly perturbations

- A. Flux and spectrum perturbations
- B. Change in k_∞^* from the equilibrium spectrum condition.

NEUTRONIC CALCULATIONS FOR FAST REACTOR FUEL TRANSIENT TESTS

U. P. Jenquin

Two highly enriched mixed oxide fuels will undergo transient tests in the Transient Reactor Test Facility (TREAT) [1] to evaluate the performance characteristics of Fast Test Reactor prototypic fuel pins. Neutronic calculations were done to determine the expected physics characteristics of the EBR-II/TREAT[2] and GETR/TREAT[3] experiments during irradiation. The power distribution in the test pins was calculated so that the regions of fuel melting could be determined during various transients. Interactions between the test assembly and the reactor have also been investigated.

Although TREAT is a thermal reactor, a significant portion of the power in the test pin is due to fissions induced by nonthermal neutrons. The test fuels are highly enriched, so the thermal neutron flux is depressed a great deal relative to the thermal neutron flux in the TREAT fuel. Thus, the ratio of nonthermal-to-thermal power becomes appreciable. Since the power distribution due to the nonthermal fissions is nearly constant, the total power distribution is much flatter than the thermal power distribution. The effect of nonthermal power on the total power distribution becomes more pronounced as fuel enrichment is increased.

The EBR-II/TREAT pins contain UO_2-25 wt% PuO_2 fuel with 93% ^{235}U. The GETR/TREAT pins contain UO_2-25 wt% PuO_2 fuel with natural uranium. A detailed description of the test pins is given in Table 4.2. The test pins are contained in an inner capsule for the transient irradiation. These capsules consist of metallic containment and thermal dam annuli which are separated from each other by NaK. The inner capsule assembly containing the test pin is then inserted in the TREAT capsule which replaces the center fuel element in the TREAT reactor.

TABLE 4.2. Description of Test Pins

Parameter	EBR-II/TREAT	GETR/TREAT
Fuel OD, in.	0.212	0.212
Clad ID, in.	0.218	0.218
Clad OD, in.	0.250	0.250
Active Length, in.	13.5	31.0
Fuel Density (93% of TD), g/cm^3	10.316	10.316
% ^{235}U in uranium	93.1	0.72
wt% PuO_2 in UO_2-PuO_2	25.0	25.0
% ^{239}Pu in plutonium	88.3	86.75
% ^{240}Pu in plutonium	10.3	11.53
% ^{241}Pu in plutonium	1.3	1.54
% ^{242}Pu in plutonium	0.1	0.13

The THERMOS/BATTELLE code[4] was used to calculate the radial thermal flux and power distribution in the test fuel. Since graphite is the primary neutron moderator, an appreciable portion of the TREAT reactor had to be included in the THERMOS calculation. Cross sections were obtained for five annuli in the test fuel. The HRG code[5] was used to calculate epithermal cross sections. The slowing down spectrum in the test pin is characteristic of TREAT fuel; therefore the broad group cross sections for the test fuels, test capsules, and TREAT capsule were calculated using the fine group slowing down spectrum of the TREAT fuel. The broad group energy boundaries were selected to be 10 MeV, 11.7 keV, 130 eV, 22.6 eV, 2.38 eV, and 0.683 eV.

The six group region average cross sections were used in a one-dimensional transport theory calculation of the complete system with DTF-IV[6] in order to normalize the epithermal to thermal flux ratio. The DTF-IV calculations were done with first order anisotropic scattering and an S_4 angular quadrature

set. The core loading was assumed to be a nominal 225 fuel elements with a graphite reflector.

The spectrum effect of the EBR-II/TREAT experiment is shown in Figure 4.5. In the TREAT fuel the maximum flux occurs at 0.035 eV. Near the edge of the EBR-II/TREAT fuel the spectrum peaks at 0.055 eV while further in the fuel the spectrum peaks at 0.075 eV. The effect of the ^{239}Pu resonance at 0.3 eV becomes more pronounced further in the fuel. The relative values among the curves indicate the spatial effects on the neutron flux.

A radial calculation was done with DTF-IV for the whole reactor with the EBR-II/TREAT assembly in the center of the reactor. Thermal and resonance energy flux distributions are shown in Figure 4.6 for the TREAT reactor with and without the assembly in it. The effect of the assembly on the thermal flux extends quite far into the TREAT fuel. The test fuel and capsules decrease the core reactivity by 2.7% $\Delta k/k$ relative to a standard TREAT fuel element.

The power distribution in the EBR-II/TREAT fuel is shown in Figure 4.7 along with the contributions of thermal and nonthermal neutron induced fissions. Considering only thermal neutron induced fissions, the surface-to-center ratio of power densities is about 13. However, thermal neutron induced fissions account for less than 30% of the power in the center of the fuel. Thus when nonthermal neutron induced fissions are also included, the power distribution is somewhat flatter. The surface-to-center ratio of power densities is 4.2, which will give acceptable results for the transient experiments.

Calculations for the GETR/TREAT experiment were done in a manner similar to the EBR-II/TREAT calculations. The power distributions in the GETR/TREAT fuel are shown in Figure 4.8. Since there is less fissionable material in this fuel than in

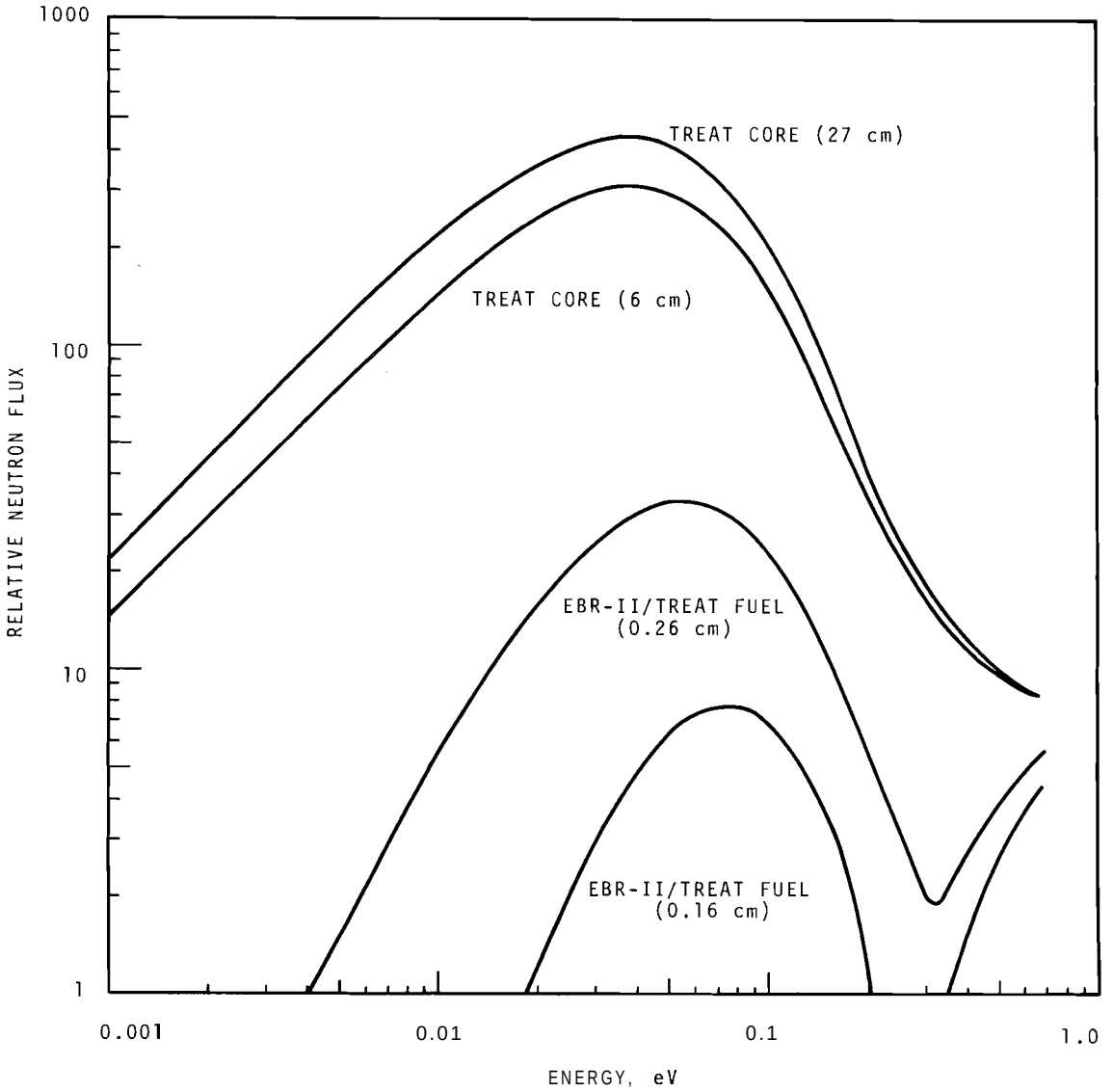

Neg 0695437-5

FIGURE 4.5. Effect of EBR-II/TREAT Experiment on Thermal Neutron Spectrum

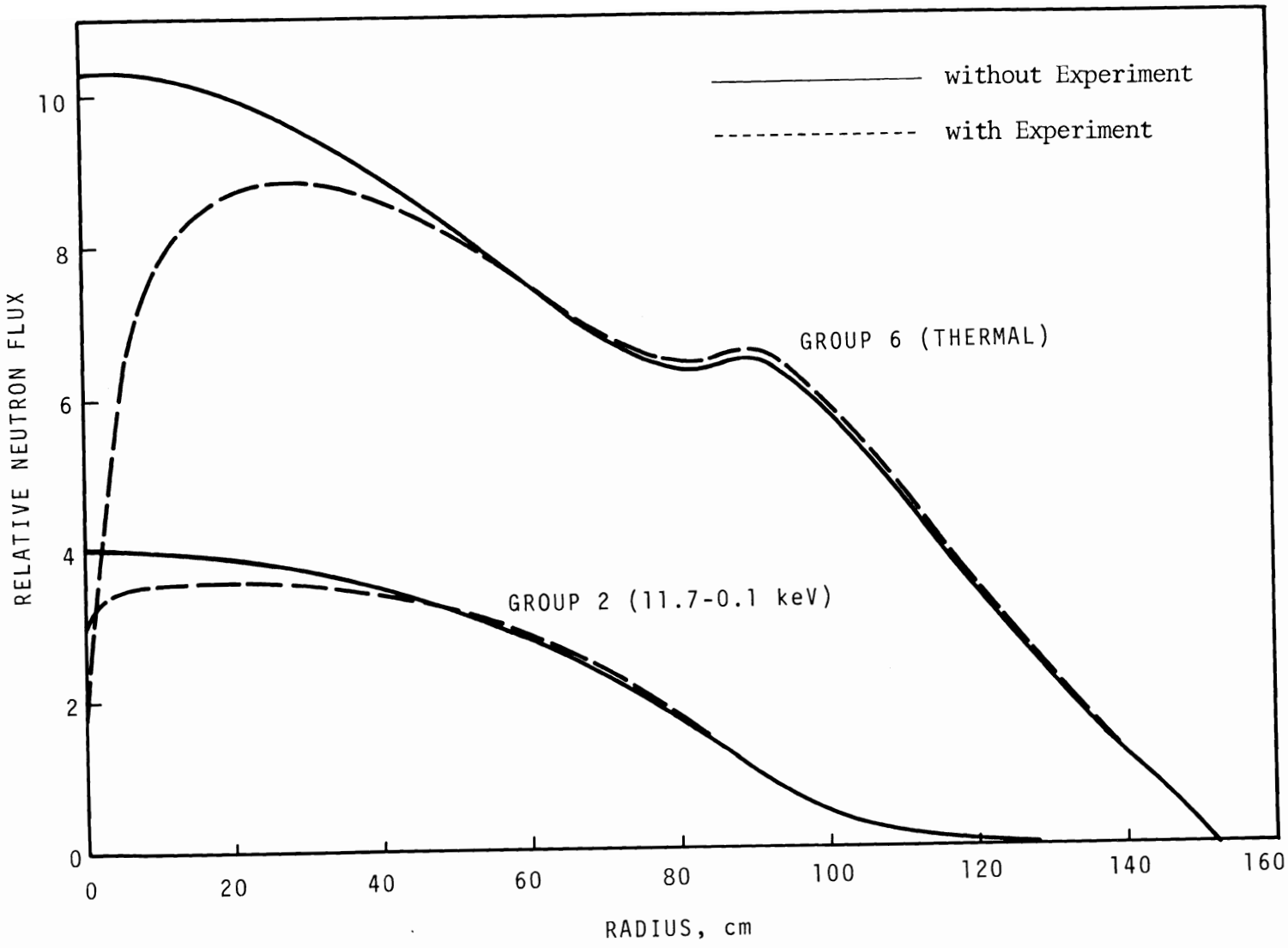

Neg 0695437-1

FIGURE 4.6. Effect of EBR-II/TREAT Experiment on Radial Flux Distributions in TREAT

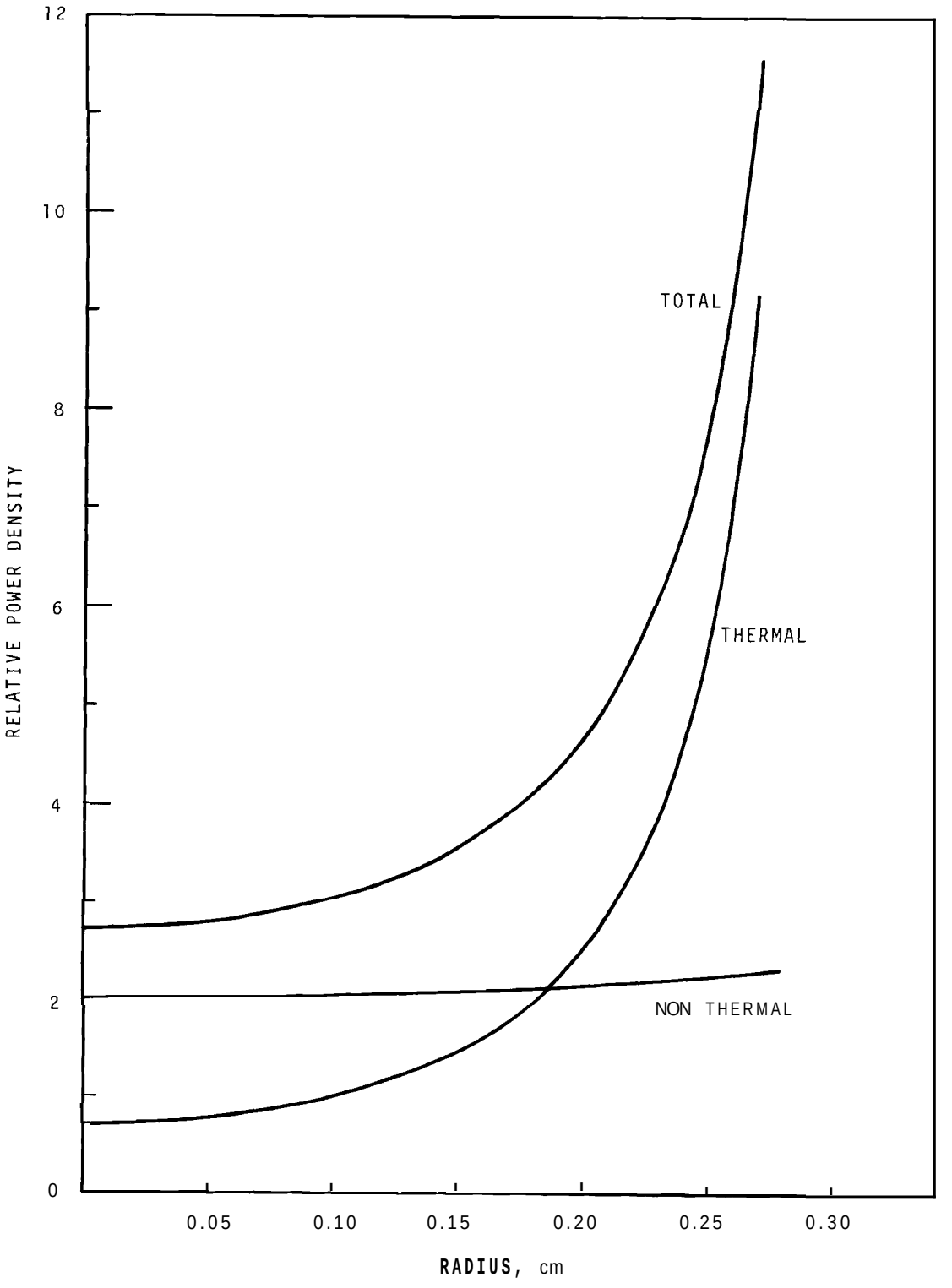

Neg 0695437-2

FIGURE 4.7. Power Distribution in EBR-II/TREAT Fuel

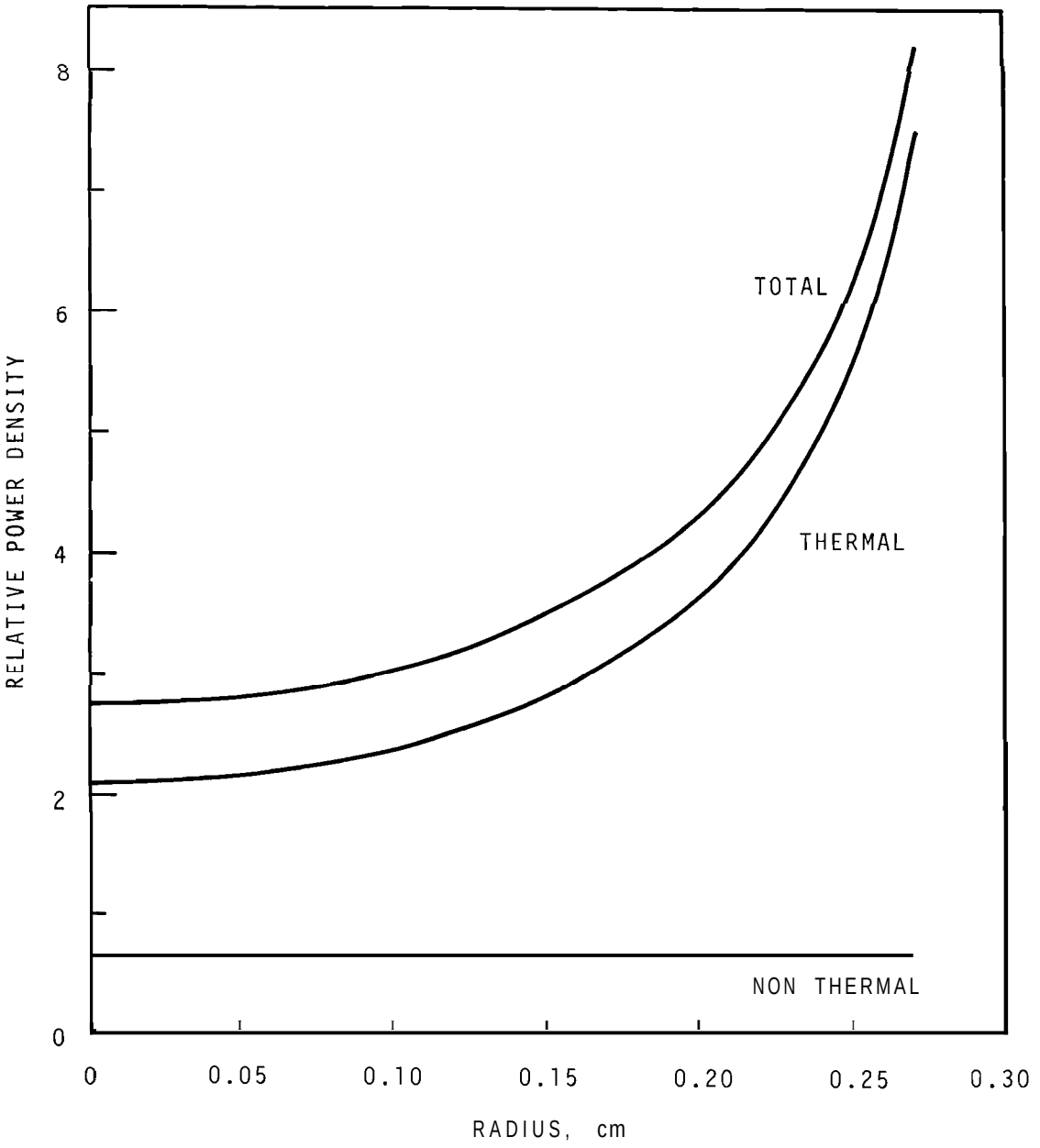

Neg 0695437-3

FIGURE 4.8. **Power Distribution in GETR/TREAT Fuel**

the EBR-II/TREAT fuel, the value of the nonthermal power distribution is much less. In addition, a greater percentage of the thermal neutrons reach the center of the fuel so that the surface-to-center ratio of power densities is 3.0, which is acceptable for the transient experiments.

Transient experiments will also be performed with these fuels after they have received a significant amount of exposure. The EBR-II/TREAT fuel was irradiated in the EBR-II reactor, so the burnup across the fuel will be nearly uniform. Therefore, the effects of burnup were estimated with hand calculations assuming an average exposure of 50,000 MWd/MTM. To obtain 50,000 MWd/MTM exposure, about 5.1% of the heavy atoms must fission. Since the uranium is fully enriched (93% ^{235}U) and 90% of the plutonium is fissionable material, then only 5.6% of the fissionable atoms must fission and the conversion of ^{238}U to ^{239}Pu and ^{240}Pu to ^{241}Pu can be neglected. Assuming an average capture-to-fission ratio of 0.5 for ^{235}U, ^{239}Pu, and ^{241}Pu, the fissionable atom concentration is decreased by about 8.4%. This gives a uniform decrease of 8.4% in the nonthermal power density. Comparing the previously calculated surface-to-center power densities for the unirradiated EBR-II/TREAT and GETR/TREAT fuels, a uniform decrease in fissionable atom concentration of 8.4% reduces the surface-to-center power densities by about 15% with the surface power density decreasing by about 7% and the center power density increasing about 8%. Combining the effect of both the thermal and nonthermal power distributions, the total power density in the center of the fuel remains constant while the total power density at the surface of the fuel is reduced by about 7%. Thus the surface-to-center ratio of power densities in the irradiated EBR-II/TREAT fuel is 3.9, and the average power density is reduced about 3%.

The GETR/TREAT fuel was irradiated in the GETR reactor up to exposures of 70,000 MWd/MTM. Since nearly all of the fissions had been induced by thermal neutrons, the exposure is not uniform across the fuel rod. The fuel received the most exposure near the cladding, so the concentration of fissionable isotopes decreases the most near the cladding and the power distribution in the fuel becomes flatter. Isotopic compositions in the fuel were obtained from burnup calculations[7] done for similar fuel irradiated in the MTR reflector which is almost identical to the GETR. THERMOS calculations were done for average exposures of 18,000 and 69,000 MWd/MTM. Comparing the previous DTF-IV results with the two types of unirradiated test fuel indicates that the fluxes in the TREAT fuel are insensitive to the type of test fuel. Therefore, these THERMOS results were normalized to the DTF-IV calculation with unirradiated GETR/TREAT fuel.

The nonthermal power density of the irradiated GETR/TREAT fuel was calculated by adjusting the results for unirradiated fuel to account for the change in isotopic concentrations of the fissile atoms. The total power distribution in the GETR/TREAT fuel as a function of exposure is shown in Figure 4.9. The surface-to-center ratio of power densities is 2.1 at 18,000 MWd/MTM. At 69,000 MWd/MTM the power distribution is nearly flat. The curves for irradiated fuel extend to a larger radius because the fuel has expanded into the gap between the clad and the initial pellet. The void in the center of the fuel is also noticeable.

From the results of DTF-IV and THERMOS calculations, the ratio of average power density in the test fuel to the total power in TREAT can be calculated. The quantities obtained from these codes incorporate radial effects only, so an axial peak-to-average power factor was included because the test pins are somewhat shorter than the TREAT elements. Since the

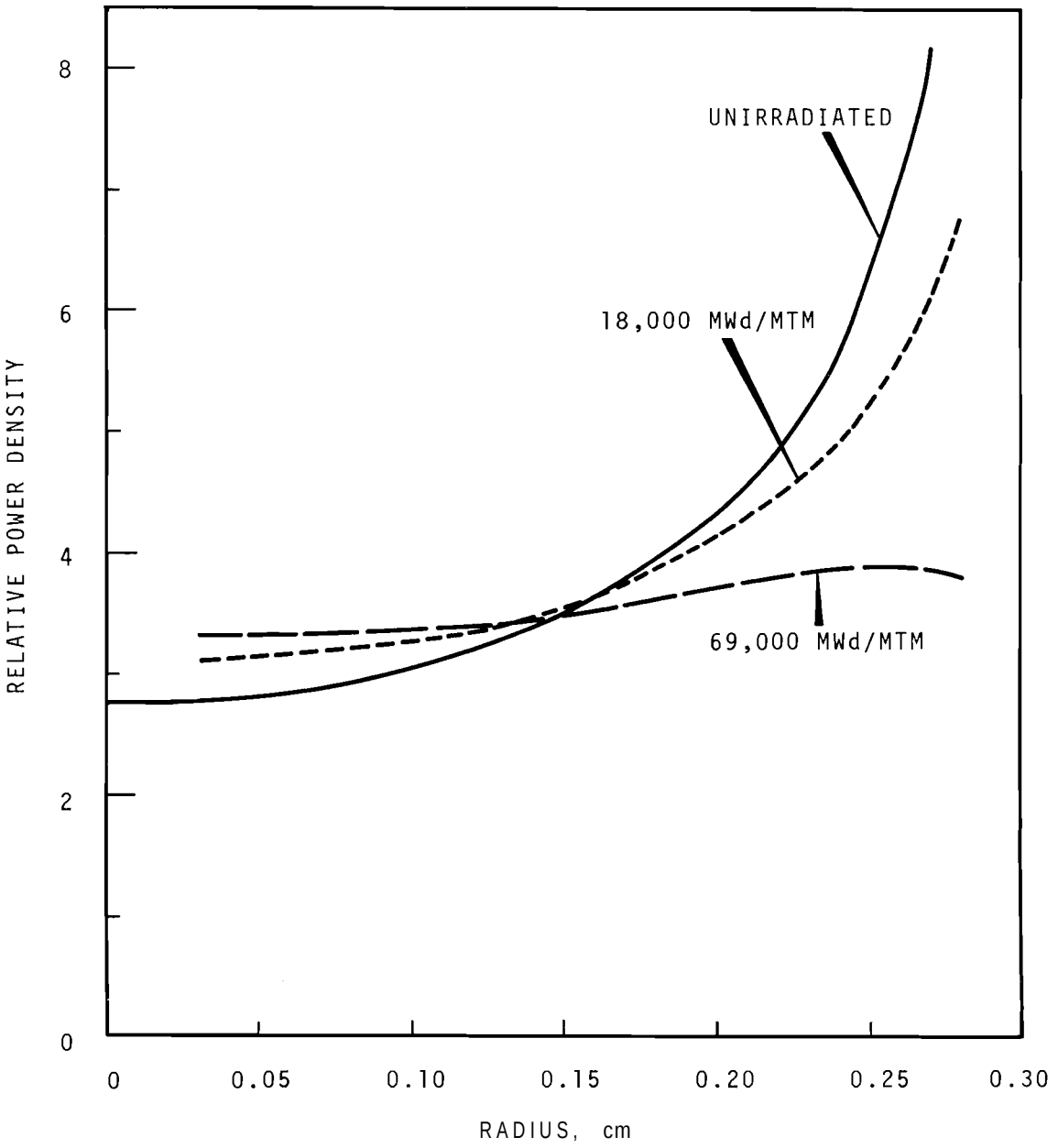

Neg 0695437-4

FIGURE 4.9. **Power Distribution in GETR/TREAT Fuel as a Function of Exposure**

EBR-II/TREAT fuel is only 13-1/2 in. long, the axial peak-to-average power factor of the TREAT core (1.19) was used. The GETR/TREAT fuel is 31 in. long, so a peak-to-average power factor of 1.12 was assumed. The ratio of average power density in the EBR-II/TREAT fuel to the total TREAT power is 0.98 $\times 10^{-4}$ which compares very favorably with the measured calibration of 1.00 $\times 10^{-4}$.[8] As indicated earlier, the calculated ratio at 50,000 MWd/MTM would be reduced by about 3% to 0.95 $\times 10^{-4}$. The ratio of average power density in the GETR/TREAT fuel to the total TREAT power is 0.81 $\times 10^{-4}$ for unirradiated fuel which agrees reasonably well with the measured calibration of 0.90 $\times 10^{-4}$.[8] At 18,000 MWd/MTM the calculated ratio is 0.77 $\times 10^{-4}$ and at 69,000 MWd/MTM the ratio is 0.65 $\times 10^{-4}$.

The measured calibrations of the average power density in the test fuel to the total TREAT power were done with a loading of 206 standard elements and 12 slotted elements. Since the calculations were done with nominal loading of 225 standard elements, the calculated ratio of powers should be about 5% lower than the measured ratio of powers. Heterogeneity effects due to the slotted elements and the control rods might also affect the ratio slightly.

From a reactivity standpoint the EBR-II/TREAT experiment is worth -2.7% $\Delta k/k$ relative to a standard TREAT fuel element. The negative worth is due to the capsules surrounding the test fuel. The capsules contain a large amount of neutron absorbing material. The GETR/TREAT experiment is worth -2.5% $\Delta k/k$ relative to a standard TREAT fuel element. From a hazards evaluation standpoint it is necessary to know the effect of test fuel relocation on the core reactivity. If the EBR-II/TREAT fuel is uniformly homogenized with the EBR-II/TREAT capsule, the core reactivity is increased by 0.4% $\Delta k/k$. This is one of the most reactive situations

imaginable. If the test fuel slumps to the bottom of the reactor, the effect will be a negative worth because the fuel is in a position of lower worth and it is in a lump so that the self shielding is greater. If the GETR/TREAT fuel is uniformly homogenized with the GETR/TREAT capsule, the core reactivity is increased by 0.1% $\Delta k/k$.

References

1. D. R. MacFarlane. Design Summary Report on the Transient Reactor Test Facility (TREAT), ANL-6034. Argonne National Laboratory, Argonne, Illinois, June 1960.

2. J. E. Hanson. Experiment Description and Hazards Evaluation for the PNL Mixed Oxide Irradiation in EBR-11, Task A, Subtask 1, Irradiations, BNWL-650. Battelle-Northwest, RichZand, Washington, July 1968.

3. T. B. Burley and J. E. Hanson. Unpublished Data. Battelle-Northwest, Richland, Washington, May 1967. [Communication: Experiment Description for Pacific Northwest Laboratories Mixed Oxide (UO_2-PuO_2) Irradiations in the General Electric Test Reactor.]

4. D. R. Skeen and L. J. Page. THERMOS/BATTELLE: The Battelle Version of the THERMOS Code, BNWL-516. Battelle-Northwest, RichZand, Washington, September 1967.

5. J. L. Carter. "Computer Code Abstracts, Computer Code - HRG," Reactor Physics Department Technical Activities Quarterly Report, July, August, September 1966, BNWL-340. Battelle-Northwest, RichZand, Washington, October 1966.

6. K. D. Lathrop. DTF-IV, a FORTRAN-IV Program for Solving the Multigroup Transport Equation with Anisotropic Scatter-&, LA-3373. Los Alamos Scientific Laboratory, November 1965.

7. U. P. Jenquin. Unpublished Data. Battelle-Northwest, RichZand, Washington, March 1970. (Communication: Burnup Calculations for BNWL Capsules.)

8. G. E. Culley. UnpubZished Data. Battelle-Northwest, RichZand, Washington, March 1970. (Personal Communication)

A NEW COMPUTATIONAL SYSTEM FOR FAST REACTOR ACCIDENT INVESTIGATION

A. E. WALTAR

Major fast reactor excursion calculations are characteristically laden with numerous parametric studies due to uncertainties in the state of the reactor during the traumatic conditions hypothesized. An improvement over earlier methods[1,2] has been developed which permits elimination of a substantial degree of arbitrariness in the range of parametrics by providing a consistent basis for establishing the reactivity ramp rate, effective Doppler coefficient, and appropriate equation of state during the disassembly process.

Basically, the method consists of a coupling of the multichannel neutronics-heat transfer computer program, MELT-II,[3] with the two-dimensional disassembly computer program, VENUS.[4] The MELT-I1 phase includes feedback effects due to Doppler broadening, sodium voiding, and fuel relocation whereas the VENUS phase includes Doppler broadening and the reactivity feedback due to core disassembly. The accident sequence is followed in MELT-I1 until fuel temperatures are elevated to the point where sizable disassembly pressures are attained. At this time the fine structure temperature information is volume-averaged over the R-Z spatial mesh structure used in VENUS and this input, along with the power distribution and all reactivity feedback components, is used directly as the starting point for the disassembly phase in VENUS. In addition, the core is scanned for liquid sodium content to determine the effective Doppler coefficient and to establish whether a sodium-in or a sodium-out equation of state should be employed at each particular VENUS mesh point.

An example of the type of problem which can be treated by this coupled system is the highly asymmetric situation arising by passing a large sodium bubble through the core. The

particular example presented is based on a 162 liter bubble passing through an FTR-like core (radius about 60 cm, height about 90 cm). Reactivity, power response, and energy yield resulting from upward movement of the bubble through the lower reflector and into the core are illustrated in Figure 4.10. Disassembly conditions are established when the center of the bubble reaches approximately the lower third of the reactor. The ramp rate is nearly 80$/sec and the effective Doppler coefficient has dropped from an initial value of -0.005 to approximately -0.0038. The amount of energy contained in the molten fuel at the end of the nuclear excursion is calculated to be 1120 MW-sec.

Tight coupling between the predisassembly and disassembly phase is essential to provide a realistic appraisal in energy release -- particularly for an accident of this type because of the core inhomogeneity (variation of sodium content) involved. For example, if analysis of the above accident is attempted using only a disassembly code, parametrics including a range of ramp rates from 50 to 100$/sec, Doppler coefficients from -0.003 to -0.005, and equations of state varying from essentially full sodium-in to full sodium-out are necessary to bound the problem. Such calculations have been performed and the energy contained in molten fuel ranges from 181 to 2407 MW-sec.

The author is indebted to Dr. William T. Sha, Argonne National Laboratory, for his keen interest and collaboration in this study.

References

1. D. E. Simpson, J. W. Hagan, A. E. Waltar, R. A. Harris, A. Padilla, and G. L. Fox. Preliminary Analysis of Postulated Maximum Accidents for the FFTF, BNWL-760. Battelle-Northwest, Richland, Washington, November 1968.

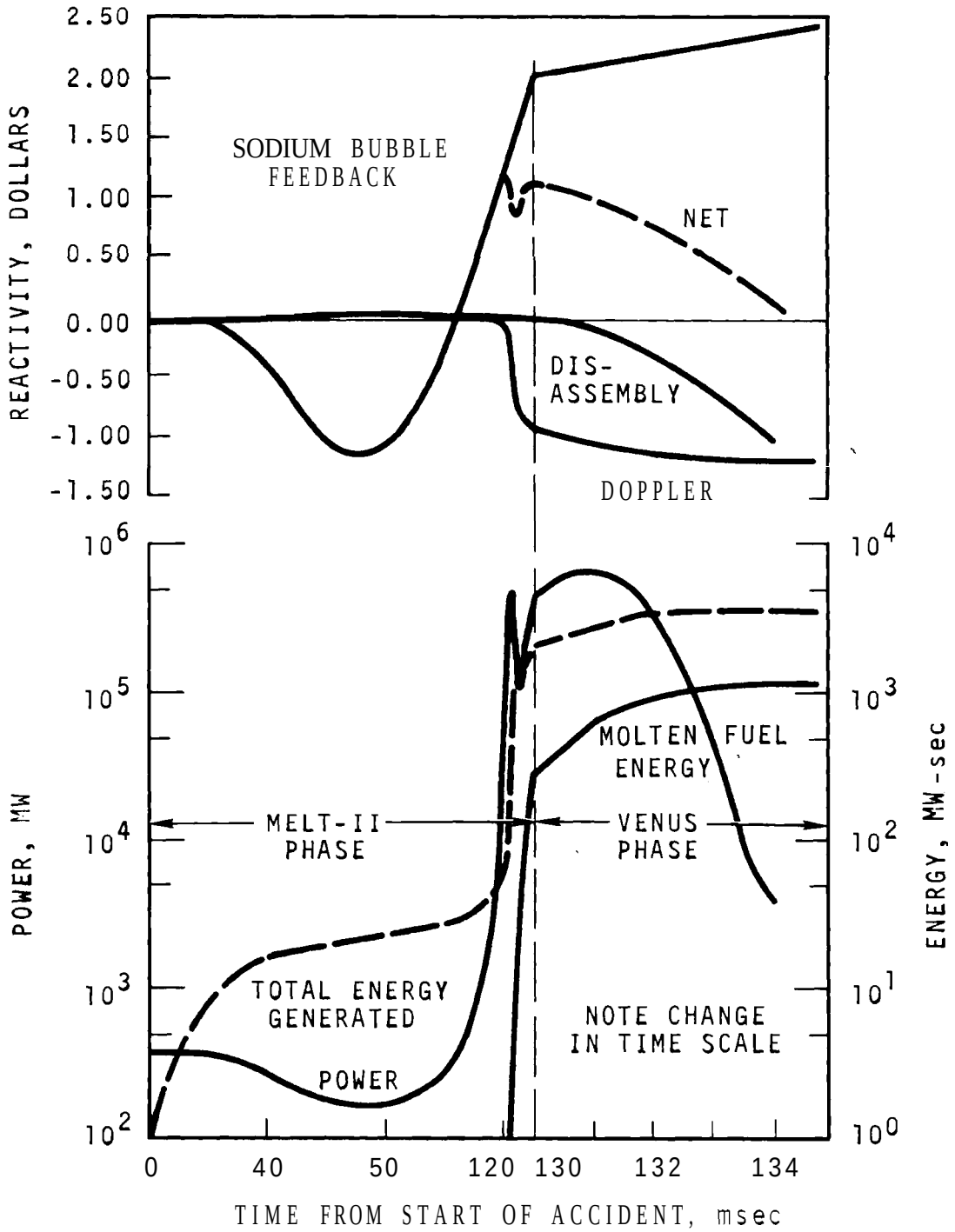

FIGURE 4.10. Transient Response for a Large Sodium Bubble Passing Through a Fast Reactor Core

2. D. R. MacFarlane, N. A. McNeal, T. J. Heames, W. T. Sha, and C. K. Youngdahl. "Reactivity Transients Leading to Disassembly in Oxide-Fueled Fast Reactors," Trans. Am. Nucl. Soc., vol. 12, p. 342. 1969.

3. A. E. Waltar, Andrew Padilla, Jr., and Richard J. Shields. MELT-11, A Two-Dimensional Neutronics-Heat Transfer Code for Fast Reactor Safety Analysis, BNWL-1320. Battelle-Northwest, Richland, Washington, to be published.

4. W. T. Sha and T. H. Hughes. VENUS - Two Dimensional Neutronic-Hydrodynamic Fast Reactor Power Excursion Computer Program, Argonne National Laboratory, to be published.

ON THE TREATMENT OF SPATIAL FEEDBACK EFFECTS IN FAST REACTOR ACCIDENT ANALYSES

A. E. Walter and W. W. Little, Jr.

Numerous papers[1-3] that have recently appeared point out the need for using a space-time kinetics package when analyzing fast reactor transients. Although the desirability of such techniques cannot be argued in an absolute sense, they introduce some very practical limitations in terms of both programming and computation time -- particularly for 2 or 3 dimensional computations. The purpose of this work is to emphasize that the discrepancy between lumped parameter and space dependent models is frequently caused by differences in the important feedback terms, and that these differences can be greatly reduced by using a lumped nuclear model coupled with a space dependent feedback model.

An example of an attempt to account for spatial feedback effects and yet retain the simplicity and speed associated with point kinetics is the treatment of Doppler feedback in the MELT-I1 code.[4] Assuming $T\frac{dk}{dT}$ remains constant over the temperature range of interest for an oxide fueled core, Doppler feedback is computed according to the following expression:

$$k_{Doppler} = \begin{cases} \dfrac{K_D \sum_{i,j} W(i,j)\, V(i,j) \ln \dfrac{T(i,j)}{T_o(i,j)}}{\text{TOTAL FUEL VOLUME}} & \text{for } T_o \le T \le T_1, \\[2ex] A + \dfrac{K_D \sum_{i,j} F\, W(i,j)\, V(i,j) \ln \dfrac{T(i,j)}{T_1(i,j)}}{\text{TOTAL FUEL VOLUME}} & \text{for } T_1 < T \end{cases} \qquad (1)$$

where K_D = original whole core Doppler coefficient,

$W(i,j)$ = local Doppler weighting factor,

$V(i,j)$ = local nodal fuel volume,

$T(i,j)$ = local nodal fuel temperature,

$T_o(i,j)$ = original local nodal fuel temperature,

$T_1(i,j)$ = local nodal fuel temperature at the time local voiding occurs,

F = effective normalized change in the Doppler coefficient for spectrum hardening due to sodium voiding,

A = feedback value evaluated at $T = T_1$.

The change in the effective Doppler coefficient (D_{eff}), calculated by dividing the change in the Doppler feedback of Equation (1) by the natural logarithm of the core-average fuel temperature change over the same time interval, is illustrated in Figure 4.11. The particular example is a guillotine break in one inlet pipe of an FTR-like core (radius about 60 cm, height about 90 cm). The overall drop in D_{eff} up to the time of initial coolant voiding results from the skewed fuel temperature buildup towards the top, lower worth region of the core. Channel 1 (central subassembly) is assumed to begin voiding at the core top due to cladding failure and fission gas release. Initial reactivity effects are negative, and the attendant drop in power accentuates the relative temperature peaking at the core periphery. As the void moves downward into the core, however, the reactivity effects are positive,

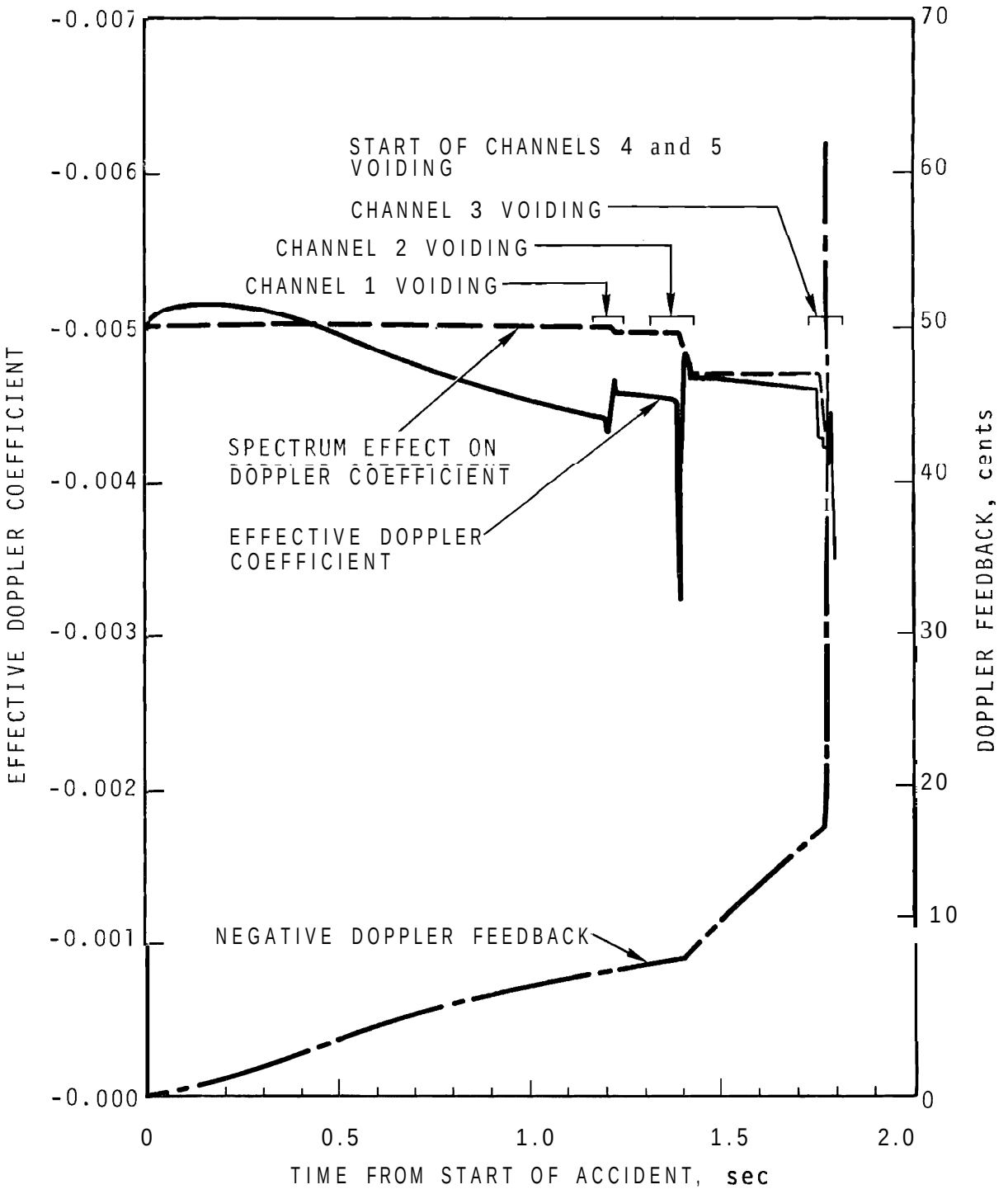

FIGURE 4.11. **Change in the Effective Doppler Coefficient During a Pipe Rupture Accident**

and the power surge peaks temperatures toward the central regions. Hence, D_{eff} increases. This phenomenon continues although the effects of spectrum hardening resulting from coolant voiding (the dashed line) become dominant and D_{eff} has dropped from -0.005 to approximately -0.0035 at the time the core nears a disassembly condition. For this type of accident, Doppler feedback is shown to be fairly small until the latter stages of the accident. Even so, however, the inclusion of a spatial Doppler feedback according to Equation (1) results in a substantially higher power and integrated energy (about 15%) relative to the lumped model which uses a Doppler feedback based on the core average temperature.

References

1. G. Kessler. "Space-Dependent Dynamic Behavior of Fast Reactors Using the Time-Discontinuous Synthesis Method," Trans. Am. Nucl. Soc., vol. 11, p. 569. 1968.
2. James F. Jackson and William E. Kastenberg. "Space-Time Dynamics Studies in Large LMFBR's with Feedback," Trans. Am. Nucl. Soc., vol. 12, p. 705. 1969.
3. D. A. Meneley and K. O. Ott, "Spectral Effects in Liquid-Metal Fast Breeder Reactor Transients," Trans. Am. Nucl. Soc., vol. 12, p. 706. 1969.
4. Alan E. Waltar, Andrew Padilla, Jr., and Richard J. Shields. MELT-11, A Two-Dimensional Neutronics-Heat Transfer Code for Fast Reactor Safety Analysis, BNWL-1320. Battelle-Northwest, Richland, Washington, 1970.

STABILITY ANALYSIS OF THE FAST TEST REACTOR

J. R. Sheff

The stability analysis of the Fast Test Reactor (FTR) merits discussion because of features of the reactor which differentiate it from other fast reactors. The most significant differences are the large size, 1033 liters, and high power level, 400 MW_t. The Doppler effect replaces the expansion effects as the dominant mechanism providing the prompt shutdown coefficient. The negative Doppler coefficient is $-3.2 \times 10^{-6}/°C$.

A standard lumped feedback path model involving a linearized set of matrix equations describing the neutronics and feedback mechanisms is used for the analysis. The approach is novel, however, in the description of the reactor via more than a single node so that such effects as the spatial dependent sodium void coefficient could be adequately treated. The sodium void coefficient is positive at the core center but becomes negative in the outer regions of the core.

The resulting feedback function for the FTR reference core, the solid line in Figure 4.12, is seen to be stable since multiplication by the zero power transfer function causes only a rather small angle clockwise rotation in the third quadrant. The measurable range from $\omega = 0.006$ to $\omega = 50$ is shown by the bars across the curve.

Extensive parametric studies have proven the system very stable. The Doppler coefficient was reduced by greater than tenfold in all cases showing any tendency toward instability. The only two cases discovered which were absolutely unstable are shown in Figure 4.12. Along with the zero Doppler coefficients, it was necessary to either let the fuel expansion coefficient go to zero or introduce a positive expansion coefficient for the fuel assembly tubes.

Conditional instability has also been found in a few cases near those producing absolute instability. Power levels of 100 times full power would be required to produce instability.

An analytic fit to the EBR-II experimental feedback function data[1] is also shown for comparison. One notes that the behavior is quite similar to the zero Doppler coefficient curves. This similarity might be expected since EBR-II has a very small Doppler coefficient.

In conclusion, the stability analysis of the FTR differs from other fast reactors primarily because of effects produced

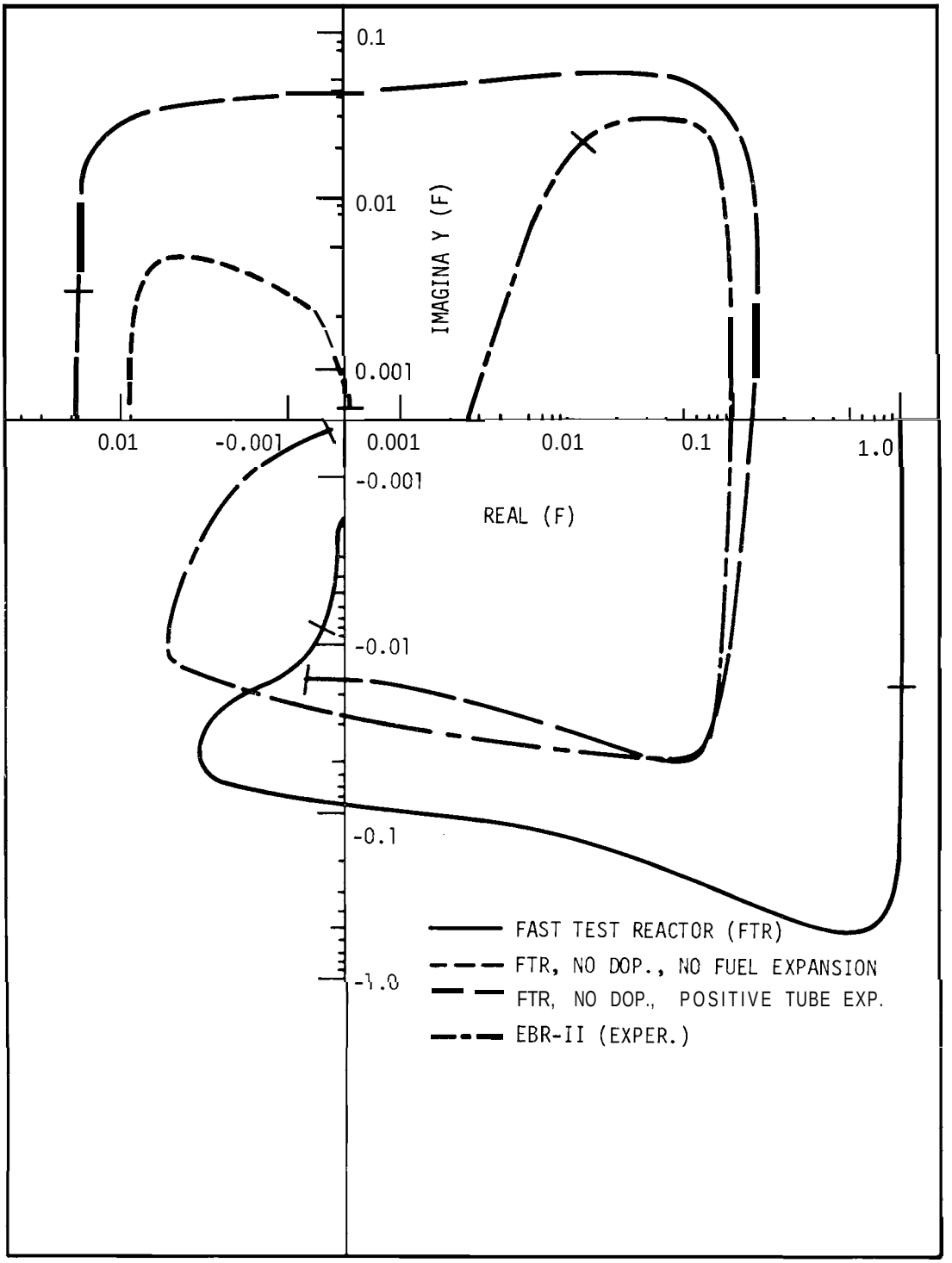

FIGURE 4.12. Phase Plane Plot of Feedback Functions. ω = 0.006 and 60 rad/sec are indicated by the dashes across the curves.

by its larger size and the systems studied are stable at least to the extent that the model is accurate. Not included at this time are effects of the system external to the reactor.

Reference

1. *Reactor Development Program Progress Report*, ANL-7391. Argonne National Laboratory, October 1967.

NOTES ON THE USE OF THE "ENGINEERING MOCKUP" AS A NUCLEAR DESIGN TOOL

R. A. Bennett, S. L. Engstrom, J. V. Nelson, and P. L. Hofmann

The use of engineering mockup, critical experiments constitutes an important element in the nuclear design of complicated and novel reactors. The goal of the mockup experiment is to verify the design values of the neutronics characteristics of the reactor to be built. The extent to which the physical characteristics of the reactor can be accurately mocked-up in the critical assembly determines its value as a design tool. If only a coarse mockup can be achieved, the required amount of extrapolation and interpolation increases, and the utility of the mockup experiment is greatly diminished.

In order to assure a useful engineering mockup configuration, detailed experimental planning, including extensive pre-calculation, is necessary. This calculational activity is presently underway in order to plan the engineering mockup experiments for the FTR.

The facilities available for the FTR engineering mockup experiments are the ANL ZPR assemblies, specifically ZPR-9. The matrix structures of these facilities are essentially square and fixed. The platelet inventories of materials are limited, and only a discrete spectrum of compositions are possible. One possible ZPR arrangement to simulate the hexagonal FTR geometry (if only whole material drawers can be used) is illustrated in Figure 4.13. Each zone in the square

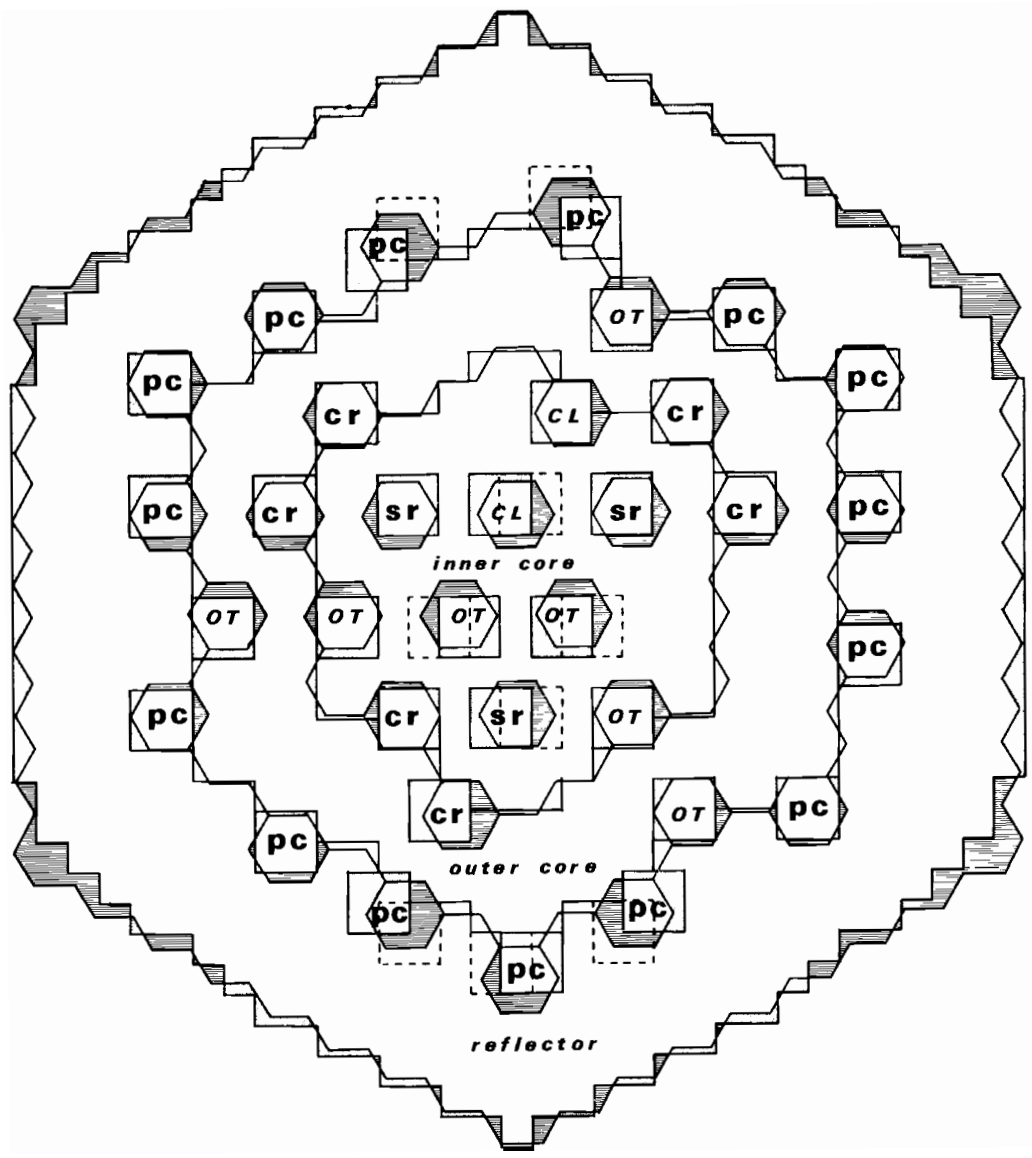

OT - OPEN TEST
CL - CLOSED LOOP
sr - SAFETY ROD
cr - CONTROL ROD
pc - PERIPHERAL CONTROL

FIGURE 4.13 Engineering Mockup - FTR Overlay

lattice mockup, although slightly different in volume from its FTR counterpart, has the same mass of materials.

Two-dimensional (x,y) and hexagonal coordinate calculations were carried out for different reactor conditions. The resulting multiplication constants are compared in Table 4.3. A comparison of different control rod worths is also shown.

For the configuration shown, the multiplication constants are consistently higher for the mockup by a few milli-k. Control strengths in the engineering mockup are consistently underestimated by 5 to 10%. These calculational trends will be used in the planning of the engineering mockup experiments in order to increase their accuracy and consequent utility.

TABLE 4.3. Results of FTR/FTR Engineering Mockup Comparative Calculations

Configuration Description	k_{eff} FTR	k_{eff} Eng. Mockup
1. Reactor shut down - all rods in	0.8858	0.8971
2. All safety rods out	0.9538	0.9606
3. All safety and in-core control rods out	1.0087	1.0124
4. All safety rods out, asymmetric in-core control rod in	0.9893	0.9939
5. All safety, control, and peripheral control rods out	1.0445	1.0465

	Calculation Numbers	Reactivity FTR	Worth (%Δk/k) Eng. Mockup
All safety rods (3)	1 and 2	8.05	7.37
All in-core control rods (4)	2 and 3	5.70	5.20
One in-core control rod	3 and 4	1.94	1.84
All peripheral control rods (15)	3 and 5	3.40	3.21
Total control strength	1 and 5	17.15	15.91
Total in-core control strength	1 and 3	13.75	12.57

INVERSE MULTIPLICATION MONITORING OF SUBCRITICAL REACTIVITY CHANGES IN FTR

S. L. Engstrom, R. A. Bennett, and V. O. Uotinen

It is presently planned that reactivity changes during refueling of FTR and those occurring during initial steps in the approaches to critical will be monitored with a portion of the Low Level Flux Monitoring System. Inverse multiplication techniques are to be used. One can very reasonably expect that changes in fuel loadings of drivers or test loops and control motions near any of the elements of the monitoring system will seriously perturb their responses and ultimately produce results that must be corrected.

This problem has been investigated experimentally in ZPR-III Assembly 56B[1] by Argonne National Laboratory as a part of the Battelle-Northwest FTR Critical Experiments Program. Control rods were inserted at the boundary of the core of the assembly, and the inverse multiplication rate was monitored with sensors located at various positions, including the core center and outside the ZPR-III matrix approximately 100 cm from the core centerline and approximately 60 cm from the nearest control zone. The areal profile and counter positions are shown in Figure 4.14. Values of the reactivity worths of rods differed by as much as 12% for the various sensors.

In an attempt to identify which counter was "best," a series of subcritical calculations were performed with a two dimensional diffusion theory model of the various experimental configurations. The distributed external source of neutrons due to α-n reaction in ^{240}Pu was represented to yield absolute flux levels. The actual calculated changes in the subcritical multiplication constants were compared with values inferred from changes in ^{235}U and ^{10}B reaction rates throughout the core. The results are presented in Table 4.4 for the specific

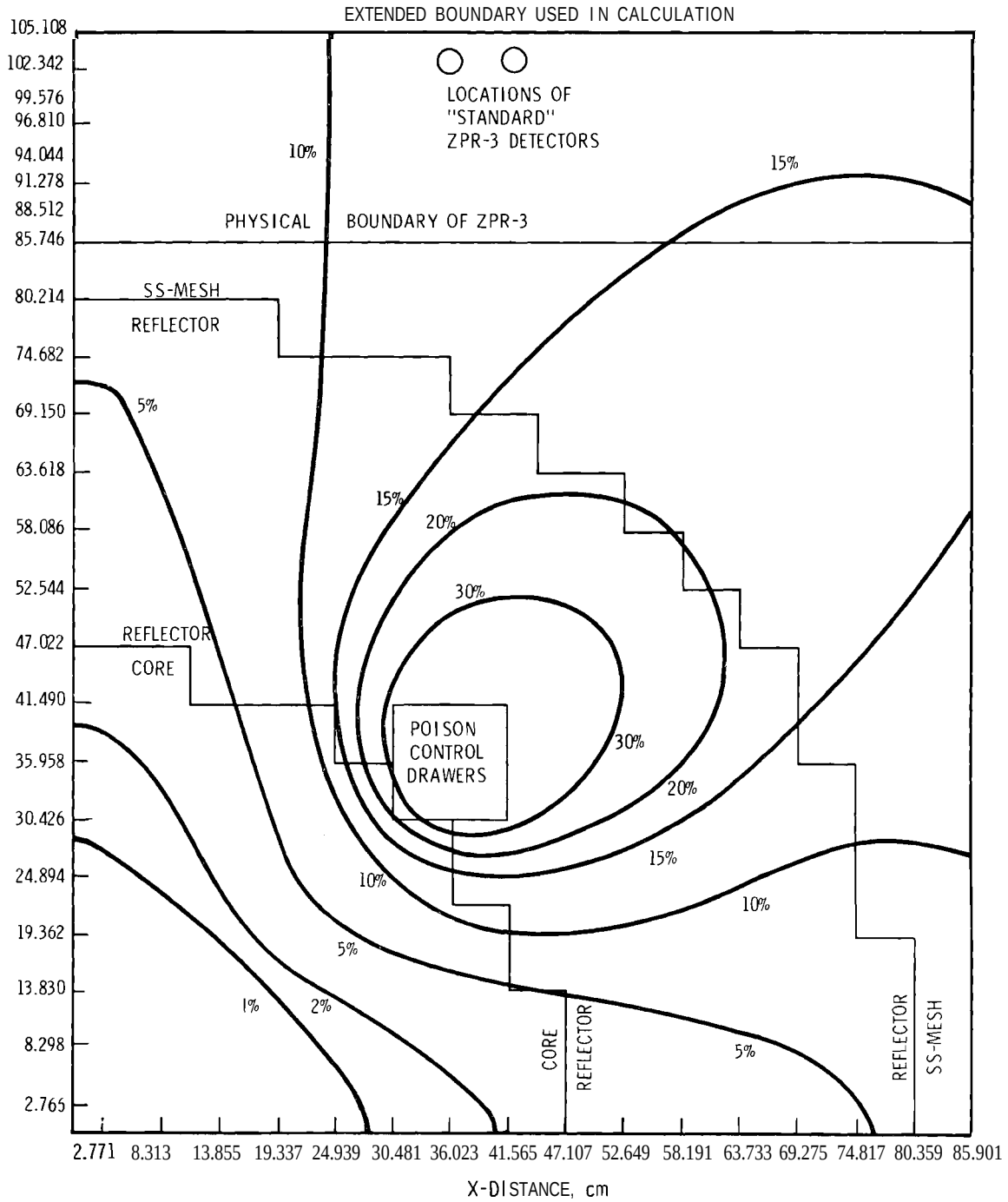

FIGURE 4.14. **Assembly 56B Quarter Core Areal Profile, Lines Showing the Percent Overestimation of the Worth of Four Large B_4C Rods**

TABLE 4.4. Calculated Reactivity Worths Deduced from Calculated Reaction Rates of Various Detectors

Sensor Location	Sensor	Four Small B_4C Rods[a] Exp. Worth, Ih	Calc. Worth, Ih	R[b]	Four Large B_4C Rods Exp. Worth, Ih	Calc. Worth, Ih	R[b]
	Reaction Rate in ^{10}B	968 510	1005	1.000	1804 ±21	1923	1.003
Center of Reactor	Fission Rate in ^{235}U		1003	0.998		1915	0.999
	ϕ Total		1002	0.997		1909	0.996
	Reaction Rate in ^{10}B	1000 510	1056	1.051	2021 ±21	2255	1.176
Standard ZPR-3	Fission Rate in ^{235}U		1052	1.047		2215	1.155
	ϕ Total		1045	1.040		2153	1.123

a. *Small rods were one-fourth the size of the range rods and occupied the quadrant of large rod closest to the core center.*

b. *R is the ratio of the worth deduced from calculated reaction rates to the worth as obtained from the calculated eigenvalues.*

experimental sensors locations and are shown graphically in Figure 4.14 for all possible sensor locations. The tabulated values show that sensors located at the core center are "best." The calculated lines of "equal over-estimation," shown in Figure 4.14, illustrate that any other position is worse.

Comparisons of calculated values with the "best" experimental results show an additional 5% disagreement or c/e ratios of approximately 1.05 for both small and large rods.

Reference

1. *Reactor Development Program Progress Report*, ANL-7577. Argonne National Laboratory, April-May 1969.

CENTRAL FUEL AND PERIPHERAL CONTROL RING REACTIVITY WORTHS IN THE FTR-2 CRITICAL •

R. A. Bennett and J. V. Nelson

Experimental measurements have been made of reactivity worths of segments of a peripheral control ring of B_4C-steel-Na and large fuel assembly-size plutonium samples from the core of a full scale simulation of the FTR. These experiments were performed by Argonne National Laboratory personnel in ZPPR Assembly-1, FTR-2 as part of the FFTF Critical Experiments Program.

An areal profile of FTR-2 is shown in Figure 4.15 which illustrates the arrangement of the core, central depleted zone, peripheral control ring, and reflector. Additional detailed descriptions of the experimental arrangements have been reported.[1] Reactivity measurements were made in alternating steps in which fissile plutonium was removed from the core and replaced by fertile uranium; those reactivity decreases were approximately compensated for by the removal of segments of the control ring, which, in turn, was replaced by reflector composition. The sequence of the experiments is indicated by the numerical scheme shown in Figure 4.15. For example,

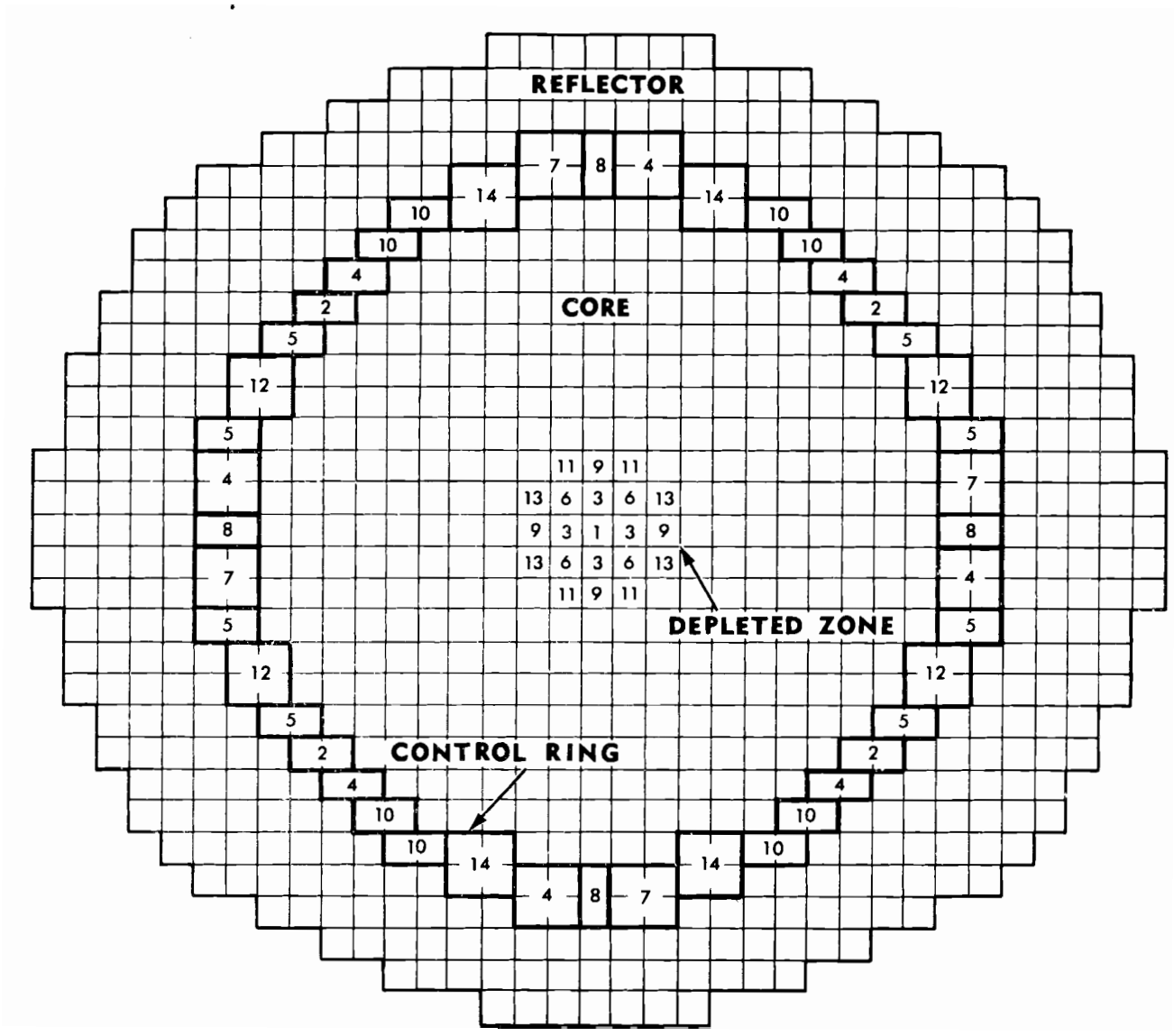

FIGURE 4.15. FTR-2, ZPPR-1-70, Areal Profile

fissile material was replaced first in Zone 1 and control material was replaced second in Zone 2. The experimental results and corresponding diffusion theory values are presented in Table 4.5.

Comparisons of the experimental data and calculated values indicate that the neutronics design requirements of the FTR should reflect approximately ±10% uncertainty (Col. 13) in the calculated values of peripheral control rod strengths, and approximately a 30% over-calculation (Col. 10) of the reactivity worths of centrally located changes in fissile plutonium densities arising from changes in the compositions of test loops or fuel burnup. These analyses also indicate that the discrepancy between calculated and measured multiplication constants, (K^E - K^C) (Col. 7), increases linearly with the mass of the plutonium test sample. One may infer from this dependence that the troublesome fractional over-calculation of reactivity worths of plutonium samples is approximately constant for sample sizes from 0 to 32 kg, the limit of these experiments.

References

1. *Reactor Development Program Progress Report*, ANL-7632. Argonne National Laboratory, October 1969.

TABLE 4.5. Experimental Results and Corresponding Diffusion Theory Values

Experiment Number	Experimental Results: Core Fuel Mass[a] kg	Experimental Results: Control[b] Drawers In Place	Experimental Results: Excess Reactivities %Δk/k	Experimental Results: Multiplication Constants, K^E	Calculation: Multiplication Constants K^C	Comparison: $K^E - K^C$	Reactivity Worths of Fertile for Fissile Exchanges: Experimental, %Δk/k(E)	Reactivity Worths of Fertile for Fissile Exchanges: Calculated %Δk/k(C)	Reactivity Worths of Fertile for Fissile Exchanges: Ratio, C/E	Reactivity Worths of Reflector for Control Exchanges: Experimental %Δk/k(E)	Reactivity Worths of Reflector for Control Exchanges: Calculated %Δk/k(C)	Reactivity Worths of Reflector for Control Exchanges: Ratio, C/E
Col. 1	Col. 2	Col. 3	Col. 4	Col. 5	Col. 6	Col. 7	Col. 8	Col. 9	Col.10	Col. 11	Col. 12	Col. 13.
0	527.041	240	+0.086±0.001	1.00086	0.98729	0.01357						
1	525.043	240	-0.480±0.030	0.99522	0.98118	0.01404	-0.566±0.030	-0.631	1.114			
2	525.043	224	-0.159±0.005	0.99841	0.98369	0.01472				+0.321±0.030	0.260	0.810
3	519.050	224	-1.618	0.98408	0.96677	0.01731	-1.459	-1.779	1.219			
4	519.050	176	-0.800±0.070	0.99206	Asymmetric	-				+0.818	Asymmetric	-
5	519.050	144	-0.226±0.003	0.99774	Asymmetric	-				+0.574±0.070	Asymmetric	-
6	515.054	144	-1.360±0.200	0.98658	Asymmetric	-	-1.134±0.200	Asymmetric	-			
7	515.054	112	-0.607±0.027	0.99397	0.97370	0.02027				+0.753±0.200	Asymmetric	-
8	515.054	96	-0.120±0.001	0.99880	0.97807	0.02073				+0.487±0.027	0.459	0.942
9	507.064	96	-1.690±0.250	0.98338	0.95959	0.02379	-1.570±0.250	1.967	1.253			
10	507.064	64	-0.849±0.061	0.99158	0.96723	0.02435				+0.841±0.260	0.823	0.978
11	503.068	64	-1.600±0.250	0.98425	0.95866	0.02559	-0.751±0.260	0.924	1.230			
12	503.068	32	-0.301±0.006	0.99700	0.97037	0.02663				+1.299±0.250	1.259	0.969
13	495.077	32	-1.520±0.180	0.98503	0.95452	0.03051	-1.219±0.180	1.711	1.404			
14	495.077	0	-0.306±0.007	0.99695	0.96671	0.03024				+1.214±0.180	1.321	1.088
							Man qu ≡r d v at ⊙ fom ⊙1-y		9%		Standard deviation = ±11% from unity	

(a) Fissile material ^{239}Pu + ^{241}Pu + ^{235}U.

(b) Two drawers per matrix location.

FTR CORE FLUX MONITORING

E. T. Boulette and C. A. Mansius

Monitoring of the FTR core neutron flux level from shutdown to full power (400 MW) is complicated by the presence of in-vessel stored fuel. At very low power levels (<1 W) a large fraction of the signal to the out-of-vessel monitor will be due to neutron flux from the stored fuel, and accurate core monitoring will be compromised. To circumvent this difficulty, the current design includes in-vessel monitors in the vicinity of the shield-reflector interface. Because of their proximity to the core, these in-vessel monitors saturate at a low reactor power level (10 to 100 W). The problem is to locate these detectors to assure adequate monitoring over the power range from shutdown to full power.

The monitoring capability of ^{235}U fission chambers is highly dependent upon the gamma:neutron flux ratio at the detector location. To determine the monitoring range of a detector of this type, one must know the variation in the gamma and neutron flux with changes in the power level. In addition, the effect of stored fuel must be taken into account.

The effect of stored fuel on the out-of-vessel monitor signal as a function of the neutron source rate in the core is depicted in Figure 4.16 for 25, 50, and 100 fuel subassemblies in storage, based on extrapolation of calculations made with 2DBS for Concept V-A. In all cases, it was assumed that a third of the stored fuel elements were placed in each 120 degree sector of the FTR. In all three cases (25, 50 and 100 stored fuel assemblies) it was assumed that the fuel densities in the stored fuel zones were the same. To check the extrapolations involved in these calculations, a two-dimensional diffusion theory calculation was made with 2DBS on Concept V-A in which the neutron source rate in the core was fixed at 1.1×10^9 n/sec (corresponding to a subcritical system with k = 0.9).

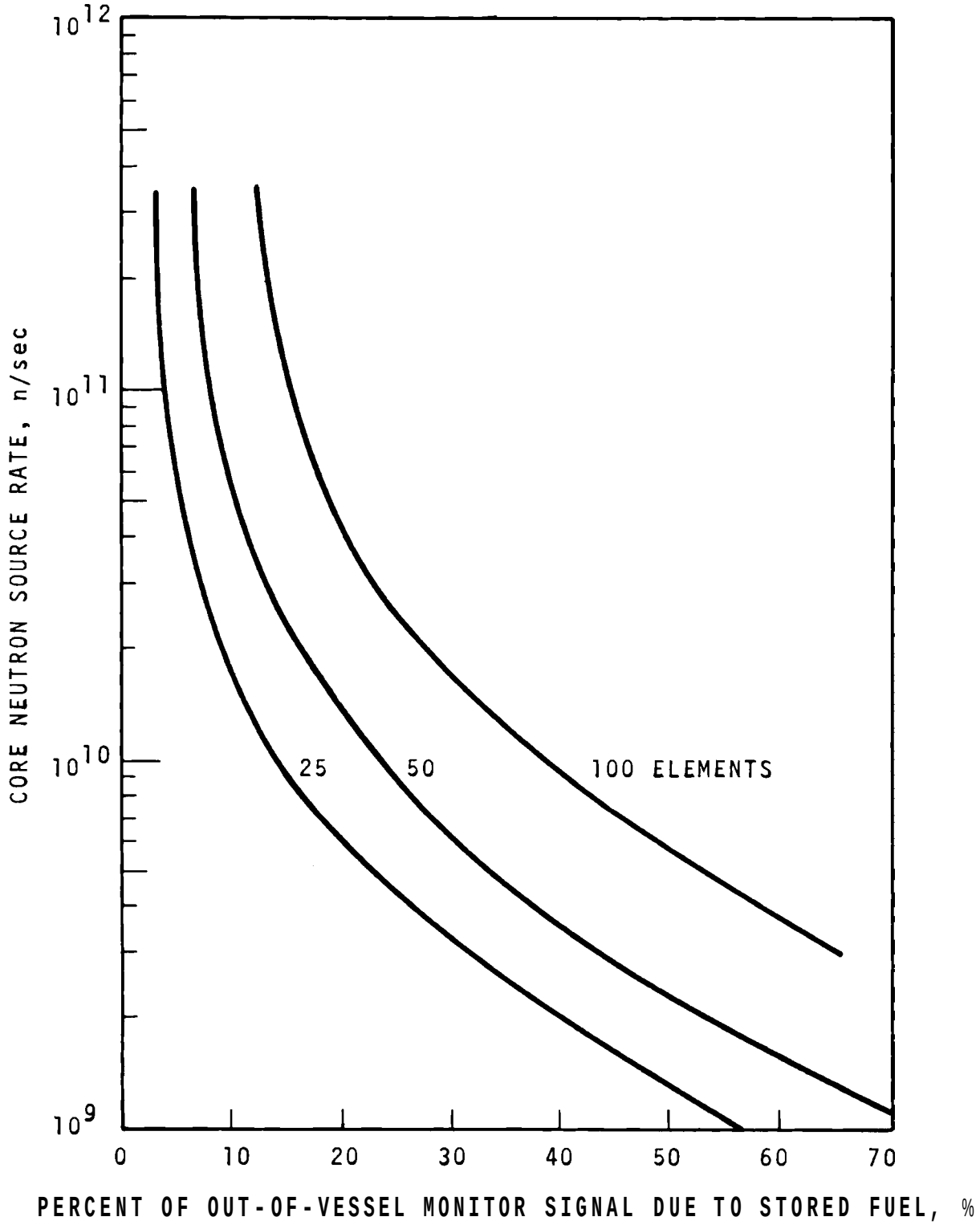

FIGURE 4.16. Percent of Out-of-Vessel Monitor Signal due to 25, 50, and 100 Stored Fuel Elements Versus Total Core Source Rate

Calculations were made with and without stored fuel in the sodium annulus. The results indicated that at full shutdown (k = 0.9) about 80 to 85% of the signal at the out-of-vessel monitor is due to stored fuel. This calculation assumed a steady state condition: i.e., the delayed neutron precursors generated at full power have decayed to the extent that the fixed source in the core (spontaneous fission and a,n reactions) predominates. The extrapolation shown in Figure 4.16 indicates that about 70% of the signal will be due to stored fuel. The agreement between these two numbers validates the extrapolation technique used to generate the curves in Figure 4.16.

In addition to these data, one must also know the time variation of the total core source rate following a large perturbation (e.g., a scram to k = 0.9). In Figure 4.17 is plotted the core neutron source rate versus time after shutdown for instantaneous scrams to k = 0.9 and k = 0.99. To generate these curves, the following assumptions were made: (1) the scrams are instantaneous, (2) at full power, 90% of the fission is ^{239}Pu fission and 10% is ^{238}U fission, (3) the neutron source rate in the core at any time following shutdown is simply $(1 - k)^{-1}$ times the sum of the fixed source in the core [spontaneous fission and (α,n) reactions with oxygen] and the delayed neutron source rate, (4) the total delayed neutron source rate, S_D, decays as the sum of exponentials

$$S_D(t) = S_o \left\{ 0.9\left(\sum_i \beta_i^{239} e^{-\lambda_i^{239} t}\right) + 0.1\left(\sum_i \beta_i^{238} e^{-\lambda_i^{238} t}\right)\right\} \quad (1)$$

where

S_o = 3.34 × 10^{19} n/sec (neutron source rate at 400 MW)

β_i^{239} = i^{-th} delayed neutron fraction for ^{239}Pu fission

β_i^{238} = i^{-th} delayed neutron fraction for ^{238}U fission

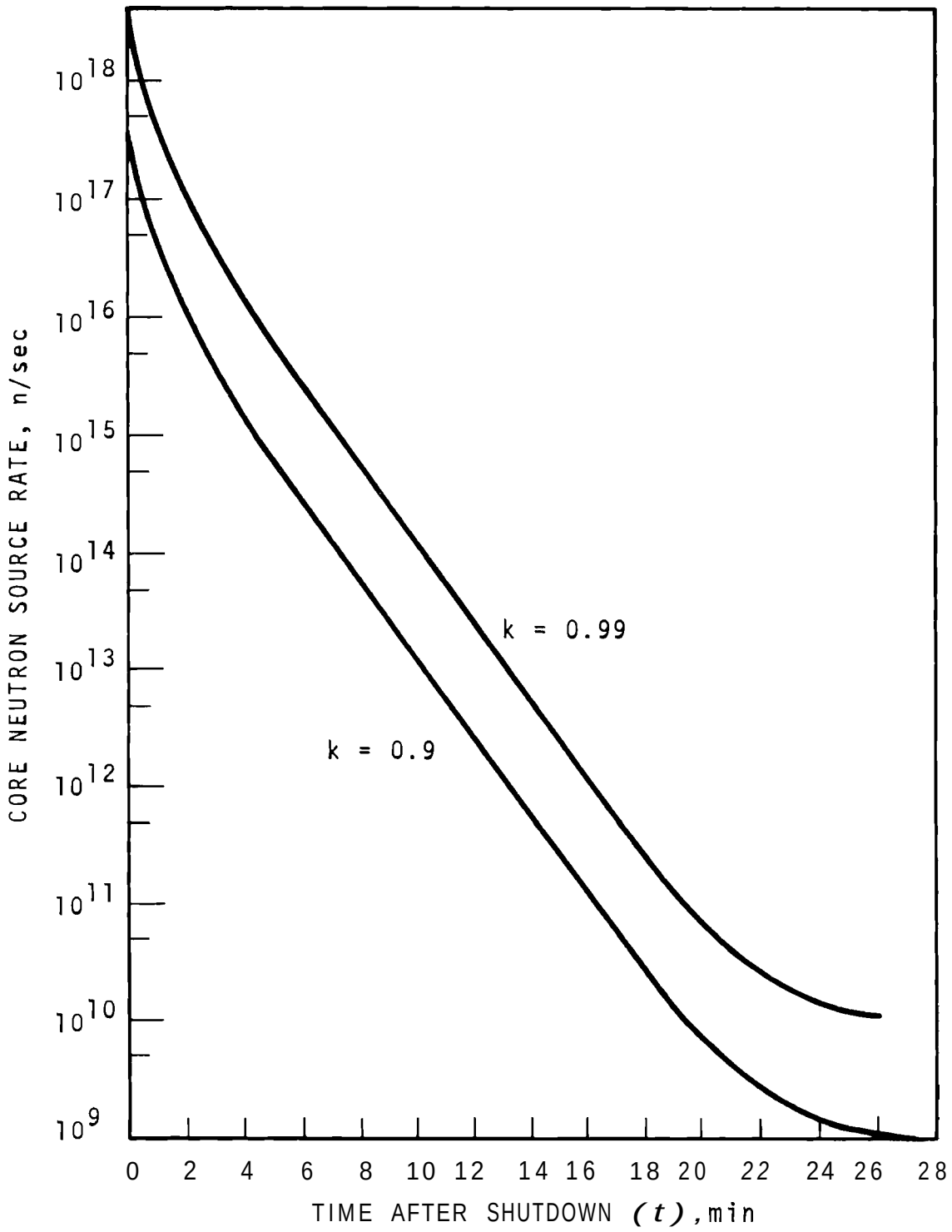

FIGURE 4.17. **Total Core Source Rate Versus Time Following Instantaneous Scrams to k = 0.9 and k = 0.99**

λ_i^{239} = decay constant associated with the i^{-th} delayed neutron fraction for ^{239}Pu fission

λ_i^{238} = decay constant associated with the i^{-th} delayed neutron fraction for ^{238}U fission

t = time in seconds.

Equation (1) does not account for secondary delayed neutrons (i.e., delayed neutrons generated by delayed-neutron-induced fission); however, this effect is believed to be negligible.

From Figures 4.16 and 4.17, one may determine at which time following a scram the out-of-vessel monitors become unreliable. The out-of-vessel monitors are considered unreliable when the percent of the out-of-vessel monitor signal due to stored fuel is so great as to mask-out changes in the signal from the core. Also from Figure 4.17, one may obtain the ^{235}U fission rate at the in-vessel detector location as a function of time following scram. At full power (core source strength = 3.34×10^{19} n/sec) the ^{235}U fission rate at the detector location is 1.4×10^{13} fissions/sec-g of ^{235}U. Since the ^{235}U fission rate at the detector location is essentially proportional to the core source strength, the ^{235}U fission rate may be obtained for any time following scram from Figure 4.17.

In addition to these data, one must know the gamma intensity at the detector location to assess the detector's monitoring capability. The total gamma dose rate at the in-vessel detector location is plotted in Figure 4.18 versus time after shutdown. The major contributors to the total dose rate are $^{55}Mn(n,\gamma)$ and $^{59}Co(n,\gamma)$ reactions. The fission product decay gammas and the $^{23}Na(n,\gamma)$ gammas will yield dose rates of the order of 10^4 R/hr and 10^5 R/hr respectively, and therefore will not contribute significantly to the total dose rate for the first few hours following a scram. Note that a buildup

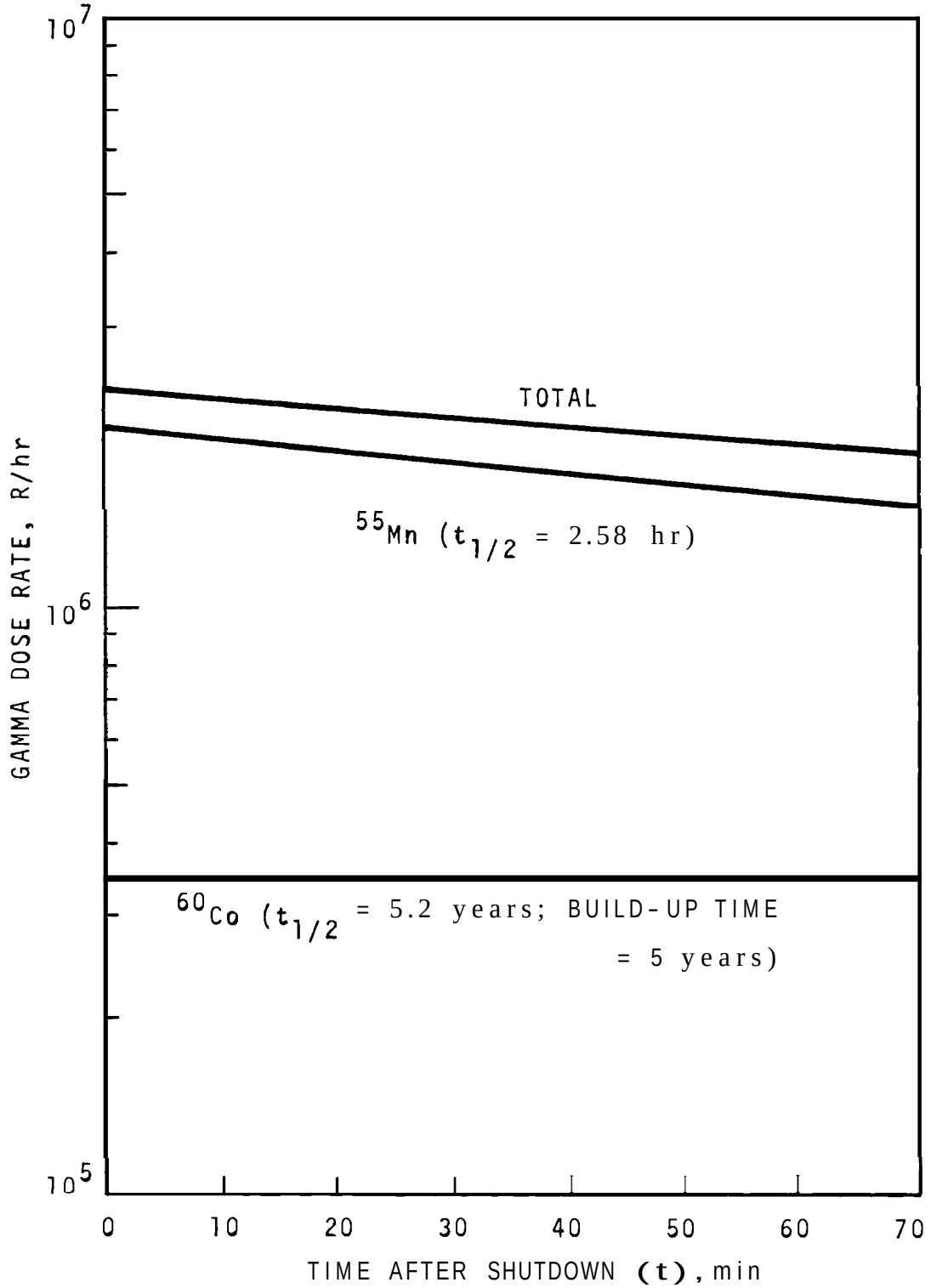

FIGURE 4.18. The Total Gamma Dose Rate (R/hr) Versus Time After Shutdown at 96.0 cm from the Core Centerline on the Core Midplane

time of 5 years has been assumed for the $^{59}Co(n,\gamma)$ reaction. Thus, it is only at about 50% saturation.

Employing the data presented in Figures 4.16 through 4.18, one may determine at which time following a scram the out-of-vessel monitors become unreliable. In addition, one can determine the required operating characteristics for the in-vessel detectors to assure continuous neutron monitoring.

EFFECT OF COBALT CONTENT IN STEEL ON SHIELD REQUIREMENTS

C. A. Mansius

It is anticipated that a number of radioactive components from the Fast Test Reactor will need to be replaced at some time during the lifetime of the facility. Replacement of large components such as the core support structure will probably require fabrication of a shielded container. The purpose of this study was to determine the effect of the cobalt content of the stainless steel used in the fabrication of the core support structure on the shielding requirements during the removal process.

Only long-lived radioisotopes will influence the shield requirements, since replacement of the core support structure would require an extended shutdown period. At the location of the support structure, the neutron spectrum is relatively degraded in energy and n,γ reactions are dominant. Based on half life, decay energy, and production rate, ^{60}Co and ^{59}Fe will be the predominant radioisotopes emitted by the support structure. The half life of ^{60}Co is 5.2 years and it emits both a 1.17 and 1.33 MeV photon per decay. The half life of ^{59}Fe is 45 days and it emits a 1.10 MeV photon in 56% of the decays and a 1.29 MeV photon in 44% of the decays. Because of the comparable photon energies from the two isotopes, the relative gamma intensity will be essentially independent of the shield thickness.

The relative radiation intensity from ^{60}Co and ^{59}Fe depends on the cobalt content of the steel together with the operating and decay history. Figure 4.19 gives the relative intensity of the two isotopes as a function of operating time and cobalt content. It is assumed the reactor operates at 400 MW for 75 days and is then shutdown for 25 days. For this assumed cycle, ^{59}Fe attains 87% of its saturated value whereas ^{60}Co would reach a maximum of about 60% of its saturated value (continuous cyclic operation). Figure 4.20 presents the decay curves for the two isotopes.

Calculations indicate that about 5 to 6 in. of lead will be required to reduce the radiation intensity from the core support structure to a level of about 25 mrem/hr at the surface of the cask, based on the maximum relative ^{59}Fe activity shown in Figure 4.19. About 0.4 in. of lead is required to effect a factor of 2 change in the radiation intensity for either the cobalt or iron radiations. The data in the two figures can be used together with this basic shield information to estimate the required shield thickness as a function of operating time, cobalt content, and shutdown time. In most cases of interest it is found that shielding requirements will depend directly on the cobalt content of the steel.

RADIATION LEVELS IN HEAT TRANSPORT CELL

W. L. Bunch, C. A. Mansius, and D. R. Marr

Access into the FFTF heat transport system (HTS) cells is desirable to permit inspection and maintenance. Estimates were made of anticipated radiation levels within the HTS cells as a function of various operating conditions to provide information for the conceptual design. The three basic conditions considered are: (1) entry into the cell following shutdown of the reactor, (2) reducing the reactor power and valving off the single HTS cell of interest to permit decay of

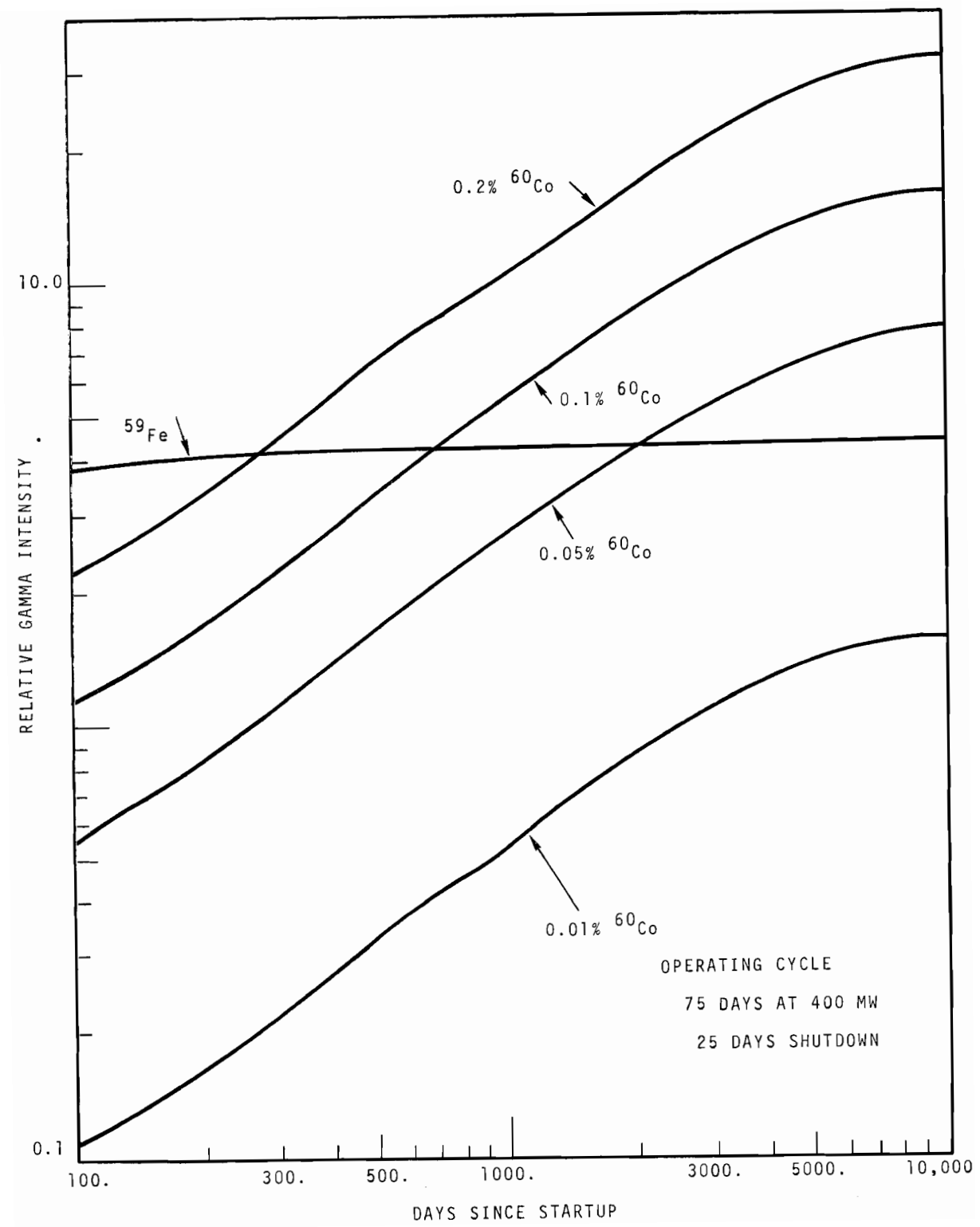

FIGURE 4.19. Relative ^{59}Fe - ^{60}Co Gamma Intensity

^{24}Na, with entry into the cell following shutdown of the reactor, and (3) entry into the valved-off cell with the reactor operating.

Entry into the HTS cell following shutdown of the reactor would be delayed about 12 days to permit decay of ^{24}Na. After that delay time, it is estimated the average radiation level in the cell will be about 30 mrem/hr because of the long-lived (2.58 year half life) ^{22}Na in the system. The radiation level could be significantly higher as a result of corrosion and fission products in the system. However, it will take significant operating time for transport of corrosion products to the cells, and fission product contamination will depend on the fuel failure history that is experienced.

By operating the reactor at reduced power while one HTS cell is valved off, it would be possible to reduce or eliminate the 12-day wait to permit ^{24}Na decay. Table 4.6 indicates the operating-shutdown intervals that would be employed as a function of valve leakage to maximize plant efficiency. It is assumed there would be no incentive to continue to operate at reduced power once the radiation level due to ^{24}Na had achieved the equilibrium value for the specific leakage rate.

TABLE 4.6. Operating and Shutdown Times to Maximize Plant Efficiency as a Function of Valve Leakage[a]

Valve Leakage			Days at 2/3 Power	^{24}Na Intensity R/hr	Days Down	^{24}Na Intensity R/hr
%	GPM	GPH				
0.01	1.5	90	2	3000	10	0.03
0.0025	0.38	23	4	300	8	0.03
0.001	0.15	9	6	30	6	0.03
0.0005	0.075	4.5	8	3	4	0.03
0.0002	0.03	1.8	12	0.03	0	0.03
0	0	0	12	0.03	0	0.03

a. *Assumes 15,000 gallons in one HTS cell, 15,000 gpm full flow rate.*

To estimate the radiation level in the HTS cell as a function of valve leakage, it was assumed the point of interest within the cell was equidistant from all of the sodium within the cell. The activity of the sodium at any point in the system was related to valve leakage or flow rate based on time since leaving the high pressure inlet plenum. The most important single factor becomes the decay time in transit from the inlet plenum to the HTS cell. It is obvious that within the cell significant radiation gradients will exist at low flow (leakage) rates. Methods are available to include the exponential variation in source strength from straight pipe sections; however, it was not deemed necessary to include such refinement in this study. Detailed calculations can be made for specific component arrangements and specific points of interest.

In order to enter a HTS cell with the reactor operating, it would first be necessary to employ a valve that permitted less than about 1.8 gal/hr leakage. It would also be necessary to increase the cavity wall thickness by about a foot, since personnel radiation levels are more restrictive than those established by protection of the secondary sodium from activation. For the same reason it would be necessary to refine the shielding around the piping penetrations through the cavity wall. The reactor would then be operated at reduced (2/3) power for about 12 days to permit decay of ^{24}Na. Under these conditions, the radiation environment in the HTS cell would be satisfactory for personnel access during operation.

From consideration of the impact of a design basis accident, entry into a HTS cell during reactor operation would require other design changes. Either an air lock would be required to permit access to the cell while maintaining the confinement boundary provided by the cell, or a vent block would be required between the cell and the reactor cavity to remove the cell entirely from the confinement region.

NEUTRON ATTENUATION CHARACTERISTICS OF STAINLESS STEELS

D. R. Marr

The decision to replace 304 stainless steel with 316 stainless steel in the duct material as well as in the cladding indicated a need to examine the relevancy of the existing neutron shielding calculations, which were based on the use of 304 stainless steel. This study provided the following results:

1. 316 SS is a slightly more effective shielding material than 304. Largest differences (up to a factor of 2) are seen in the lower energy reactions.
2. Previously reported results based on the use of 304 SS are thus conservative.
3. The higher shielding effectiveness of 316 SS is due to molybdenum, present only in small percentage amounts, which has a much higher absorption cross-section than any of the other components of stainless steel.
4. The shielding characteristics of stainless steel are not sensitive to the chromium-nickel content within the ranges established for 316 SS and 304 SS.
5. Most of the difference in neutron attenuation between 316 SS and 304 SS is effected in transmission through the reflector and about half way into the shield.

The compositions of 316 and 304 SS as shown in Table 4.7 together with the composition assumed in this study. Type 316 differs from 304 in higher nickel content offset by a corresponding decrease in the chromium content and by the inclusion of about 2.5% molybdenum, which replaces some of the iron. Type 316 also has a slightly higher density. For the purpose of this comparison, a one-dimensional spherical geometry model based on the radial configuration of Concept V-A was selected. This configuration is shown in Table 4.8. The core barrel dimension was arbitrarily thickened to one foot to study the attenuation in pure stainless steel.

TABLE 4.7. Weight Percent Composition of 316 and 304 Stainless Steels

	304 SS (7.90 g/cm^3)		316 SS (7.98 g/cm^3)	
	Yevick[1]	This Study	Yevick	This Study
Fe	64.92-70.92	68.92	61.92-68.92	66.42
C	<0.08	0.0	<0.08	0.0
Cr	18.00-20.00	19.00	16.00-18.00	17.00
Ni	8.00-1200	10.00	10.00-14.00	12.00
Mn	<2.00	1.50	<2.00	1.50
Si	<1.00	0.50	<1.00	0.50
Co	<0.20	0.08	<0.20	0.08
Mo	∿0	0.0	2.00-3.00	2.50

TABLE 4.8. Model Configuration and Composition

Zone	Outside Radius, cm	Material Composition, vol %				
		Na	SS	Fuel	Void	Ni
Core I	38.6	38.89	29.40	25.91	3.53	2.27
Core II	60.2	38.89	28.06	26.26	3.58	3.12
Reflector I	72.14	35.00	37.20	--	--	27.80
Reflector II	96.0	33.00	33.70	--	--	32.30
Shield	144.8	34.00	66.00	--	--	--
Core Barrel	179.3	--	100.00	--	--	--

Twelve integral quantities of possible shielding interest were calculated using the converged fluxes from the discrete ordinates transport code ANISN. An S_8 calculation was made with ANISN using the HOMSET cross sections on each of the four following cases:

CASE I (304) - All stainless used in this case was 304 SS as described above.

CASE II (316) - All stainless used in this case was 316 SS as described above.

CASE III (316A) - All stainless used was modified 316 SS, having a modified chromium and nickel content (10% Ni, 19% Cr).

CASE IV (316B) - All stainless used was 316 SS, but without the molybdenum.

The results of this study are shown in Table 4.9 where, taking 316 SS as a base case, the effect of replacing it with each of the other materials is shown at four selected points.

Several items should be noted:

1. There is little effect in the core.
2. The 316A case shows there is little effect due to changing the chromium-nickel ratio over the range that can be expected to encompass variations within each type steel or between the two steels.
3. Having excluded an appreciable effect due to the change in chromium-nickel ratio, case 316B (316 with no molybdenum) shows that the primary difference due to replacement of 304 by 316 steel is due to the molybdenum content of the 316. A close check of the HOMSET absorption cross sections for molybdenum shows values which are slightly high with respect to the latest experimental data, a bias not thought to grossly affect the results of this study.
4. Reactions with a significant high energy contribution such as ^{238}U (n,f) or biological dose do not show a large effect due to 316 replacement.
5. For those quantities such as ^{59}Co (n,γ), which have an elevated low energy response, there is a point approximately midway in the shield where subsequent attenuation is relatively independent of the steel used.

TABLE 4.9 Reaction Rates Effect

Reaction Rate	Ratio of Reaction Rate to Reaction Rate in 316 SS Case											
	Core r = 1128 cm			Reflector r = 70.1 cm			Shield r = 115.8 cm			Core Barrel r = 145.8 cm		
	304	316A	316B	304	316A	316B	304	316A	316B	304	316A	316B
^{239}Pu (n,f)	1.00	1.00	1.01	1.21	1.00	1.21	1.70	1.01	1.71	1.93	1.04	1.93
Na(n,γ)	1.00	1.00	1.01	1.14	1.00	1.14	1.49	1.02	1.49	1.69	1.04	1.69
^{235}U(n,f)	1.00	1.00	1.01	1.19	1.00	1.19	1.66	1.01	1.66	1.86	1.04	1.86
^{238}U(n,f)	0.99	1.00	1.00	1.01	1.01	1.02	1.03	1.02	1.08	1.04	1.02	1.14
Biological Dose	0.99	1.00	1.00	1.01	1.00	1.01	1.06	1.02	1.08	1.12	1.03	1.16
^{59}Co(n,γ)	1.01	1.00	1.01	1.26	1.00	1.26	1.82	1.01	1.82	2.09	1.04	2.10
^{55}Mn(n,γ)	1.02	0.99	1.03	1.10	1.00	1.10	1.35	1.01	1.34	1.49	1.04	1.49
^{58}Fe (n,γ)	1.00	1.00	1.01	1.08	1.00	1.08	1.33	1.02	1.33	1.46	1.05	1.46
B(n,α)	1.01	1.00	1.01	1.24	1.00	1.24	1.77	1.01	1.78	2.02	1.04	2.02
Total Flux	1.00	1.00	1.00	1.04	1.01	1.04	1.20	1.02	1.20	1.31	1.05	1.31
Flux Above 0.8 MeV	0.99	1.00	1.00	1.01	1.01	1.01	1.02	01	1.07	04	1.02	1.13
Flux Between 0.07-0.8 MeV	1.00	1.00	1.00	1.01	01	1.01	1.05	1.02	1.06	1.09	1.03	1.12

ZPPR/FTR-2 SHIELD EXPERIMENTS

E. T. Boulette

Experiments in support of the design of the Fast Test Reactor (FTR) shields were conducted at Argonne National Laboratory in the Zero Power Plutonium Reactor (ZPPR). The experimental arrangement approximated the basic features of the FTR: a 1000 liter, two-zone core surrounded by a 1 ft thick nickel reflector and a stainless steel-sodium shield. Although the FTR shield is surrounded by an annular sodium zone in which fuel and other reactor components may be stored, the ZPPR facility is not large enough to incorporate this feature. Provisions were therefore made to include a stored fuel zone in the experimental shield. Neutron and gamma distributions were measured throughout the core, reflector, and shield, with and without stored fuel in position.

Neutron Distribution

The neutron distribution was obtained by measuring the reaction rate traverses of ^{239}Pu and ^{238}U with fission counters and of ^{10}B with a BF_3 counter. In addition, sodium and manganese foils were dispersed throughout the system and irradiated. These foils were selected not only because of their different response functions, but also because of the impact these reaction rates have on the FTR design.

The two-dimensional diffusion theory code 2DBS,[1] and the one-dimensional discrete ordinates code ANISN[2] were used to calculate the reaction rate distributions for comparison to the experimental results. The nuclear data used was extracted from the HOMSET[3] 31-group transport-corrected cross section set. The measured and calculated ^{10}B reaction rate distribution with no stored fuel in the shield are compared in Figure 4.21. Similar agreement was found for the other reaction rate distributions.

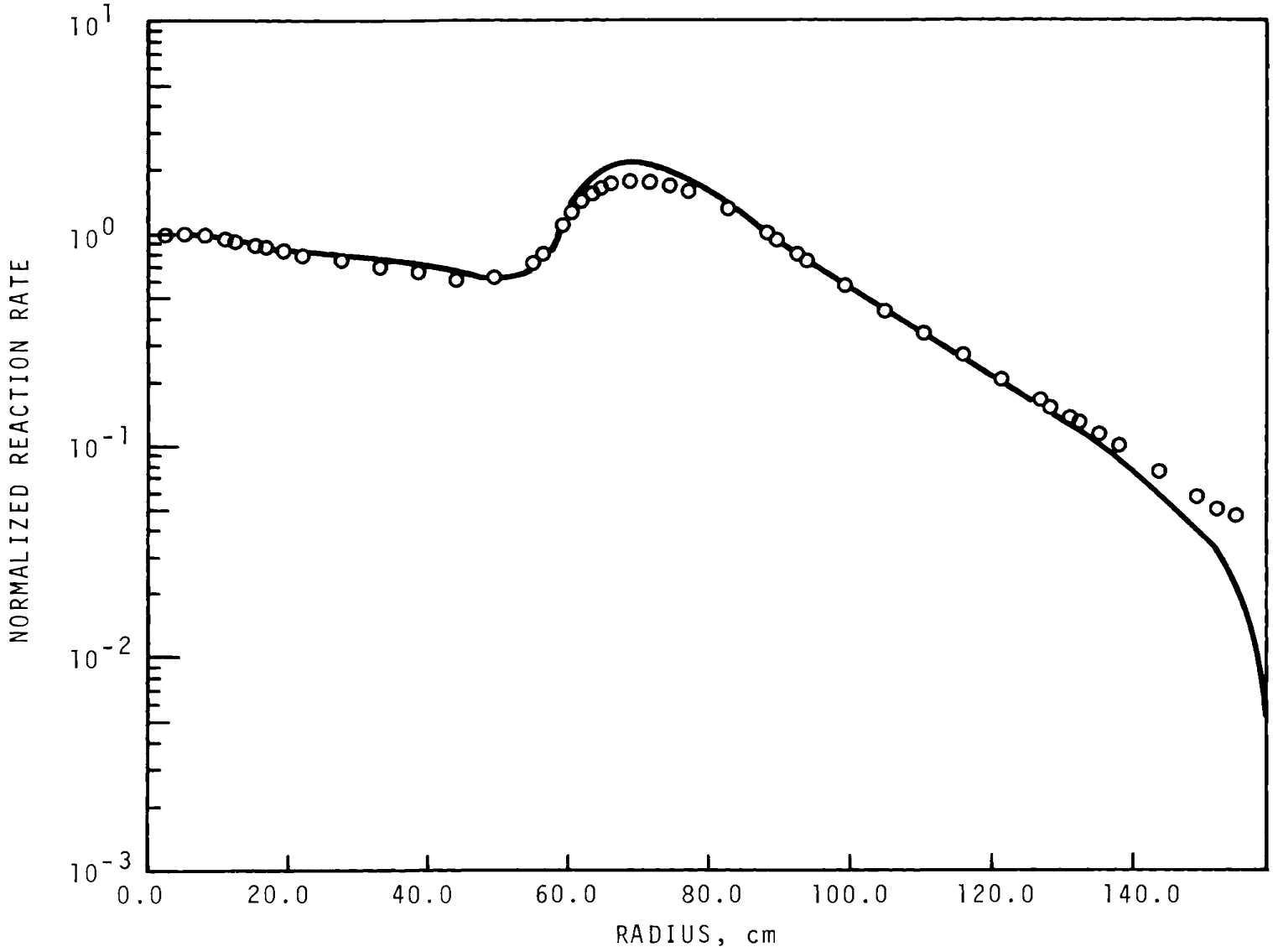

FIGURE 4.21. A Comparison of Calculated and Measured $^{10}B(n,\alpha)$ Radial Reaction Rate Distribution in the ZPPR/FTR 2

Gamma Distribution

The gamma distribution was measured by irradiating lithium fluoride thermoluminescent dosimeters (TLD's), which were dispersed radially and axially throughout the core, reflector and shield. Dosimeters were irradiated to a suitable integrated exposure, one set with and one set without stored fuel in the shield. Light output of each TLD was measured subsequently and compared to calibrated standards.

The discrete ordinates transport theory codes ANISN and DOT[4] were employed to calculate the gamma distribution for comparison to the experimental results. A ten-group gamma transport cross section set was generated employing the MUG[5] code. The energy range of the calculation extended from 10 MeV down to 0.015 MeV with equal (1 MeV) group widths except for the last group. The volume distributed gamma source was calculated from the neutron flux solution and included prompt fission gammas, fission product gammas, and neutron capture gammas. A ^{235}U prompt fission gamma spectrum[6] was employed in the calculation; however, evidence suggests this spectrum to be a realistic approximation for ^{239}Pu fission also. The fission product gamma spectrum was generated using the computer code ISOSHLD[7] based on a fission product inventory obtained from the code RIBD.[8] The neutron capture gamma ray spectra were extracted from data on thermal neutron capture reported in the literature.

A comparison of the calculated and measured radial gamma dose distribution is shown in Figure 4.22, based on a S_8-P_3 ANISN cylindrical calculation with no stored fuel present. The calculated ten-group gamma fluxes were converted to roentgens[9] and normalized to the integrated experimental exposure. Similar agreement was found at the other elevations.

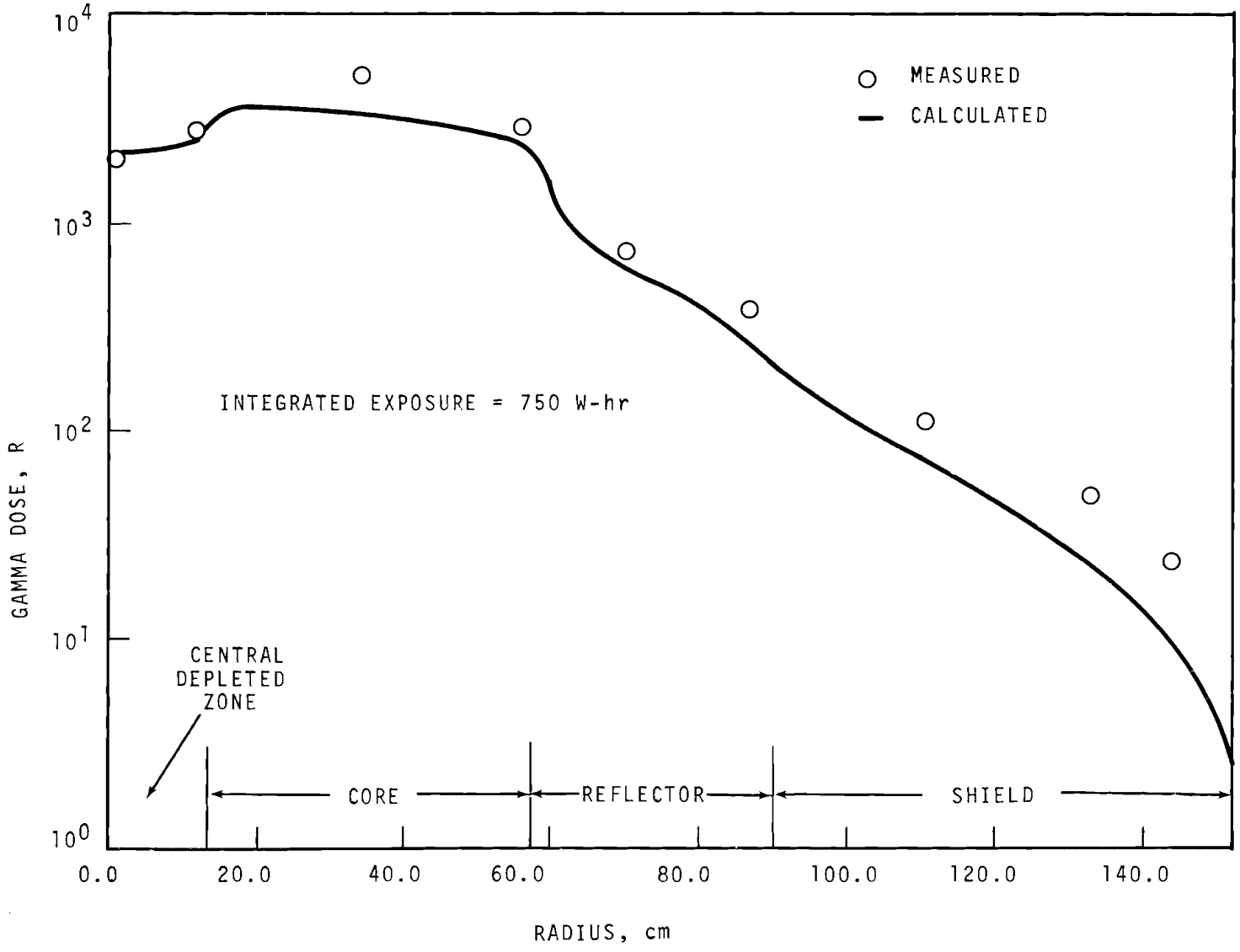

FIGURE 4.22. A Comparison of Calculated and Measured Radial Gamma Dose Distribution in the ZPPR/FTR2

Overall, the agreement between the calculated and experimental results is believed adequate to permit use of these techniques and nuclear data compilations in the preliminary design of the FTR shields. Basis of the relatively consistent difference between the experimental and calculated gamma results is being sought.

References

1. D. R. Marr. A User's Manual for 2DBS, A Diffusion Theory Shielding Code, BNWL-1291. Battelle-Northwest, Richland, Washington. February 1970.

2. W. W. Engle. A User's Manual for ANISN, A One-Dimensional Discrete Ordinate Transport Code with Anisotropic Scattering, K-1693. Carbide and Carbon Chemical Corporation, Oak Ridge, Tennessee. 1967.

3. D. R. Marr and M. G. Zimmerman. FTR Shield Design Cross Sections--A Partial Evaluation, BNWL-1197. Battelle-Northwest, Richland, Washington. 1969.

4. F. R. Mynatt. User's Manual for DOT, A Two-Dimensional Discrete Ordinate Transport Code with Anisotropic Scattering, K-1694. Carbide and Carbon Chemical Corporation, Oak Ridge, Tennessee. (to be published)

5. J. R. Knight and F. R. Mynatt. MUG - A Program for Generating Multigroup Photon Cross Sections, CTC-17. Union Carbide and Chemical Corporation, Oak Ridge, Tennessee. (to be published)

6. R. W. Peele, W. Zobel, and F. C. Maienschein. "Spectrum of Prompt Gamma Rays from Thermal Fission of ^{235}U," Trans. Am. Nucl. Soc., vol. 12, p. 384, 1969.

7. C. A. Mansius. A Revised Photon Probability Library for Use with ISOSHLD-111, BNWL-236 Supplement 2, Battelle-Northwest, Richland, Washington. April 1969.

8. R. O. Gumprecht. Mathematical Basis of Computer Code MDD, DUN-4136. Douglas United Nuclear, Inc., Richland, Washington, 1968.

9. Reactor Physics Constants, ANL-5800. Argonne National Laboratory, Second Edition, July 1963.

5.0 NO CONTRIBUTIONS

6.0 PUBLICATIONS AND PRESENTATIONS

PUBLICATIONS

B. H. Duane. Compressible Fluid Flow (BNW Program Gas), BNWL-1317.* September 1969.

R. W. Hardie and W. W. Little, Jr. 3DB, A Three-Dimensional Diffusion Theory Burnup Code, BNWL-1264. March 1970.

W. W. Little, R. B. Kidman, L. D. O'Dell, R. W. Hardie, R. E. Schenter, and K. B. Stewart. Unpublished Data. Battelle-Northwest, Richland, Washington. (Preliminary Report: Analysis of Selected Critical Experiments Using Version 11 of ENDF/B)

D. R. Marr. A User's Manual for 2DBS, A Diffusion Theory Shielding Code, BNWL-1291. February 1970.

James R. Sheff. Reactivity and the FTR, BNWL-2313. (To be published)

James R. Sheff. Justification and Specification of an FTR Oscillator, BNWL-1314. (To be published)

James R. Sheff. User's Manual for NOISY1, A Program for Calculation of Space Dependent Spectral Densities in Cubical Reactors, BNWL-1260. (To be published)

R. E. Wilson, R. J. Hall, and E. D. Clayton. "Surface Multiplication," (Technical Note) Nucl. Sci. Eng., vol.39, pp. 119-120. January 1970.

W. R. Young and R. A. Bennett. Analysis of FTR Phase B Critical Experiments Part-I ZPR-111 Assembly 51, BNWL-1138. January 1970.

W. R. Young and R. A. Bennett. Analysis of FTR Phase B Critical Experiments Part 2 ZPR-111 Assemblies 52a, b, c, d, e, and f, BNWL-1139. February 1970.

PRESENTATIONS

Papers to be Presented at the Summer Meeting of the American Nuclear Society, Los Angeles, California, June 28-July 2, 1970.

R. A. Bennett, S. L. Engstrom, J. V. Nelson, and W. R. Young. Statistically Significant Biases in the FTR Neutronics Model, BNWL-SA-3154-S.

---

* BNWL-numbered reports are published by Battelle-Northwest, Richland, Washington.

R. A. Bennett, S. L. Engstrom, J. V. Nelson, and P. L. Hofmann. Notes on the Use of the "Engineering Mockup" as a Nuclear Design Tool, BNWL-SA-3115.

R. A. Bennett and J. V. Nelson. Central Fuel and Peripheral Control Ring Reactivity Worths in the FTR-2 Critical, BNWL-SA-3116.

S. R. Bierman and E. D. Clayton. Critical Experiments with Homogeneous PuO_2, BNWL-SA-4030-S.

E. T. Boulette, W. L. Bunch, and L. F. Kocher. ZPPR/FTR-2 Shield Experiments: Gamma Distribution, BNWL-SA-3071.

E. T. Boulette. ZPPR/FTR-2 Shield Experiments: Neutron Distribution, BNWL-SA-3089.

R. H. Chow. Analyzer Recycling Between Neutron Bursts Using Gozani's Pulsed Neutron Technique, BNWL-SA-2722-S.

D. E. Christensen, R. P. Matsen and R. A. Schneider. Significant Properties of Chemical Reprocessing Plant Accountability Data, BNWL-SA-4036-A.

S. L. Engstrom, R. A. Bennett, V. O. Uotinen. Inverse Multiplication Monitoring of Subcritical Reactivity Changes in FTR, BNWL-SA-3114.

R. J. Jackson, W. H. Sutherland, and I. L. Metcalf. Swelling and Creep Effects upon Fast Reactor Core Structural Design, BNWL-SA-4018.

J. W. Kutcher, E. C. Davis and C. M. Heeb. MTR-Phoenix Fuel Critical Experiments and Analysis, BNWL-SA-3249-S.

E. P. Lippincott. Measurement of k_∞ of ThO_2-$^{233}UO_2$ HTGR Lattice, BNWL-SA-4026-S.

W. W. Little, R. B. Kidman, R. E. Schenter, L. D. O'Dell, R. W. Hardie, and K. B. Stewart. Analysis of Critical Experiments Using Version 11 of the Evaluated Nuclear Data File (ENDF/B), BNWL-SA-3202-S.

J. R. Sheff. Stability Analysis of the Fast Test Reactor, BNWL-SA-3101-S.

Alan E. Waltar and W. W. Little, Jr. On The Treatment of Spatial Feedback Effects in Fast Reactor Accident Analyses, BNWL-SA-3103-S.

Alan E. Waltar and William T. Sha. A New Computational System for Fast Reactor Accident Investigation, BNWL-SA-3102-S.

DISTRIBUTION

No. of Copies	
OFFSITE	
2	AEC Chicago Patent Group G. H. Lee
8	AEC Division of Reactor Development and Technology Asst. Dir. for Project Management Chief, Water Projects Branch (2) Chief, Gas Cooled Projects Branch Asst. Dir. for Reactor Technology Chief, Reactor Physics Branch (2) Chief, Core Design Branch
1	AEC Division of Nuclear Materials Safeguards H. Werner
1	AEC Division of International Affairs M. B. Kratzer
1	AEC Division of Production F. P. Baranowski
2	AEC Division of Licensing and Regulations C. D. Luke R. J. Odegaarden
1	AEC Division of Research G. A. Kolstad
218	AEC Division of Technical Information Extension
1	AEC Savannah River Operations Office R. Thorne
6	Argonne National Laboratory Reactor Physics Constants Center (4) R. Avery P. Gast

No. of Copies	
3	Atomic Energy of Canada Limited M. Duret C. Millar L. Pease
3	Atomic International H. Alter N. Ketzlach Liquid Metals Engineering Center (LMEC)
1	Australian Atomic Energy Commission AAEC Research Establishment Private Mail Bag, Sutherland 2232 N.S.W., Australia Dr. J. L. Symonds Chief, Physics Division
3	Babcock and Wilcox Company H. Jones D. H. Roy W. A. Wittkopf
1	Bechtel Corporation Vernon, California M. Aronchick
1	Bettis Laboratory, Westinghouse Electric Company J. J. Taylor
1	Bhabha Atomic Research Centre Trombay, Bombay-85, India S. R. Dwivedi, Theoretical Physics Section/RED Central Complex Bldg.
3	Brookhaven National Laboratory J. Chernick H. Kouts S. Pearlstein
1	California Institute of Technology H. Lurie, Engineering Div.

No. of Copies	
1	Catholic University of America Dept. of Nuclear Sci. & Eng. Washington, D.C. G. L. Simmons
10	C.E.N. - Saclay Boite Postale 2 Gif-Sur-Yvette (S et 0), France B. LaPonche P. Lecorche G. Vendryes
1	CNEN - Casaccia 00060 - S. Maria Di Galeria Rome, Italy Paolo Loizzo
2	CNEN-Centro Studi-Nucleaire Casaccia, Rome, Italy Ugo Farinelli Augusto Gandini
1	Combustion Engineering, Nuclear Division R. Harding
2	Cornell Univeristy, Ithaca, N.Y. R. T. Cuykendall, Eng. Physics M. Nelkin
2	Assoc. C.E.N. Belgo Nucleaire 35 Rue Des Colonies, Belgium H. Bairiot L. Bindler
2	Duke University Durham, N.C. H. W. Newson, Physics Dept. W. J. Seeley, School of Eng.

No. of Copies	
6	E. I. du Pont de Nemours & Co., Inc., Savannah River Laboratory H. K. Clark J. L. Crandall G. Dessauer E. J. Hennelly H. Honeck J. Suich
10	EURATOM 53, Rue Billiard Brussels 4, Belgium A. de Stordeur
1	FFR - AB Afomenergi Studsvik, Pa NYKOPING Sweden Evelyn Sokolowski
4	General Atomic J. M. Neill L. W. Nordheim H. B. Stewart G. D. Trimble
3	General Electric Company Knolls Atomic Power Laboratory R. Ehrlich C. Lubitz K. W. Seeman
4	General Electric Company San Jose R. L. Crowther M. R. Egan D. L. Fischer P. Greebler S. Levy

No. of Copies	
1	General Electric Company Nucleonics Laboratory H. W. Alter
1	Idaho Nuclear Inc. R. A. Grimesey
1	Istanbul Technical University Giimiis, Suyer, Istanbul, Turkey Director, Nuclear Energy Institute
1	Japan Atomic Energy Research Institute (JAERI) Tokaimura, Naka-gun, Ibarakiken, Japan Hjime Sakata
1	Japan Atomic Energy Institute (JPDR-TCA) Tokaimura, Ibarakiken, Japan Shojiro Matsuura
1	Kansas State University Manhattan, Kansas W. R. Kimel, Nuclear Eng.
1	Kernforschungszentrum Karlsruhe Professor W. Haefele
1	Los Alamos Scientific Laboratory G. E. Hansen
1	Manhattan College Riverdale, New York, N.Y. Brother Gabriel Kane
3	Massachusetts Institute of Technology Professor Irving Kaplan D. D. Lanning T. J. Thompson

No. of Copies	
1	North American Aviation Science Center E. R. Cohen
1	North Carolina State College R. L. Murray
1	Nuclear Materials and Equipment Corp. Apollo, Pennsylvania Karl Puechl
2	Oak Ridge National Laboratory F. C. Maienschein A. M. Perry
1	Pakistan Institute of Nuclear Science & Technology P. O. Nilore, Rawalpindi, Pakistan M. A. Mannan
1	Penn. State College W. F. Witzig
1	Phillips Petroleum Company Idaho Falls, Idaho W. B. Lewis
1	Power Reactor and Nuclear Fuel Development Corp. Minato-ku, Tokyo, Japan Setsuo Kobayashi
1	Purdue University P. N. Powers, Nucl. Eng. Dept.
1	Rensselaer Polytechnic Institute E. R. Gaerttner
1	S. C. K. - C. E. N. BRL, Mol-Donk, Belgium Dr. H. Vanden Broeck

No. of Copies	
1	Tennessee Valley Authority 310 Power Bldg., Chattanoga, Tenn. H. B. Brooks
1	Union Carbide Corporation (ORNL) E. B. Johnson
2	United Kingdom Atomic Energy Agency Atomic Weapons Research Establishment Aldermaston, Berkshire, UK R. C. Lane (1) Authority Health and Safety Branch, Safeguards Division, Risley, Warrington, UK J. H. Chalmers (1)
1	United Kingdom Atomic Energy Authority General Reactor Phvsics Division Winfrith, England C. G. Campbell
1	United Nuclear Corporation White Plains, N.Y. J. R. Tomonto
1	University of Arizona Tucson, Arizona Monte V. Davis, Nucl. Eng. Dept.
1	University of Florida Gainesville, Florida R. E. Uhrig, Nucl. Eng.
1	University of Illinois Urbana, Illinois Frederick Seitz, Physics Dept.
1	University of Minnesota Minneapolis, Minnesota H. S. Isben, Chem. Eng. Dept.

No. of Copies	
1	University of Nevada Reno, Nevada T. V. Frazier, Physics Dept.
1	University of Notre Dame Notre Dame, Indiana E. W. Jerger, Dept. of Mech. Eng.
1	University of Oregon Eugene, Oregon J. L. Powell, Physics Dept.
2	University of Tennessee Knoxville, Tennessee A. H. Nielsen, Physics Dept. P. F. Pasqua, Nucl. Eng. Dept.
1	University of Toledo Toledo, Ohio J. J. Turin
2	University of Washington Seattle, Washington A. L. Babb, Dept. of Nucl. Eng. K. L. Garlid
1	University of Wisconsin Madison 6, Wisconsin M. W. Carbon, Nucl. Eng. Com.
1	U.S. Atomic Energy Commission DNR A. Radkowsky
1	Virginia Polytechnic Institute Blacksburg, Virginia A. Robeson, Physics Dept.
1	Washington State University Pullman, Washington J. P. Spielman, Col. of Eng.

No. of Copies	
6	Westinghouse Electric
	C. A. Anderson
	R. J. French
	W. D. Leggett
	W. L. Orr
	J. B. Roll
	J. R. Worden

ONSITE-HANFORD

1	AEC Chicago Patent Group
	R. K. Sharp (Richland)
2	RDT Assistant Director for Pacific Northwest Programs
2	AEC Richland Operations Office
	C. L. Robinson (2)
8	Atlantic Richfield Hanford Company
	S. J. Beard
	M. H. Campbell
	R. D. Carter
	R. E. Isaacson
	G. R. Kiel
	A. E. Smith
	R. E. Tomlinson
	ARHCO File
3	Battelle Memorial Institute
2	Computer Sciences Corporation
	E. Z. Block
	R. J. Shields
1	Donald W. Douglas Laboratories
	J. Greenborg

No. of Copies	
9	Douglas United Nuclear
	G. F. Bailey
	C. E. Bowers
	G. C. Fullmer
	L. L. Grumme
	R. O. Gumprecht
	J. P. Hamric
	R. H. Meichle
	R. Nilson
	DUN File
108	Battelle-Northwest
	F. W. Albaugh
	C. A. Bennett
	C. L. Bennett
	S. R. Bierman
	E. T. Boulette
	C. L. Brown
	W. L. Bunch
	S. H. Bush
	G. J. Busselman
	J. J. Cadwell
	J. L. Carter
	N. E. Carter
	D. E. Christensen
	R. G. Clark
	E. D. Clayton
	G. M. Dalen
	E. C. Davis
	F. G. Dawson
	D. R. de Halas
	B. H. Duane
	J. B. Edgar
	G. W. R. Endres
	E. A. Eschbach
	E. A. Evans
	L. J. Federico
	J. R. Fishbaugher
	H. A. Fowler
	J. J. Fuquay
	G. L. Gelhaus
	A. G. Gibbs
	V. W. Gustafson

No. of
Copies

Battelle-Northwest (contd)

R. J. Hall
L. E. Hansen
G. E. Hanson
O. K. Harling
W. M. Harris
C. M. Heeb
R. E. Heineman
H. L. Henry
R. J. Hoch
P. L. Hofmann
R. H. Holeman
U. P. Jenquin
R. D. Johnson
R. L. Junkins
G. J. Konzek
D. A. Kottwitz
J. W. Kutcher
C. R. Lagergren
J. H. Lauby
B. R. Leonard, Jr.
D. L. Lessor
W. R. Lewis
R. C. Liikala
C. W. Lindenmeier
E. P. Lippincott
W. W. Little
R. C. Lloyd
R. P. Matsen
G. C. Moore
D. F. Newman
R. E. Nightingale
T. J. Oakes
D. R. Oden, Jr.
H. M. Parker
R. S. Paul
R. E. Peterson
W. W. Porath
D. L. Prezbindowski
W. L. Purcell
W. A. Reardon
C. R. Richey
C. A. Rogers
W. C. Roesch
J. T. Russell
R. E. Schenter
L. C. Schmid (6)
G. D. Seybold
R. I. Smith
K. B. Stewart
W. P. Stinson
H. J. Svoboda, Jr.
D. H. Thomsen
V. O. Uotinen
A. D. Vaughn
L. D. Williams
N. G. Wittenbrock
B. Wolfe
W. C. Wolkenhauer
D. C. Worlton
W. P. Walsh
M. G. Zimmerman
Technical Publications (2)
Technical Information Files (5)